TECHNICAL
MEMORANDUM
NCSC TM 347-82

AUGUST 1982

METHODS FOR PREDICTING TAIL CONTROL EFFECTS ON CONICAL AFTERBODIES OF SUBMERSIBLES

Prepared under Contract No. N61331-78-C-0032
By:
NIELSEN ENGINEERING & RESEARCH, INC.
Mountain View, California 94043
For:
NAVAL COASTAL SYSTEMS CENTER
Panama City, Florida 32407

Approved for public release;
distribution unlimited

NAVAL COASTAL SYSTEMS CENTER
NCSC
PANAMA CITY, FLORIDA 32407

NAVAL COASTAL SYSTEMS CENTER

PANAMA CITY, FLORIDA 32407

CAPT RAYMOND D. BENNETT, USN
Commanding Officer

GUY C. DILWORTH
Technical Director

ADMINISTRATIVE INFORMATION

The work described in this report was performed during fiscal years 1980-1981 and was supported by contract N61331-78-C-0032. Funding for this effort was supplied by the Naval Sea Systems Command under Program Element 61153N. The work produced engineering methods for predicting the effect of the deflection of tail fins mounted on a conical boattail on the hydrodynamic characteristics of a submersible.

Nielsen Engineering and Research Company of Mountain View, California, prepared the report under contract (N61331-78-C-0032) to the Naval Coastal Systems Center (NCSC). Jack N. Nielsen, Frederick K. Goodwin, and Charles A. Smith of Nielsen Engineering were authors of the report. Neill Smith of Code 794 monitored the work for NCSC.

Released by
D. C. Summey, Acting Head
Vehicle Technology Division
August 1982

Under authority of
M. J. Wynn, Head
Research and Technology
Department

Unclassified

SECURITY CLASSIFICATION OF THIS PAGE (When Data Entered)

REPORT DOCUMENTATION PAGE	READ INSTRUCTIONS BEFORE COMPLETING FORM
1. REPORT NUMBER: NCSC TM 347-82	2. GOVT ACCESSION NO.: AD-A121 263
	3. RECIPIENT'S CATALOG NUMBER:
4. TITLE (and Subtitle): METHOD FOR PREDICTING TAIL CONTROL EFFECTS ON CONICAL AFTERBODIES OF SUBMERSIBLES	5. TYPE OF REPORT & PERIOD COVERED: Final Technical Report 8/11/78 to 3/15/81
	6. PERFORMING ORG. REPORT NUMBER: NEAR TR 241
7. AUTHOR(s): Jack N. Nielsen, Frederick K. Goodwin, Charles A. Smith	8. CONTRACT OR GRANT NUMBER(s): N61331-78-C-0032
9. PERFORMING ORGANIZATION NAME AND ADDRESS: Nielsen Engineering & Research, Inc. 510 Clyde Avenue Mountain View, California 94043	10. PROGRAM ELEMENT, PROJECT, TASK AREA & WORK UNIT NUMBERS: Program Element 61153N
11. CONTROLLING OFFICE NAME AND ADDRESS: Naval Coastal Systems Center Panama City, Florida 32407	12. REPORT DATE: August 1982
	13. NUMBER OF PAGES: 111
14. MONITORING AGENCY NAME & ADDRESS (if different from Controlling Office)	15. SECURITY CLASS. (of this report): Unclassified
	15a. DECLASSIFICATION/DOWNGRADING SCHEDULE: N/A

16. DISTRIBUTION STATEMENT (of this Report)

Approved for public release; distribution unlimited.

17. DISTRIBUTION STATEMENT (of the abstract entered in Block 20, if different from Report)

18. SUPPLEMENTARY NOTES

19. KEY WORDS (Continue on reverse side if necessary and identify by block number)

Hydrodynamic Configurations
Submersibles
Predictions
Methods
Wind Tunnels
Testing

20. ABSTRACT (Continue on reverse side if necessary and identify by block number)

Methods were constructed for predicting the effects of all-movable tail fins mounted on a conical afterbody on the longitudinal stability and control characteristics of submersible vehicles. A set of wind tunnel tests were conducted to obtain systematic data as functions of tail fin aspect ratio, taper ratio, span-to-body diameter ratio and deflection angle and vehicle angles of attack and sideslip. These data were then

DD FORM 1 JAN 73 1473

Unclassified

20. ABSTRACT (Concluded)

used, coupled with theoretical results, to develop the prediction methods. The methods deal with the characteristics of individual vehicle components (bodies, tails) and their mutual interactions when combined into complete configurations. Each method is presented in self-contained form, along with appropriate directions for its use. It is shown that the methods provide good accuracy for prediction of hydrodynamic control characteristics.

SUMMARY

This document covers the wind-tunnel tests and construction of methods for estimating the effects of all-movable tail fins mounted on a conical afterbody on the longitudinal stability and control characteristics of a submersible vehicle. A systematic set of tests was made varying tail fin aspect ratio and taper ratio as well as fin span to establish a data base for the estimating methodology. With the help of the data base and analytical techniques a series of methods were constructed for estimating the tail fin characteristics and the complete configuration characteristics as a function of tail fin deflection angle. A calculative example is included of the use of the method which is fully contained within this document. The comparisons between data and prediction methods show generally good agreement.

SYMBOLS

AR	aspect ratio of fin alone
b_0, b_1, b_2	coefficients in Equation (1)
c_r	fin root chord
c_t	fin tip chord
C_ℓ	rolling-moment coefficient of body-tail combination with S_R and D as reference area and reference length, respectively
C_n	yawing-moment coefficient of body-tail combination with S_R and D as reference area and reference length, respectively
C_A	axial-force coefficient of body-tail combination with S_R as reference area
C_B	fin root-bending-moment coefficient, $M_B/q_\infty S_T s$
C_H	Fin hinge-moment coefficient, $M_H/q_\infty S_T c_r$
C_N	normal-force coefficient of tail fin, $N/q_\infty S_T$
C_Y	side-force coefficient of body-tail combination with S_R as reference length
C_Z	component of $(C_N)_{T(B)}$ normal to body longitudinal axis
$(C_m)_B$	pitching-moment coefficient of body alone about lateral axis through center of moments with S_R and D as reference area and length, respectively
$(C_m)_{B(T)}$	pitching-moment coefficient of body loading due to one fin about lateral axis through center of moments with S_T and c_r as reference quantities
$(C_m)_{BT}$	pitching-moment coefficient of body-tail combination about lateral axis through center of moments with S_R and D as reference quantities
$(C_m)_{T(B)}$	pitching-moment coefficient due to one deflected fin about lateral axis through center of moments with S_T and c_r as reference quantities
$C_{m_{Y'}}$	body-tail pitching-moment coefficient about Y' axis with S_R and D as reference area and reference length, respectively

SYMBOLS (Continued)

$C_{m_{Y''}}$	body-tail pitching-moment coefficient about Y" axis with S_R and D as reference area and reference length, respectively
$(C_N)_B$	normal-force coefficient of body alone with S_R as reference area
$(C_N)_{B(T)}$	normal-force coefficient of body loading due to deflection of one fin based on S_T as reference area
$(C_N)_{BT}$	normal-force coefficient of body-tail combination with S_R as reference area
$(C_N)_{T(B)}$	normal-force coefficient of one deflected fin based on S_T as reference area
$\left(\frac{dC_L}{d\alpha}\right)_{DAT}$	lift-curve slope of fin alone estimated from DATCOM based on fin alone planform area, S_T
$\left(\frac{dC_N}{d\alpha}\right)_{T(B)}$	normal-force curve slope, due to angle of attack, of fin in presence of body based on fin planform area, S_T
$\left(\frac{dC_N}{d\delta}\right)_{T(B)}$	normal-force curve slope, due to fin deflection, of fin in presence of body based on fin planform area, S_T
D	body diameter ahead of conical boattail
k_B	interference factor for body loading due to tail fin deflection
k_T	interference factor for tail fin normal force due to δ
k_T^*	value of k_T for s/R = .714
$M_{B(T)}$	moment corresponding to $(C_m)_{B(T)}$
M_B	fin root-bending moment
M_H	fin hinge moment
M_∞	free-stream Mach number
N	normal force
N_T	normal force of tail fin as part of tail alone
q_∞	free-stream dynamic pressure
R	radius of body before conical boattail

SYMBOLS (Continued)

s	fin semispan, distance from root chord to fin tip measured normal to root chord
S_R	reference area for body alone and body-tail combination forces and moments
S_T	planform area of tail fin
x_{cp}	fin center-of-pressure position with x_{cp} measured aft of the leading dege of the root chord parallel to it
$\left(\frac{x_{cp}}{c_r}\right)_T$	nondimensional center-of-pressure position of tail fin alone
x_s	distance to start of conical boattail from lateral axis through center of moments
x_B	distance along boattail to fin hinge-line position measured from start of boattail
x_H	distance of fin hinge line behind leading edge of root chord measured parallel to root chord
$(x_{cp})_T$	values of x_{cp} for tail alone
X	distance measured positive rearward in axial direction from lateral axis through center-of-moment reference point
$\overline{X}_{B(T)}$	axial position of center-of-pressure of body loading due to fin deflection
Y_{cp}	distance of fin center-of-pressure position outboard of root chord measured normal to root chord
Y'	lateral axis through juncture of hinge line and conical boattail
Y''	lateral axis through center-of-moments reference point
α	Angle of attack of body-tail combination; angle between body longitudinal axis and free-stream direction
γ	half-angle of conical boattail

SYMBOLS (Concluded)

δ	fin deflection angle, positive trailing edge downward or to the left at $\phi = 0°$
λ	fin taper ratio, c_t/c_r
$\Lambda_{c/2}$	sweep angle of tail-fin midchord line
Λ_{te}	sweep angle of tail-fin trailing edge

Subscripts

B	body alone
BT	body-tail combination
B(T)	body in presence of one tail fin
DAT	DATCOM
T	tail fin alond
T(B)	tail fin in presence of body
δ	due to control deflection

TABLE OF CONTENTS

Section		Page No.
1.	INTRODUCTION	1
2.	WIND-TUNNEL MODELS	2
3.	WIND-TUNNEL TESTS	9
4.	DATA REDUCTION AND ACCURACY	15
5.	PREDICTION METHODS	22
5.1	NORMAL FORCE ON A DEFLECTED TAIL FIN ON CONICAL BOATTAIL	22
5.1.1	Preliminary Remarks	22
5.1.2	Comparison Between Prediction and Data	26
5.1.3	Prediction Method	30
5.1.4	Nonlinear Effects on Fin Normal Force	31
5.2	CHORDWISE CENTER-OF-PRESSURE LOCATION ON DEFLECTED FIN ON CONICAL BOATTAIL (HINGE MOMENT)	35
5.2.1	Preliminary Remarks	35
5.2.2	Comparison Between Prediction and Data	36
5.2.3	Prediction Method	40
5.3	SPANWISE CENTER-OF-PRESSURE LOCATION OF DEFLECTED FIN ON CONICAL BOATTAIL (ROOT-BENDING MOMENT)	40
5.3.1	Preliminary Remarks	40
5.3.2	Comparison Between Prediction and Data	42
5.3.3	Prediction Method	43
5.4	LIFT CARRYOVER ONTO CONICAL BOATTAIL DUE TO DEFLECTED FINS	43
5.4.1	Preliminary Remarks	43
5.4.2	Correlation of Lift Carryover Data	45
5.4.3	Prediction Method	58

TABLE OF CONTENTS (Concluded)

Section		Page No.
5.5	CENTER-OF-PRESSURE POSITION OF LOADING ON CONICAL AFTERBODY DUE TO FIN DEFLECTION	60
5.5.1	Preliminary Remarks	60
5.5.2	Correlation of Center-of-Pressure Position of Body Loading	61
5.5.3	Prediction Method	75
5.6	CHARACTERISTICS OF COMPLETE CONFIGURATION	79
5.6.1	Preliminary Remarks	79
5.6.2	Method of Calculation	79
6.	USE OF METHODS TO PREDICT CHARACTERISTICS OF COMPLETE CONFIGURATIONS	80
6.1	INTRODUCTORY REMARKS	80
6.2	EXAMPLE CONFIGURATION	80
6.3	FIN NORMAL-FORCE COEFFICIENT, $(C_N)_{T(B)}$	81
6.4	FIN HINGE-MOMENT COEFFICIENT, $(C_H)_{T(B)}$	83
6.5	FIN ROOT-BENDING-MOMENT COEFFICIENT, $(C_B)_{T(B)}$	89
6.6	NORMAL FORCE ON CONICAL BOATTAIL DUE TO FIN DEFLECTION, $(C_N)_{B(T)}$	89
6.7	CENTER-OF-PRESSURE OF LOADING ON CONICAL AFTERBODY, $(x_{cp}/c_r)_{B(T)}$	90
6.8	COMPLETE CONFIGURATION CHARACTERISTICS	90
6.8.1	Normal-Force Coefficient	90
6.8.2	Pitching-Moment Coefficient	91
7.	CONCLUSIONS AND RECOMMENDATIONS	93
7.1	CONCLUSIONS	93
7.2	RECOMMENDATIONS	94
APPENDIX A		A-1

LIST OF ILLUSTRATIONS

Figure No.		Page No.
1	BASIC TEST MODEL	3
2	FIN GEOMETRY	5
3	FIN PROFILES	6
4	FIN TEST MATRIX	7
5	TANGENT-OGIVE BASE SECTION	8
6	FIN BALANCE	10
7	TYPICAL MODEL INSTALLATION IN THE 12-FOOT PRESSURE WIND TUNNEL	12
8	CLOSE UP OF FINS MOUNTED ON THE CONICAL AFTERBODY	13
9	COEFFICIENT DEFINITIONS AND SIGN CONVENTION	14
10	NORMAL-FORCE CURVE SLOPE DUE TO FIN DEFLECTION FOR THE TWO HORIZONTAL FINS IN THE PRESENCE OF THE BODY AT $\delta = 0°$	17
11	EXPERIMENTAL NORMAL-FORCE COEFFICIENT VARIATION WITH δ FOR FIN T12	18
12	CENTER-OF-PRESSURE LOCATION OF THE FINS IN THE PRESENCE OF THE BODY, $\delta = 0°$	20
13	COMPARISON OF FIN CHARACTERISTICS DUE TO α VARIATION	23
14	COMPARISON OF EXPERIMENTAL FIN-ALONE NORMAL-FORCE-CURVE SLOPES WITH VALUES PREDICTED FROM DATCOM	28
15	CORRELATION OF WING-BODY INTERFERENCE FACTOR k_T FOR VARIOUS FINS MOUNTED ON CONICAL BOATTAIL	29
16	VARIATION OF $F(s'/R)$ WITH (s/R)	32
17	VALUE OF b_2 FOR OBTAINING NONLINEAR COMPONENT OF FIN NORMAL FORCE IN PRESENCE OF CONICAL BOATTAIL	34

LIST OF ILLUSTRATIONS (Concluded)

Figure No.		Page No.
18	COMPARISON OF EXPERIMENTAL AND THEORETICAL CENTER-OF-PRESSURE POSITIONS FOR FINS ALONE	37
19	CENTER-OF-PRESSURE POSITION OF FIN ON BOATTAIL BASE CORRELATED AS FUNCTION OF FIN ALONE POSITIONS	39
20	CHARTS FOR TAIL-ALONE CENTER OF PRESSURE AT SUBSONIC SPEEDS AS DETERMINED BY LIFTING-LINE THEORY	41
21	CORRELATION OF LATERAL CENTER-OF-PRESSURE POSITION OF DEFLECTED FIN ON CONICAL BOATTAIL	44
22	PLOTS OF NORMAL FORCE ON BODY VERSUS NORMAL FORCE ON FIN MOUNTED ON BOATTAIL	47
23	CORRELATION OF k_B/k_T WITH s/R	59
24	PLOTS FOR DETERMINING CENTER-OF-PRESSURE LOCATION OF LOADING ON BODY DUE TO FIN DEFLECTIONS	63
25	COMPARISON BETWEEN EXPERIMENTAL AND PREDICTED VALUES OF $\left(\frac{x_{cp}}{c_r}\right)_{B(T)}$	76
26	COMPARISON BETWEEN MEASURED AND PREDICTED QUANTITIES FOR TAIL FINS T11 ON BODY-TAIL COMBINATION	84

1. INTRODUCTION

Submersible vehicle design has achieved considerable importance in recent years, but preliminary design methods for such vehicles have not received the attention they warrant. It is desirable to develop such methods to avoid expensive and time-comsuming parametric studies of designs in testing facilities.

In order to make a rational start at developing preliminary design methods it has been necessary to define a set of configurations of interest. The bodies chosen have been bodies of revolution with blunt noses and boattail bases. Fins of various planforms may be mounted on the body between the nose and the base. The problems of interest include predicting the six components of forces and moments on the complete configuration as a function of angle-of-attack and roll angle. In addition, the fin and configuration forces and moments as affected by angle-of-attack and fin deflection angle are of interest.

Special problems arise in connection with the prediction of the forces and moments. For the high angles-of-attaok of interest, the body may shed vortices which interact with the fins mounted on it. The flow may separate over the boattail at angle-of-attack. Also, the tail fins or boattail may undergo separation as a result of deflecting the fins. The possibility of gap effects due to deflecting the tail fins also exists. Thus a number of effects may occur which are generally beyond the scope of classical hydrodynamics.

A special approach has been adapted to cope with the problems arising in trying to develop a preliminary design method for submersible vehicles. This method, sometimes called rational modeling, is based on obtaining a systematic data base over the parameter ranges of interest in the design space. Then analysis is used to interpolate within or extrapolate the data base as far as possible. The extent to which the method can be extended beyond the design space depends to the extent that rational models can be used to predict or correlate the data base. By careful choice of the systematic parameter variations in compiling the data base, it is possible to cover a larger design space while still keeping the test program within bounds.

This report supplements the work of Fidler and Smith[1] and concerns the same basic models. Fidler and Smith tested a series of isolated bodies, isolated tails, and body-tail combinations in a wind tunnel to determine a systematic data base of forces and moments with zero deflection angle of the tail fins. They have

---

[1] Fidler, J.E. and Smith, C.A.: Methods for Predicting Submersible Hydrodynamic Characteristics. NCSC TM-238-78, July 1978.

developed methods for predicting the variations of the forces and moments of body-tail combinations and their components as a function of angle of attack. This report describes tests to obtain the effects of tail-fin deflections on the forces and moments. Also methods are developed based on the resulting data base for predicting these quantities for body-tail combinations not in the data base.

Three sections of the report are devoted to wind-tunnel models, test program, and the data reduction and accuracy. Another section discusses the development of methods for predicting the forces and moments on the various components of the body-tail combination as a function of fin deflection angle δ with $\alpha = 0$ degrees. The normal force, pitching moment, and root-bending moment of the fins are predicted. The body normal force and its center of pressure due to fin deflection are predicted. Finally the normal force and pitching moment of the body-tail combination are predicted. A detailed calculative example is included which encompasses all the methods.

With the methods of Reference 1 for $\delta = 0$ degrees and $\alpha \neq 0$ degrees together with the present methods for $\delta \neq 0$ degrees, $\alpha = 0$ degrees, estimates can be made for $\alpha \neq 0$ degrees, $\delta \neq 0$ degrees using superposition. Nonlinear coupling effects between α and δ are not covered herein.

2. WIND-TUNNEL MODELS

The wind-tunnel models used in the present investigation were designed to cover systematically those ranges of geometry typical of submersible vehicles. Changes in body length, nose shape, and afterbody length were investigated in a previous test[1]. A single nose and body were used in the present test with two different afterbodies and 12 different sets of control surfaces.

The basic model, a body of revolution, is shown in Figure 1 without control surfaces attached. The overall length is 70.28 inches (178.51 cm). The diameter of the centerbody section is 7 inches (17.78 cm). Thus, the slenderness ratio is 10.05. Details of the various sections are:

Nose section:	1 caliber ellipse
Centerbody section:	49.28 inches long (125.17 cm)
Afterbody section:	2 caliber cone

[1] ibid.

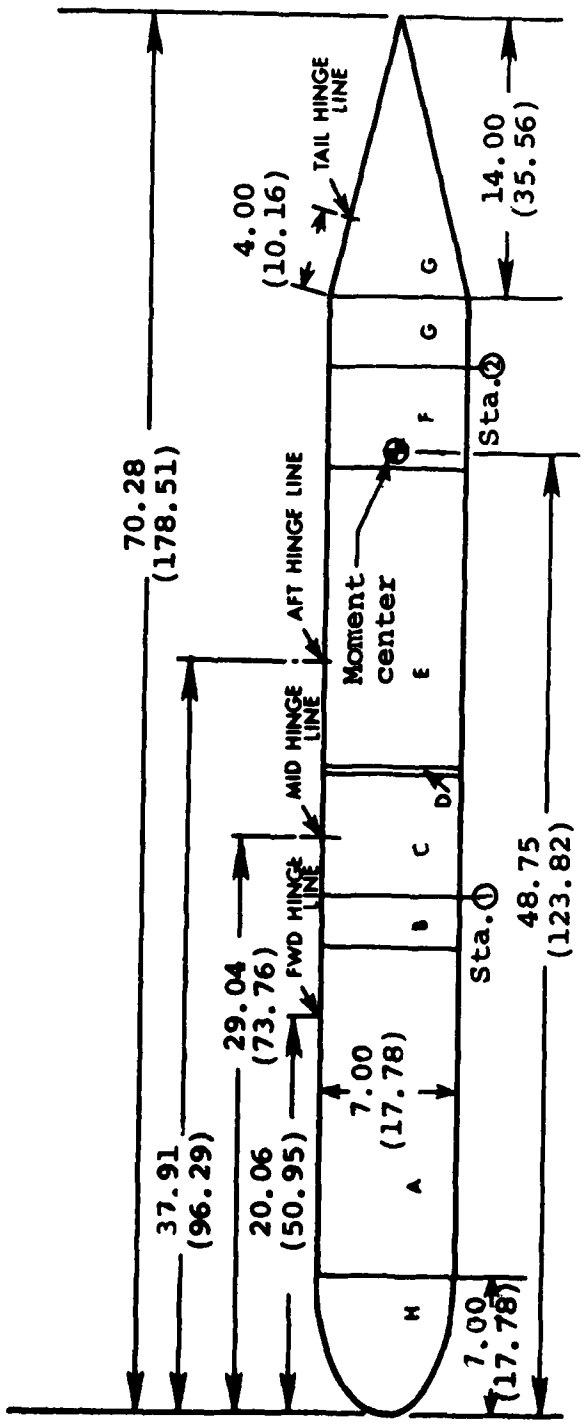

All dimensions in inches (centimeters)

Body section	Length
A	16.560 (42.06)
B	2.625 (6.67)
C	6.100 (15.49)
D	0.375 (0.95)
E	15.000 (38.10)
F	5.120 (13.00)
G	17.500 (44.45)
H	7.000 (17.78)

FIGURE 1. BASIC TEST MODEL

There is room for a six-component, 2-inch diameter balance to be located inside the body. This balance is used to measure the forces and moments on the overall configuration.

Control surfaces of various aspect ratio, taper ratio, and body diameter to exposed semispan ratio can be mounted to the basic model at any of the four hinge lines indicated in Figure 1. Dimensions of the control surfaces are tabulated in Figure 2. One to four control surfaces can be attached individually to the body at the forward and tail hinge-line locations in a cruciform arrangement. Only a single fin can be mounted at the mid and aft hinge lines, at the right horizontal position looking forward (corresponding to $\phi = 90$ degrees). All of the fins, with the exception of fin 4, have the section profile shown in Figure 3(a). These fins are flat plates with rounded leading edges. Fin 4 has a NACA 0018 profile, as shown in Figure 3(b).

The fin test matrix is shown pictorially in Figure 4. Across the top of the figure, the nominal aspect ratios are listed and down the left-hand side, the various taper ratio, λ, and fin span, s, combinations. The planforms of the fins listed in Figure 2 are drawn in the appropriate boxes.

A separate afterbody section was tested in addition to the conical afterbody shown in Figure 1. This second afterbody was a 2-caliber tangent ogive and is shown in Figure 5.

Each of the body sections (nose, afterbody, etc.) has been given a combination letter-number designation to differentiate among various body components. The designations for components used in the previous test[1] have not been changed. The designations are listed below.

Section	Designation
Nose	N2
Centerbody	C4
Conical afterbody	B2
Tangent-ogive afterbody	B4

When a control surface was mounted at the tail hinge line its number designation was preceded by a T. When it was mounted on one of the other hinge lines it was preceded by an S and followed by a subscript indicating the particular hinge line (F, M, or A for forward, mid, and aft). Thus, an example of a complete body-tail configuration would be N2C4B2T11, and a body-sail configuration would be $N2C4S4_FB2$.

(1) ibid.

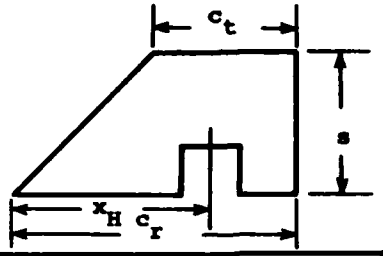

Fin No.	Taper Ratio λ	Aspect Ratio, AR 2 Panels	Span s in. (cm)	Tip Chord c_t in. (cm)	Root Chord c_r in. (cm)	Single Panel Area, S_T $in.^2$ (cm^2)	Hinge Line x_H in. (cm)
2	0.5	1.0	1.95 (4.95)	2.597 (6.596)	5.187 (13.175)	7.581 (48.910)	4.000 (10.160)
4	0.5	1.0	2.50 (6.35)	3.332 (8.463)	6.664 (16.927)	12.495 (80.613)	4.000 (10.160)
5	0.5	1.0	3.50 (8.89)	4.620 (11.735)	9.310 (23.647)	24.260 (156.516)	4.000 (10.160)
9	0.0	2.0	2.50 (6.35)	0.000 (0.000)	5.000 (12.700)	6.250 (40.322)	4.000 (10.160)
11	0.5	1.0	2.50 (6.35)	3.332 (8.463)	6.664 (16.927)	12.500 (80.645)	4.000 (10.160)
12	0.5	2.0	2.50 (6.35)	1.666 (4.232)	3.332 (8.463)	6.250 (40.322)	1.875 (4.762)
13	1.0	0.5	2.50 (6.35)	10.00 (25.400)	10.000 (25.400)	25.000 (161.290)	4.000 (10.160)
14	1.0	1.0	2.50 (6.35)	5.000 (12.700)	5.000 (12.700)	12.500 (80.645)	4.000 (10.160)
15	1.0	1.905	2.50 (6.35)	2.625 (6.668)	2.625 (6.668)	6.563 (42.342)	1.875 (4.762)
19	0.5	2.5	3.50 (8.89)	1.867 (4.742)	3.733 (9.482)	9.800 (63.226)	1.876 (4.765)
20	0.523	2.352	2.50 (6.35)	1.459 (3.706)	2.792 (7.092)	5.314 (34.283)	2.043 (5.189)
24	0.526	3.733	3.50 (8.89)	1.292 (3.282)	2.458 (6.243)	6.563 (42.342)	1.709 (4.341)

FIGURE 2. FIN GEOMETRY

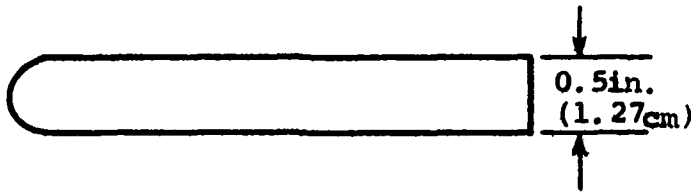

(a) Basic Fin Profile.

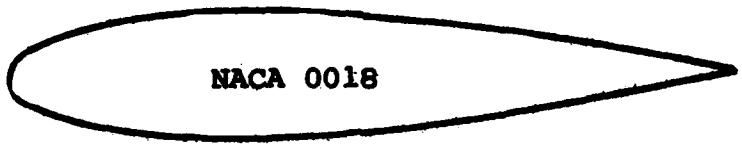

(b) Profile of Fin 4.

FIGURE 3. FIN PROFILES

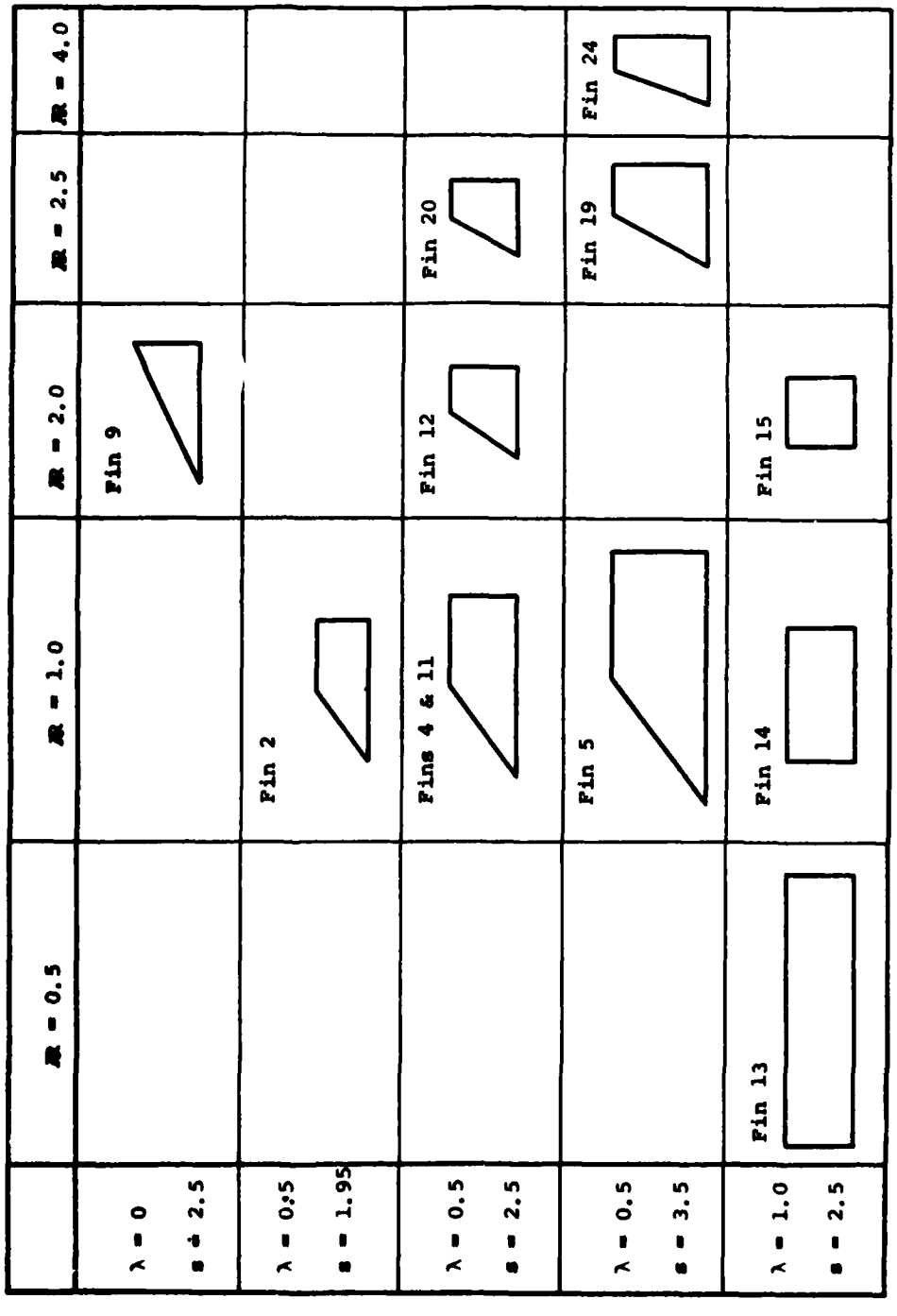

FIGURE 4. FIN TEST MATRIX

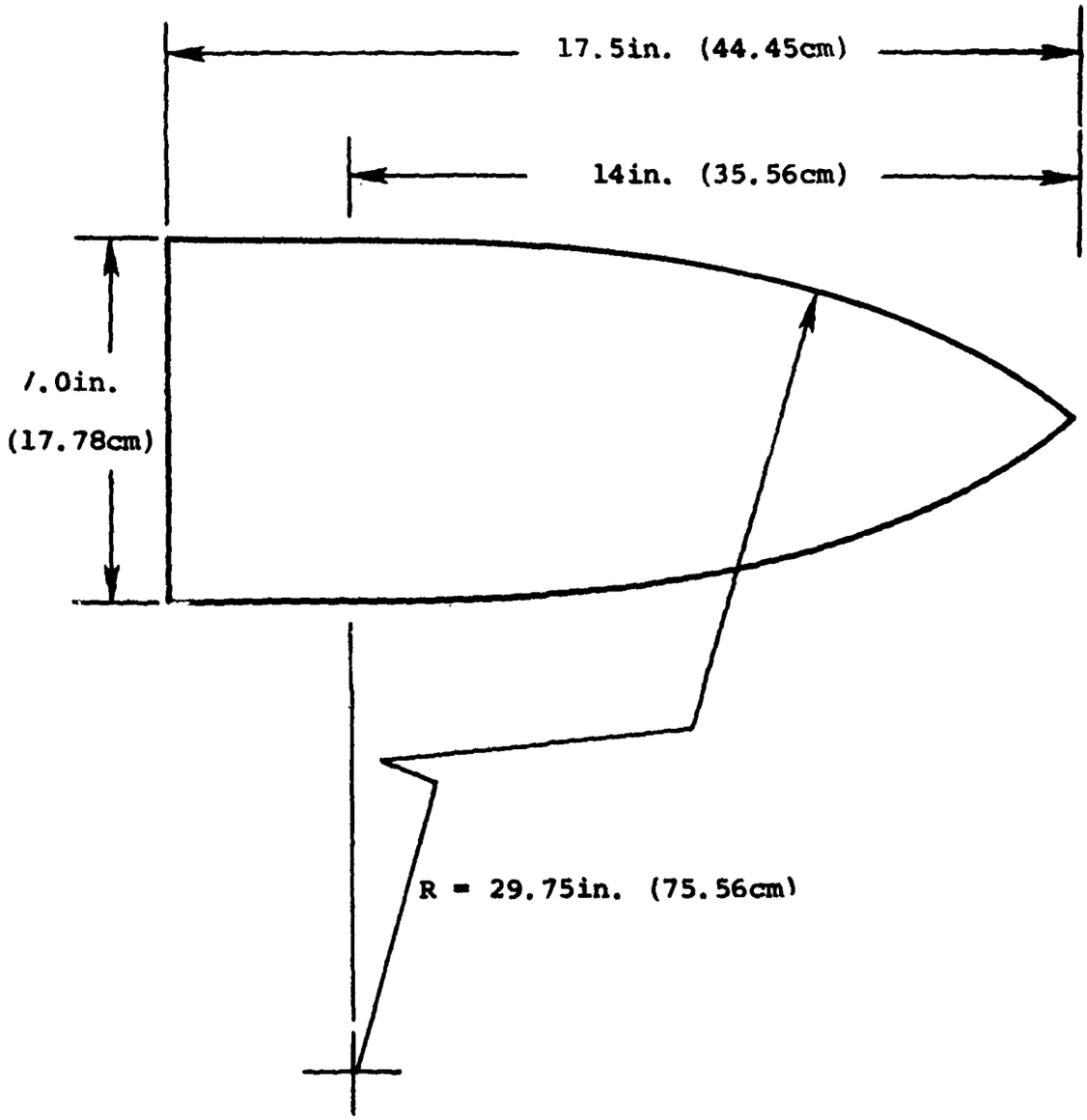

FIGURE 5. TANGENT-OGIVE BASE SECTION

Each control surface located at the forward or tail hinge line can be deflected independently any angle from -30 to +30 degrees relative to the body longitudinal axis. Fins at the mid and aft hinge lines cannot be deflected. In addition, the body forward of station 1 and aft of station 2 (Figure 1) can be rolled any angle ϕ about the body longitudinal axis.

Each control surface is mounted on a three-component strain gauge balance designed specially for this program. Figure 6 shows the fin balance post to which the strain gauges were applied. This type balance is capable of measuring normal force, root-bending moment, and hinge moment. It does not measure axial force.

3. WIND-TUNNEL TESTS

Wind-tunnel tests were conducted in the 12-foot Pressure Wind Tunnel at NASA/Ames Research Center, Moffett Field, California. This is a variable density, low turbulence facility that operates at subsonic speeds up to slightly less than a Mach number of 1.0. It can be operated at any internal stagnation pressure from 2.5 to 75 pounds per square inch absolute. The Reynolds number can be varied from 0 to approximately 9.5×10^6 per foot. These tests consisted of force and moment tests on a series of body-tail combinations, isolated bodies, and body-sail configurations. In addition, a single oil-flow visualization test was conducted on an isolated body.

The objectives of these tests were to investigate the effects of:

a. tail surface deflection angle
b. model roll angle
c. afterbody base planform
d. control surface section profile
e. forward-mounted single fin (i.e., sail)

Nominal tunnel flow conditions throughout the test were:

Reynolds number	7.5×10^6/ft
Mach number	0.28
Dynamic pressure	500 lb/ft^2
Total pressure	9500 lb/ft^2

The body-alone configurations and the body-sail configurations were also tested at lower Reynolds numbers.

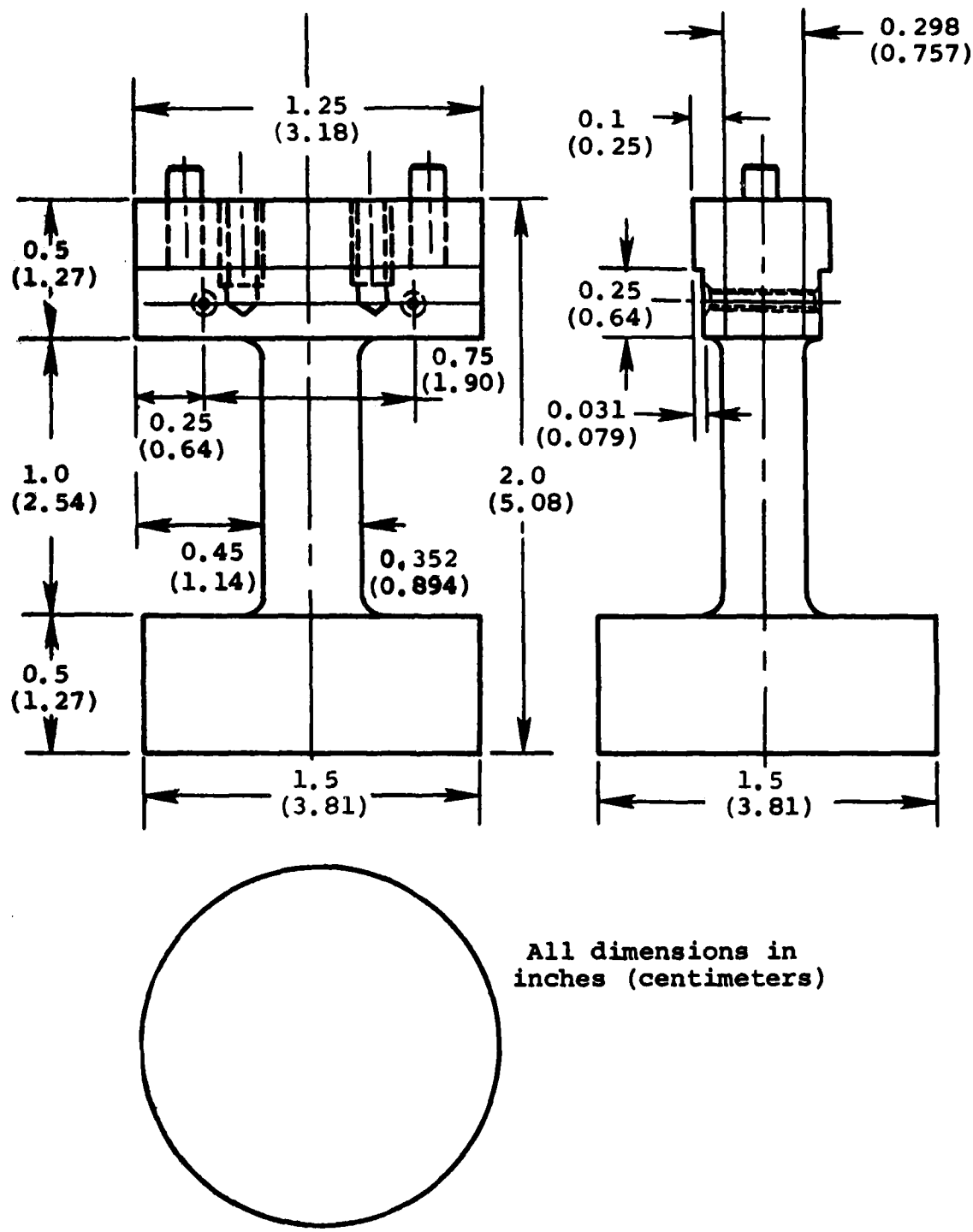

FIGURE 6. FIN BALANCE

A typical model installation in the wind tunnel is shown in Figure 7. The model was strut mounted from the floor of the tunnel. In order to minimize strut interference on the model the upper section had an airfoil shape fairing. In addition, angle of attack testing was done at negative angles, model nose down in the tunnel. This kept the tail fins as far out of the strut wake as possible.

Data were obtained from a six-component main balance located inside the body and separate three-component balances connected to each fin. Figure 8 shows two different sets of fins attached to the conical afterbody. The rectangular areas which can be seen on each fin are the balances.

The force and moment coefficients measured by the main balance in the body were axial force, C_A, normal force, C_N, side force, C_Y, rolling moment, C_ℓ, pitching moment, C_m, and yawing moment, C_n. These last two moments were taken about the moment center shown in Figure 1. Positive directions of the force and moment coefficients are shown at the top of Figure 9. As the forward and aft sections of the model were rolled, these directions remained fixed in the wind tunnel.

The tail fin numbering system is also shown in Figure 9. At zero degrees roll, $\phi = 0$ degrees, fin 1 is on the top of the model when looking upstream in the tunnel. Positive roll is clockwise looking upstream. The bottom part of Figure 9 defines the directions of positive fin deflection, δ, positive fin normal force, N_T, positive fin root-bending moment, M_B, and positive hinge moment, M_H. These positive directions roll with the fin as the model is rolled. Thus, at $\phi = 90$ degrees the positive directions for fin 1 are opposite to those for fin 2 at $\phi = 0$ degrees. The root-bending moment is taken about the fin root chord and the hinge moment about the fin hinge line. The hinge line locations for the various fins are listed in Figure 2.

Each configuration was tested through an angle-of-attack range from +2 to -15 degrees. Body-tail configurations were tested at roll angles from 0 to 90 degrees with undeflected fins, and at the two roll angles 0 and 90 degrees with the two opposing fins, fins 2 and 4, deflected through the range -12 to +30 degrees. The configurations tested are tabulated in Table 1.

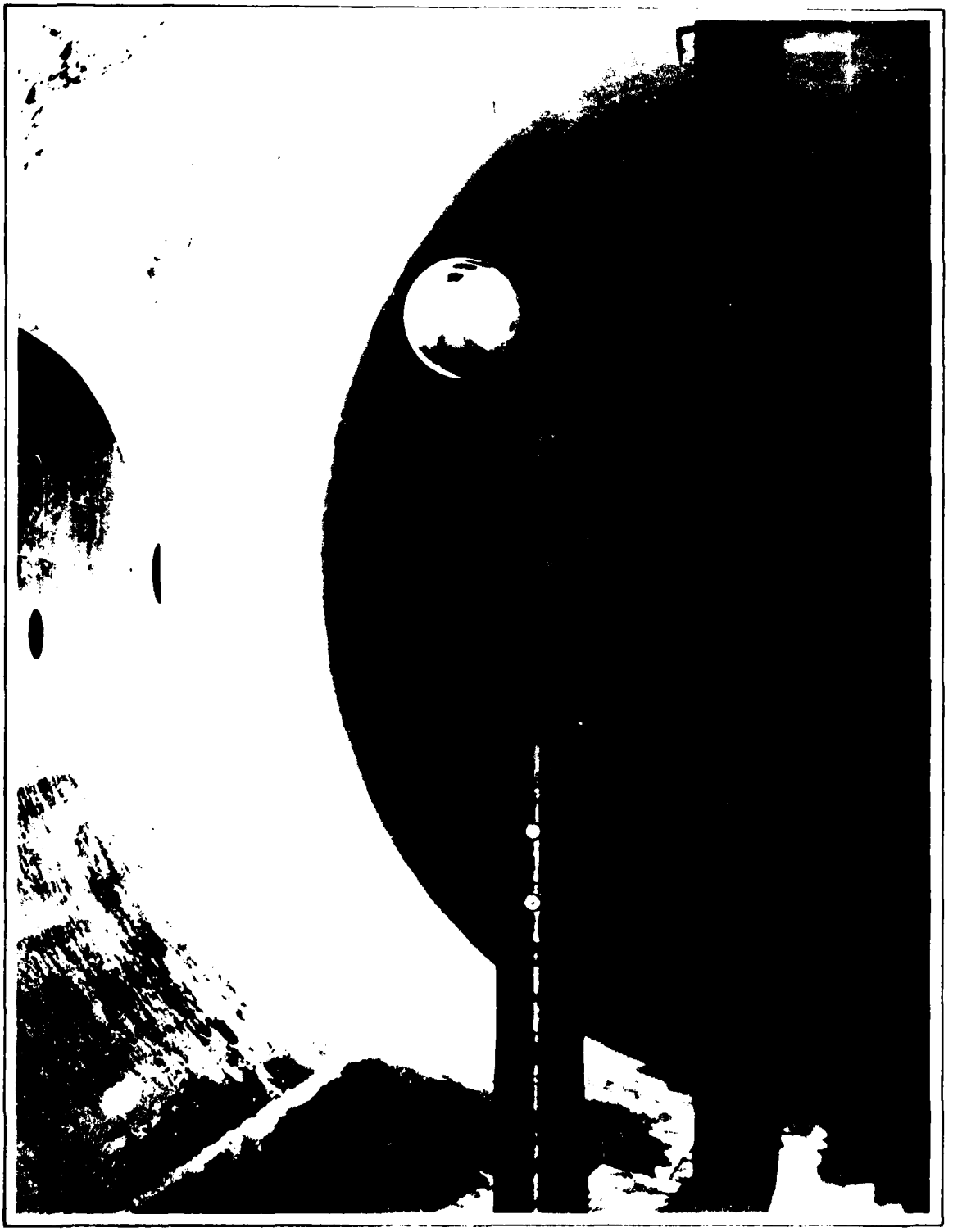

FIGURE 7. TYPICAL MODEL INSTALLATION IN THE 12-FOOT PRESSURE WIND TUNNEL

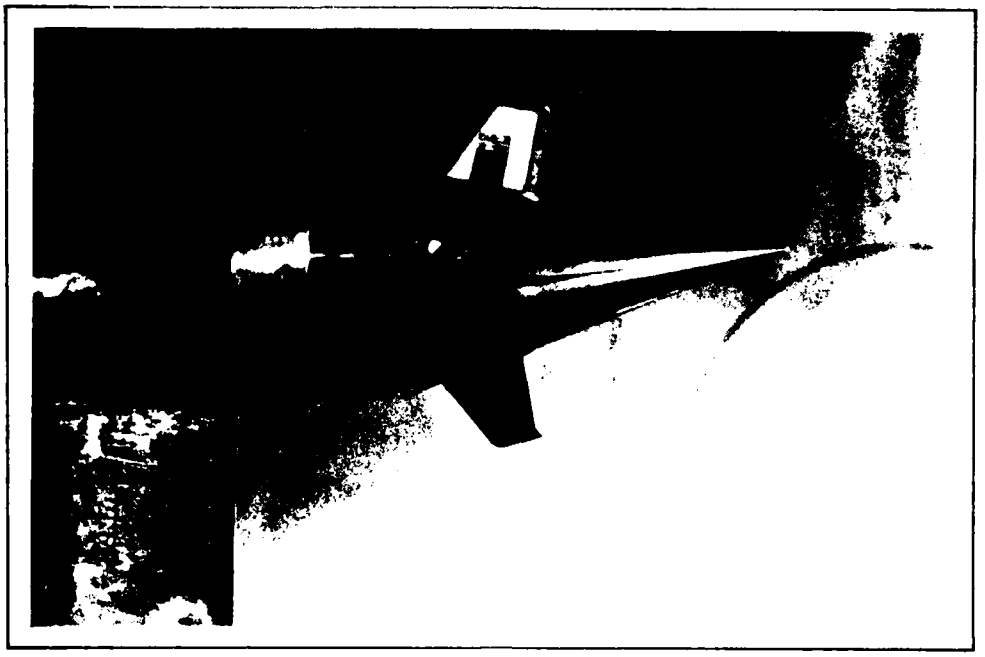

(a) Configuration N2C4B2T12

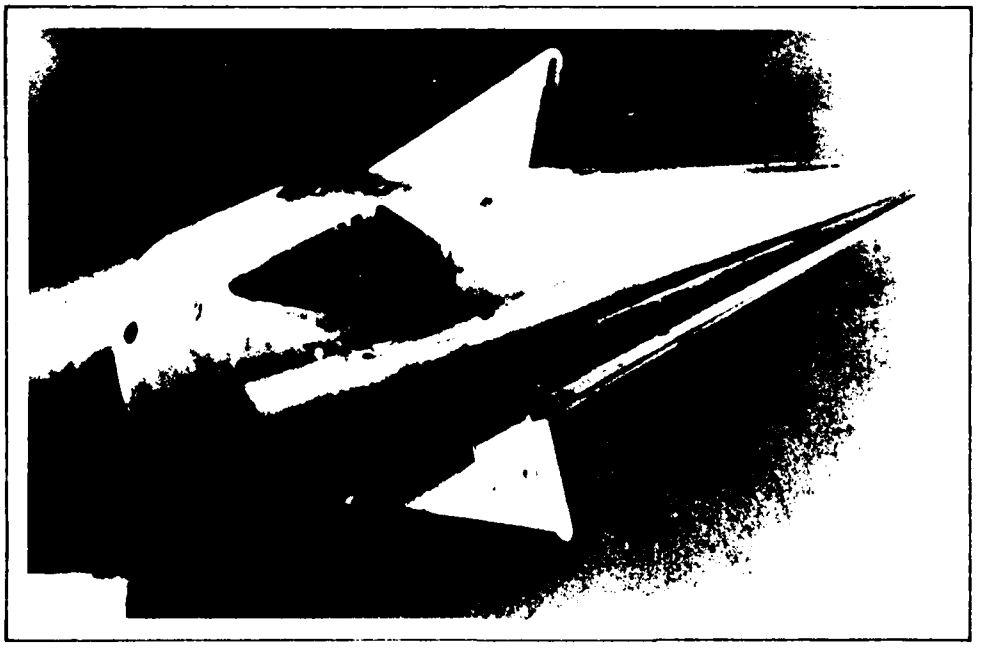

(b) Configuration N2C4B2T9

FIGURE 8. CLOSE UP OF FINS MOUNTED ON THE CONICAL AFTERBODY

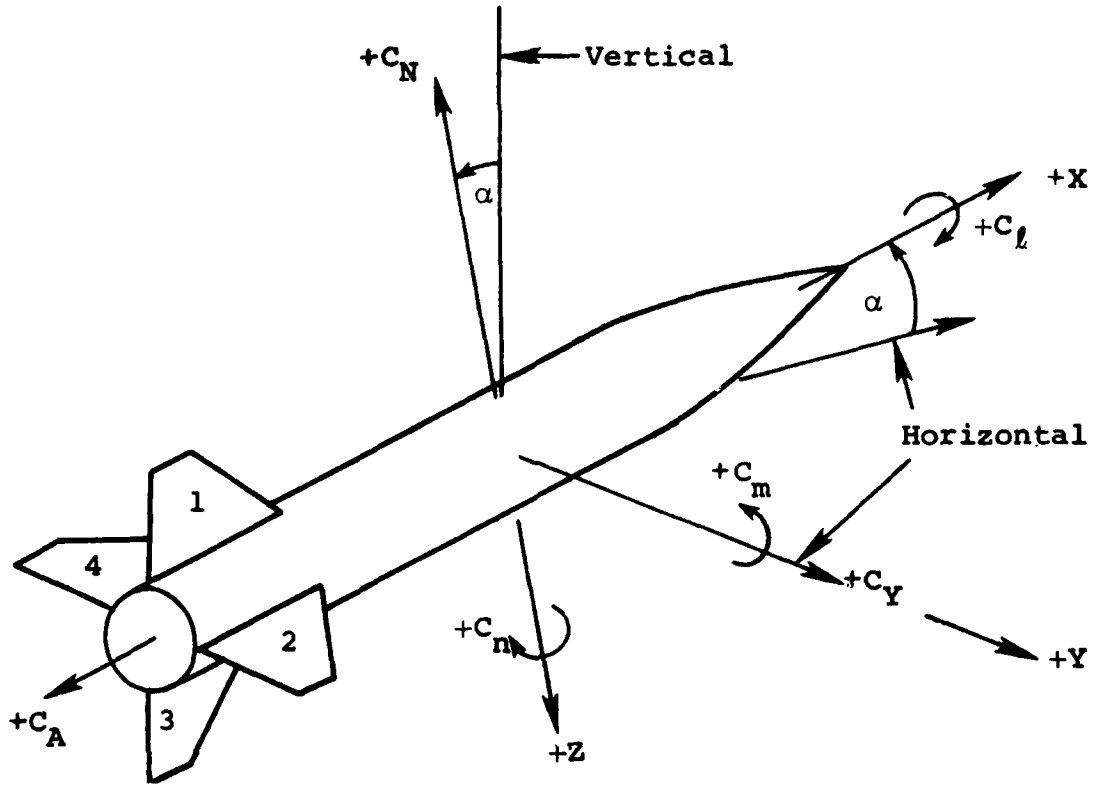

Fin	+δ at φ = 0°
1	Trailing edge left
2	" " down
3	" " left
4	" " down
$+M_{H_{1\&3}}$	Trailing edge left
$+M_{H_{2\&4}}$	Trailing edge down

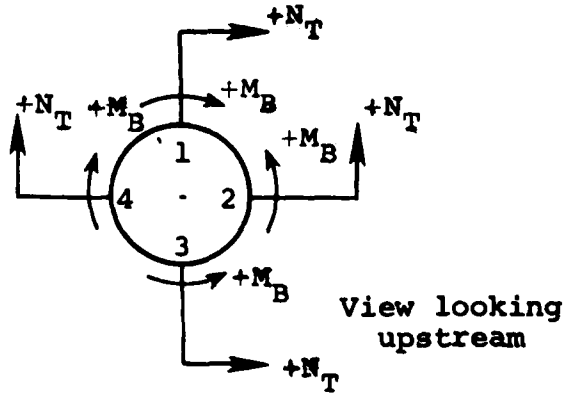

FIGURE 9. COEFFICIENT DEFINITIONS AND SIGN CONVENTION

TABLE 1

CONFIGURATIONS TESTED

1. Body-Tail Series

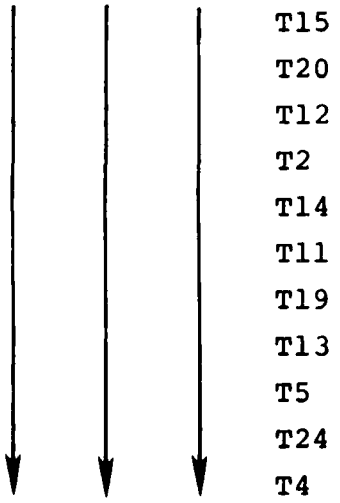

2. Body-Alone Series

N2 C4 B2

N2 C4 B4

3. Body-Sail Series

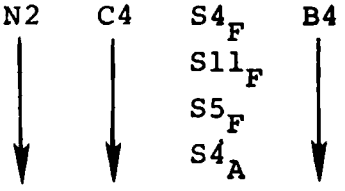

4. Flow-Visualization Series

N2 C4 B4

4.0 DATA REDUCTION AND ACCURACY

The wind-tunnel test data reduction program provided the following force and moment coefficients for the body-tail combination:

$(C_A)_{BT}$ body-tail axial force/$q_\infty S_R$

$(C_N)_{BT}$ body-tail normal force/$q_\infty S_R$

$(C_Y)_{BT}$ body-tail side force/$q_\infty S_R$

$(C_\ell)_{BT}$ body-tail rolling moment/$q_\infty S_R D$

$(C_m)_{BT}$ body-tail pitching moment/$q_\infty S_R D$

$(C_n)_{BT}$ body-tail yawing moment/$q_\infty S_R D$

where q_∞ is the tunnel free-stream dynamic pressure; S_R is the body frontal area, 38.485 in.^{2} (248.29 cm^2); and D is the body maximum diameter, 7.0 in. (17.78 cm).

In the prediction methods, developed in the following sections of this report, only the normal-force and pitching-moment coefficients will be used since the methods are for zero degrees angle-of-attack, α = 0 degrees, and zero degrees roll

angle, ϕ = 0 degrees. The values of these coefficients are influenced by the interference of the strut supporting the model, see Figure 7, on the model. Strut interference causes nonzero values of the body alone normal-force and pitching-moment coefficients at $\alpha = \phi = 0$ degrees. Average values of these coefficients obtained during the test program were:

$$(C_N)_B = 0.0771$$

$$(C_m)_B = -0.2447$$

The wind-tunnel test data reduction program also provided the following force and moment coefficients for each of the fins:

$(C_N)_{T(B)}$ fin normal force/$q_\infty S_T$

$(C_H)_{T(B)}$ fin hinge moment/$q_\infty S_T c_r$

$(C_B)_{T(B)}$ fin root-bending moment/$q_\infty S_T s$

where q_∞ is the tunnel free-stream dynamic pressure, S_T is the fin area, c_r is the fin root-chord length, and s is the fin semispan, the distance from the root chord to the tip chord measured normal to the root chord. The values of S_T, c_r, and s for each of the fins tested are listed in Figure 2.

During the test program, the deflection angles of the fins could not be set precisely. Thus, uncertainties in the angles are present in the data. Before using the fin data in the prediction methods, the three coefficients were fit by least squares using a polynomial of the following form

$$C = b_0 + b_1\delta + b_2|\delta|\delta \quad . \qquad (1)$$

After fitting the data, the b_0 coefficients were set to zero to cause the force and moment coefficients to be zero when the deflection angle, δ, is zero.

Figure 10 shows the normal-force curve slopes for the two horizontal fins due to fin deflection. These fins are fins 2 and 4 shown in Figure 9. Data for each of the fins were least squares fitted using Equation (1). Of the seven fins, all but T12 and T19 exhibit nearly the same slope for fins 2 and 4. The reason for the disagreement shown for T12 and T19 can be seen by examining Figure 11. This shows the experimental normal force variation with δ for fin T12. Data for the right and left horizontal fins (2 and 4) are shown. As can be seen, the data for

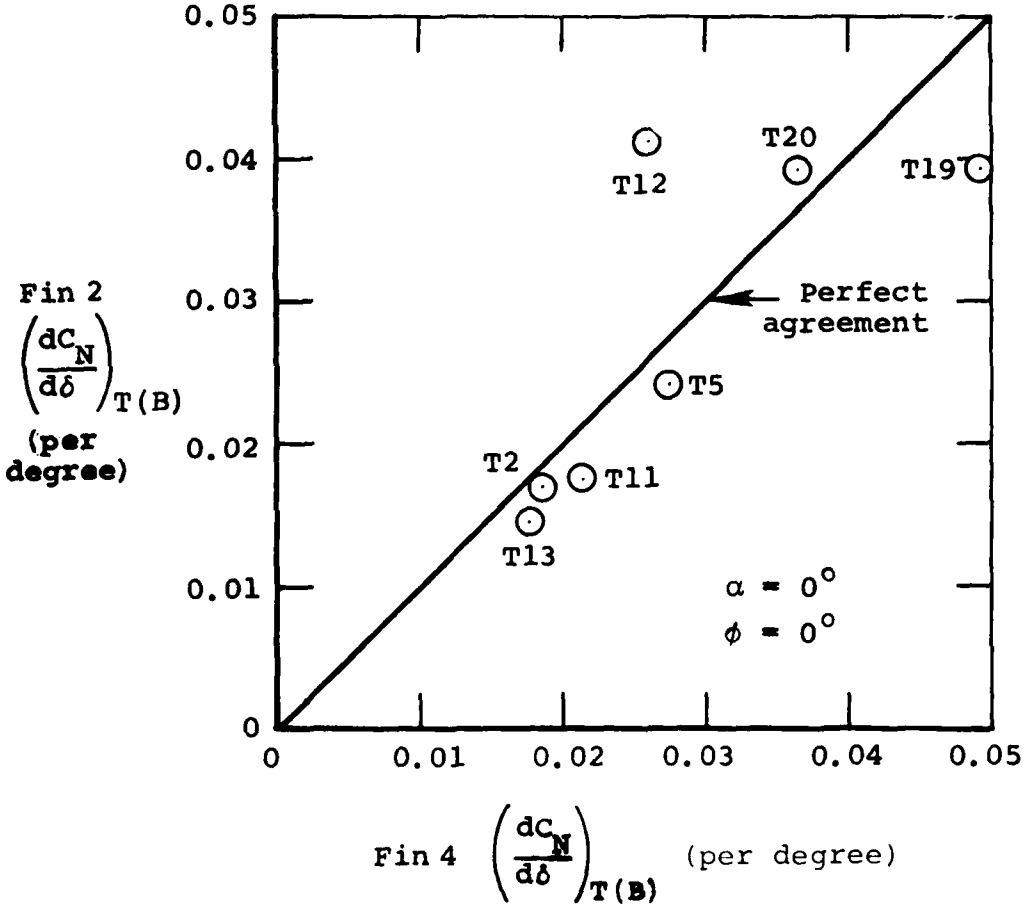

FIGURE 10. NORMAL-FORCE CURVE SLOPE DUE TO FIN DEFLECTION FOR THE TWO HORIZONTAL FINS IN THE PRESENCE OF THE BODY AT $\delta = 0^{\circ}$

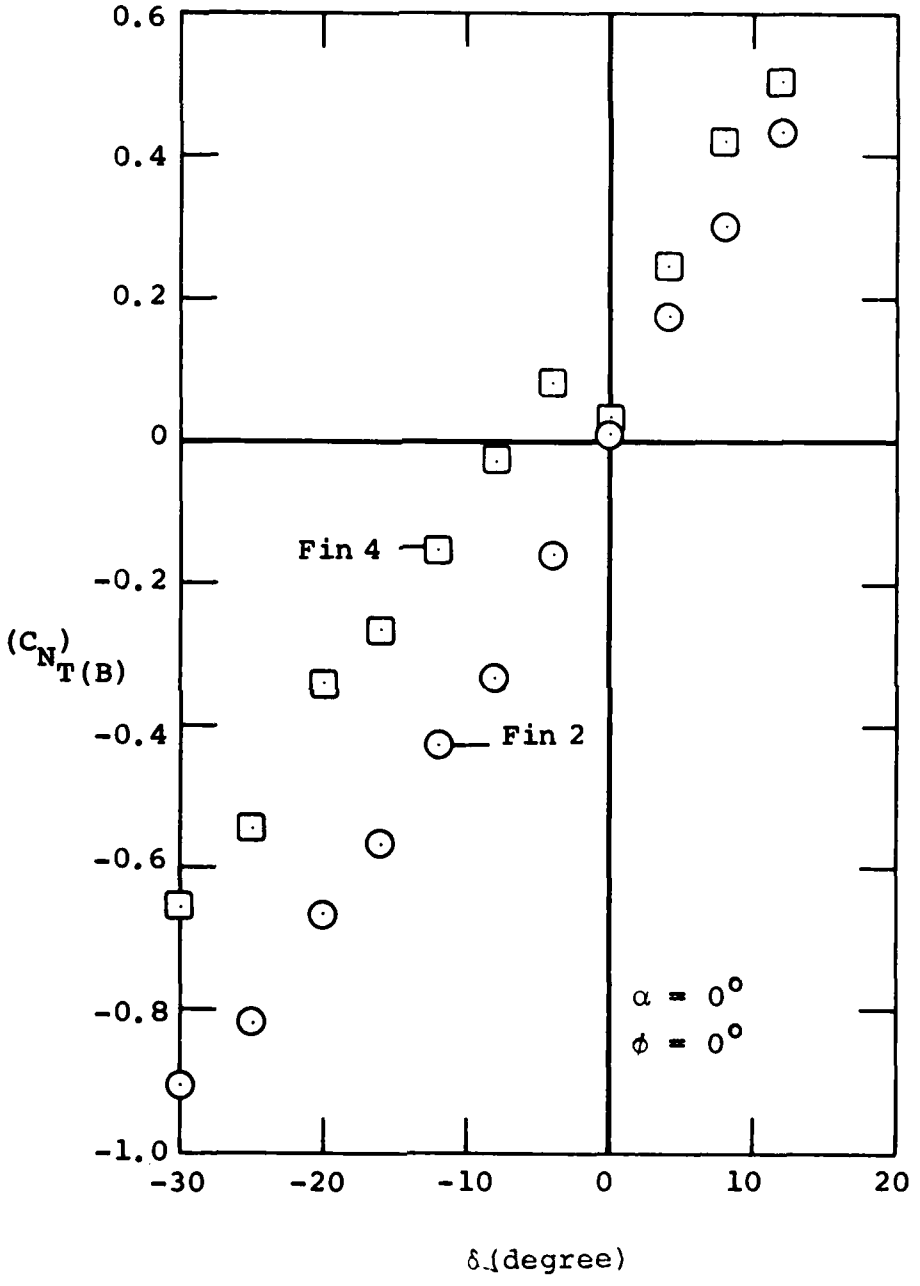

FIGURE 11. EXPERIMENTAL NORMAL-FORCE COEFFICIENT VARIATION WITH δ FOR FIN T12

the two fins do not agree and, furthermore, the slopes of the two variations with δ are different. It is not known which is correct. In performing the least square fits to provide the data to be used in developing the prediction methods, the average of the data for the two fins was used. This uas done for all of the fins listed in Figure 2 except where the left or right fin data were obviously bad, then only the good data were used.

After least squares fitting the $(C_N)_{T(B)}$, $(C_H)_{T(B)}$, and $(C_B)_{T(B)}$ data, the longitudinal center of pressure, x_{cp}/c_r, and lateral center of pressure, y_{cp}/s, were calculated as a function of δ.

$$\left(\frac{x_{cp}}{c_r}\right)_{T(B)} = \frac{x_H}{c_r} - \left(\frac{C_H}{C_N}\right)_{T(B)}$$
$$\left(\frac{y_{cp}}{s}\right)_{T(B)} = \left(\frac{C_B}{C_N}\right)_{T(B)} \qquad (2)$$

At δ = 0 degrees they are given by

$$\left(\frac{x_{cp}}{c_r}\right)_{T(B)} = \frac{x_H}{c_r} - \left(\frac{dC_H/d\delta}{dC_N/d\delta}\right)_{T(B),\delta=0}$$
$$\left(\frac{y_{cp}}{s}\right)_{T(B)} = \left(\frac{dC_B/d\delta}{dC_N/d\delta}\right)_{T(B),\delta=0} . \qquad (3)$$

A comparison similar to that presented in Figure 10 for $(dC_N/d\delta)_{T(B)}$ is shown in Figure 12 for the two center-of-pressure locations. The agreement between right and left fin data (2 and 4) is good.

Seven of the fins listed in Figure 2 had been tested in the earlier test program[1], however not on the same body. The body used in that program had the same nose and tail cone as shown in Figure 1 but the cylindrical center section was three diameters shorter making the fineness ratio 7 rather than 10. This should not have a large effect on the fin characteristics so it is of interest to compare data from the two programs to examine repeatability.

---

[1] ibid.

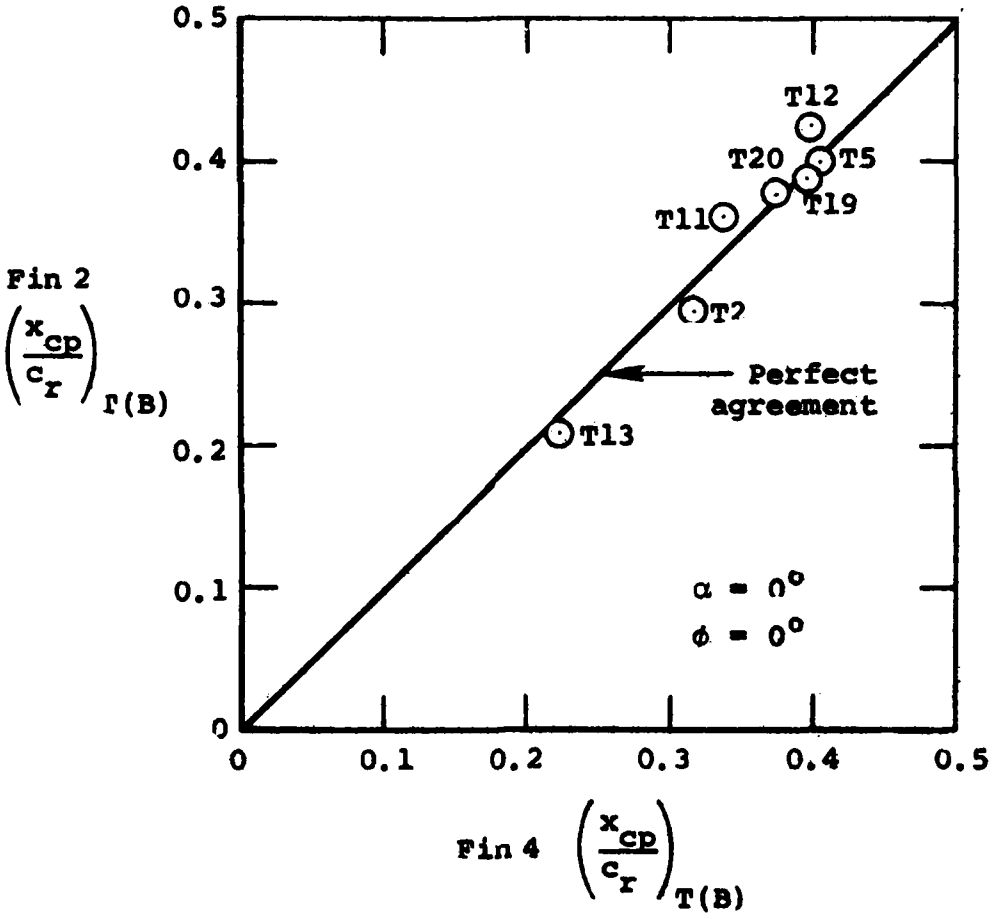

(a) Longitudinal Center of Pressure

FIGURE 12. CENTER-OF-PRESSURE LOCATION OF THE FINS IN THE PRESENCE OF THE BODY, $\delta = 0^{\circ}$

(Sheet 1 of 2)

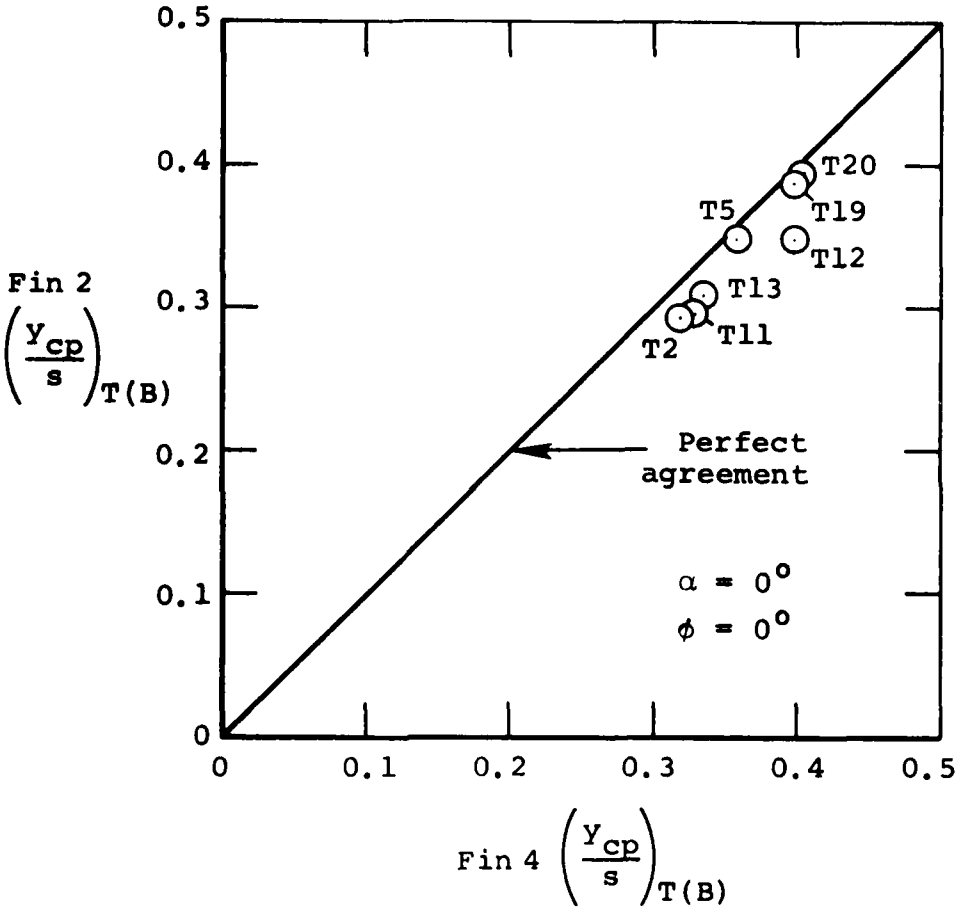

(b) Lateral Center of Pressure

FIGURE 12. (Sheet 2 of 2)

In the earlier test program, the tail fins could not be deflected so that the comparisons will be made for angle-of-attack effects with $\delta = \phi = 0$ degrees. The comparisons are shown in Figure 13. Good agreement is shown for the normal-force curve slope and both center-of-pressure locations.

5. PREDICTION METHODS

5.1 NORMAL FORCE ON A DEFLECTED TAIL FIN ON CONICAL BOATTAIL

5.1.1 Preliminary Remarks

The amount of normal force developed by the deflected tail fin in the presence of the body will depend on a number of geometric factors in addition to the deflection angle δ. The first two geometric factors are those defining the shape of the fin planform, AR and λ, for the fins which have unswept trailing edges. The relationship of the size of the fin to the body is characterized by the third geometric parameter, s/R. A fourth parameter is needed to fix the planform geometry completely; this one locates the position of the fin axially on the conical boattail. It will turn out that the method will not use this parameter. It will apply only to fins located well forward on the boattail with the leading edges of the fins not projecting in front of the boattail. A fifth parameter, the hinge-line location, must be known to specify the fin geometry in the deflected condition.

The present report developes prediction methods for δ effects at $\alpha = 0$ degrees. The previous work[1] predicted α effects at $\delta = 0$ degrees. Combined effects of α and δ can thus be predicted by linear superposition until more precise methods are developed.

Knowledge of the nature of the interference between fin and body in the present case for $\alpha = 0$ degrees and $\delta \neq 0$ degrees should be of value in interpreting the data and constructing the prediction methods. The flow field of the body alone at $\alpha = 0$ degrees is due to displacement effects of the body, and an axisymmetric flow field is generated. It will generally vary in dynamic pressure in the region to be occupied by the fin. The fin can therefore generate more or less normal force depending on the level of dynamic pressure at its particular location.

Another factor which affects the mutual interference is the kind of reflection plane the body presents to the fin. For a

[1] ibid.

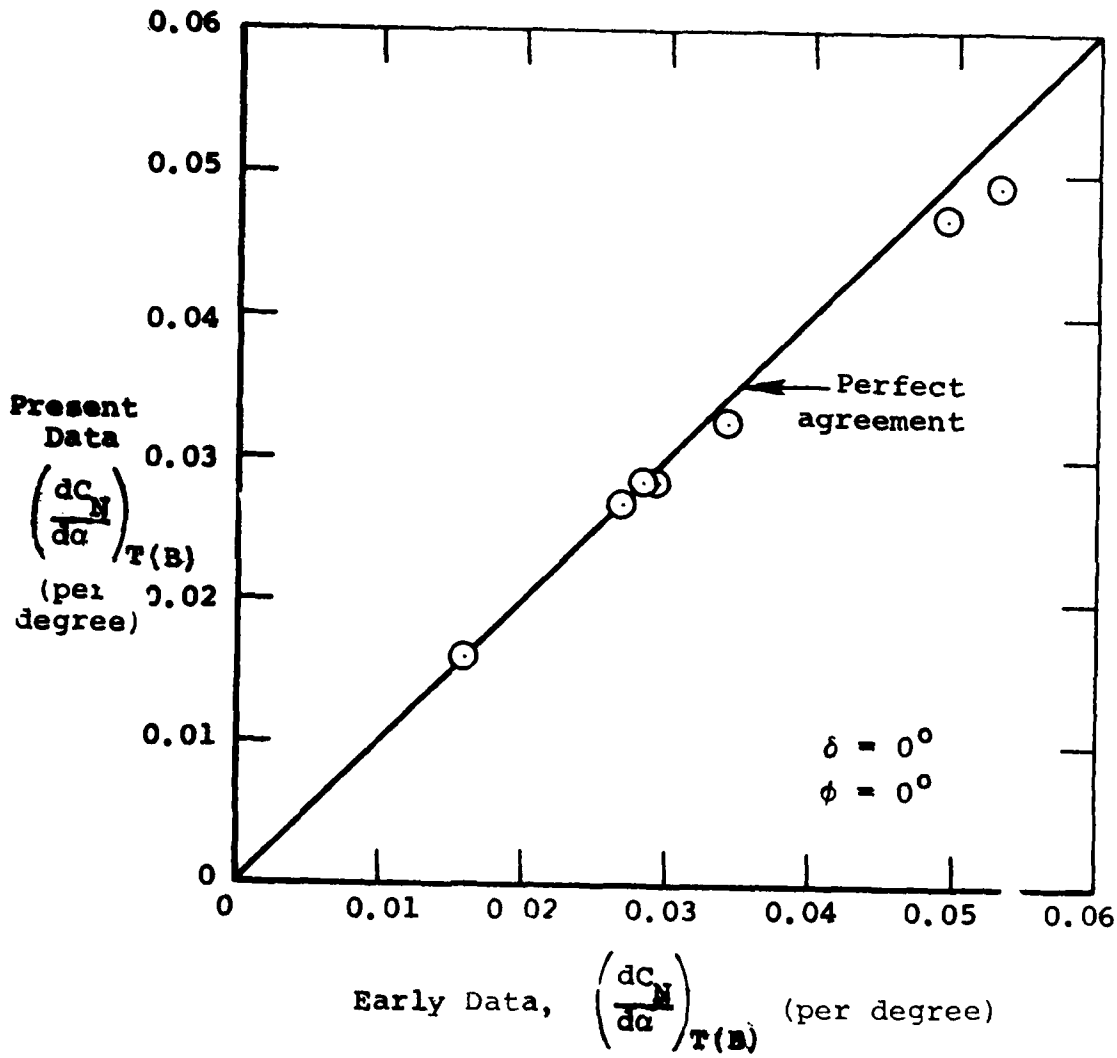

(a) Normal-Force Curve Slope at $\alpha = 0^\circ$

FIGURE 13. COMPARISON OF FIN CHARACTERISTICS DUE TO α VARIATION

(Sheet 1 of 3)

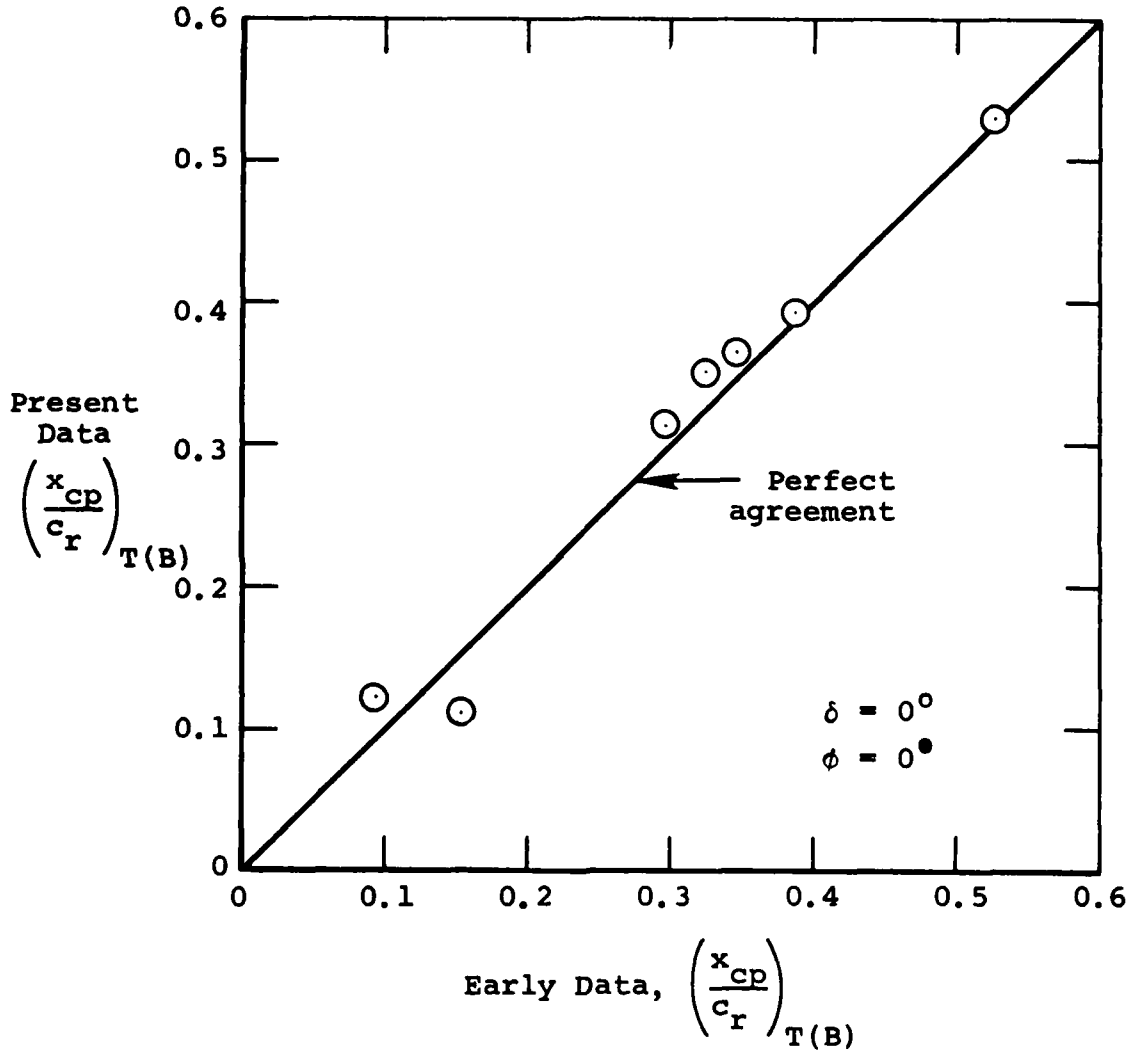

(b) Longitudinal Center of Pressure

FIGURE 13. (Sheet 2 of 3)

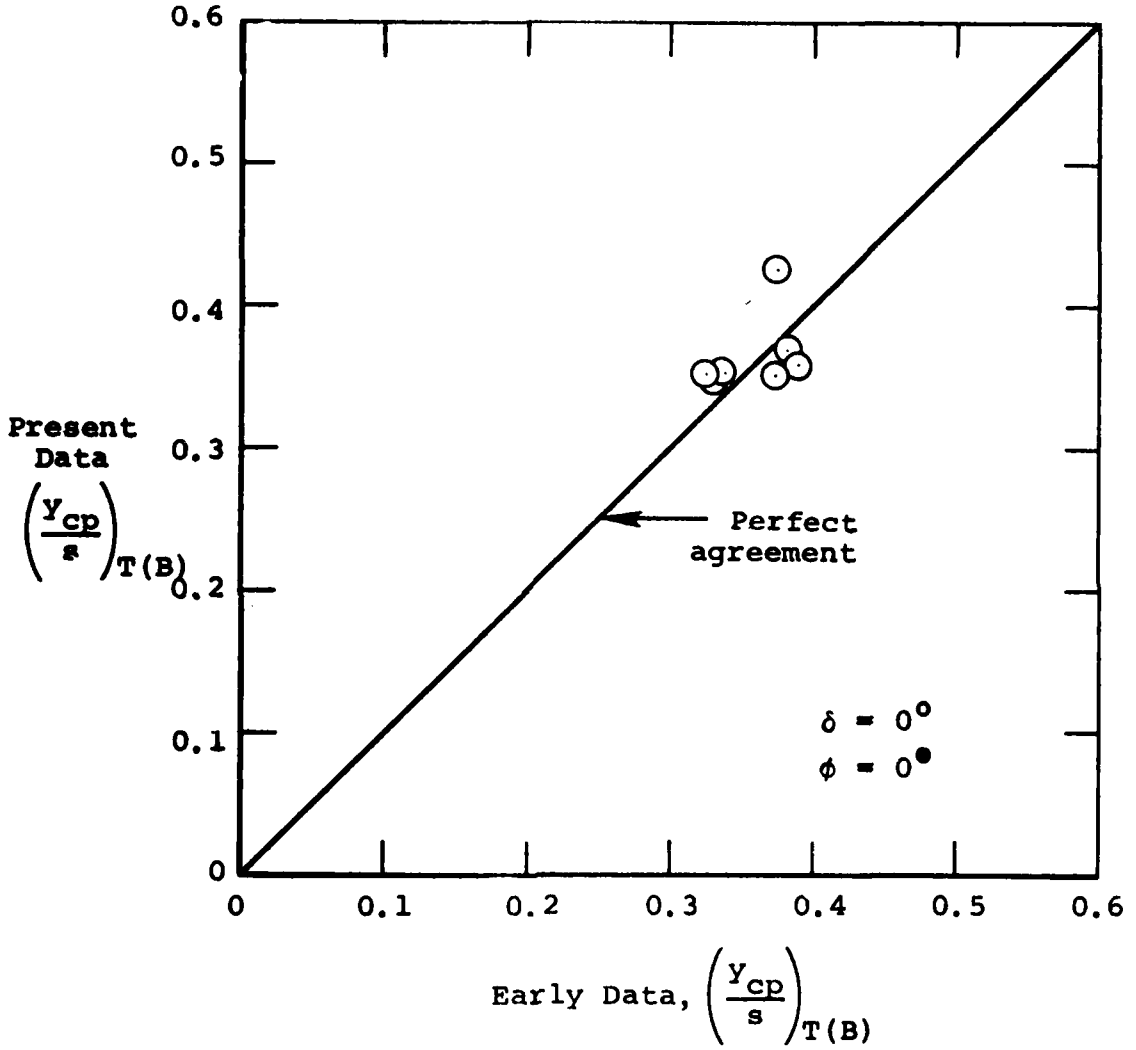

(c) Lateral Center of Pressure

FIGURE 13. (Sheet 3 of 3)

very small fin the body looks like a large normal reflection plane but for a large fin, it does not. For a large normal reflection plane, it would be expected that the fin would act as if it were half of the fin alone at the same angle-of-attack, where the fin alone is defined to be two fins joined together.

A third factor influencing the mutual interference between fin and body is the gap geometry which changes with δ. The effect of this parameter is complicated from the geometric point of view. Its aerodynamic effects appear less complicated. A flow characteristic which could greatly affect the fin-body interference is flow separation over the boattail.

A parameter which has been used to specify the interference of the body on the fin for $\alpha = 0$ degrees and $\delta \neq 0$ degrees is the interference factor, k_T, defined as follows[2]:

$$k_T = \frac{\text{normal force on fin at } \delta}{(1/2)\ \text{normal force on fin alone at } \alpha = \delta} = \frac{N_{T(B)}}{N_T} \quad . \quad (4)$$

The fin alone is two fins which are mirror images joined together at their root chords. Values for k_T vary between about 0.93 and 1.0 for a slender fin mounted on a circular cylinder (Reference 2, p. 218). The ratio k_T is used in the present method.

Nonlinearities occur in the force and moment data which have been determined by the least-squares fit to the data. The prediction method handles the nonlinear effects for the fin normal force, and normalizes other forces and moments by the fin normal force.

5.1.2 Comparison Between Prediction and Data

In predicting the fin normal force in the presence of the body, we usually base the calculation on the normal force of the fin alone. One source of normal-force curve slope for a fin alone is experiment and another is DATCOM[3]. However, we frequently do not have fin-alone data, so that DATCOM is used as a convenient reference. It is thus relevant to inquire about the accuracy of the DATCOM prediction method. At $M_\infty = 0$, DATCOM gives for lift-curve slope per radian

---

[2] Nielsen, Jack N: Missile Aerodynamics. McGraw Hill Book Company, Inc., 1960.

[3] McDonnell-Douglas Aircraft Co.: USAF Stability and Control DATCOM. Revised April 1978.

$$\left(\frac{dC_L}{d\alpha}\right)_{DAT} = \frac{2\pi AR}{2 + \sqrt{AR^2(1 + \tan^2\Lambda_{c/2}) + 4}} \quad . \qquad (5)$$

Table 2 shows the comparisons in $(dC_L/d\alpha)$ from Equation (5) with measured values of $(dC_N/d\alpha)$ for five of the present fins as given in Reference 1.

TABLE 2

COMPARISON BETWEEN EXPERIMENT AND THEORY FOR TAIL ALONE LIFT-CIRVE SCOPE

Fin	AR	λ	$\left(\frac{dC_N}{d\alpha}\right)_{exp}$	$\left(\frac{dC_L}{d\alpha}\right)_{DAT}$
T9	2	0	0.0425	0.0401
T12	2	1/2	0.0467	0.0447
T14	1	1	0.0275	0.0259
T11	1	1/2	0.0272	0.0253
T13	1/2	1	0.0152	0.0135

The theory and experiment are plotted versus each other in Figure 14. The experimental values are about 5 percent greater than the predicted values. This result shows that the fins are acting like aerodynamic lifting surfaces. We will use the DATCOM method in our correlation methods, and the 5 percent error will be absorbed in the correlation. We also ignore the difference between the normal-force curve slope and the lift-curve slope in the DATCOM prediction.

The normal-force correlation method is based on determining k_T for each of the fins, and then finding a correlation for k_T. Table 3 gives the values of k_T as determined using DATCOM and the data. The two correlating parameters for k_T are AR and s/R as shown in Figure 15. The data for s/R = 0.714 correlate well independent of λ. The three points for λ = 0.5 and s/R = 1.00 also correlate well, and fit in with the s/R = 0.714 data. The three points for λ = 0.5, AR = 1 with variable s/R show a systematic increase in k_T as s/R increases. Surprisingly, the AR = 0.5 wing shows a value of k_T greater than unity.

(1) ibid.

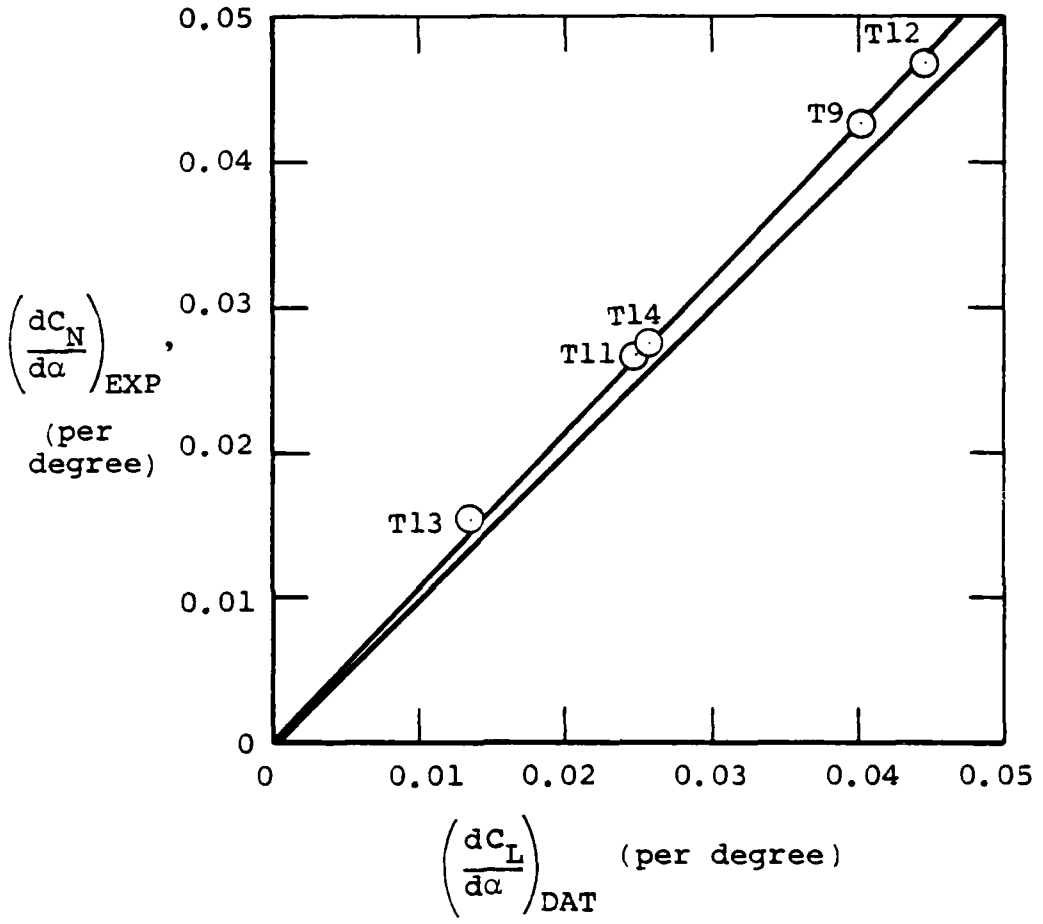

FIGURE 14. COMPARISON OF EXPERIMENTAL FIN-ALONE NORMAL-FORCE-CURVE SLOPES WITH VALUES PREDICTED FROM DATCOM

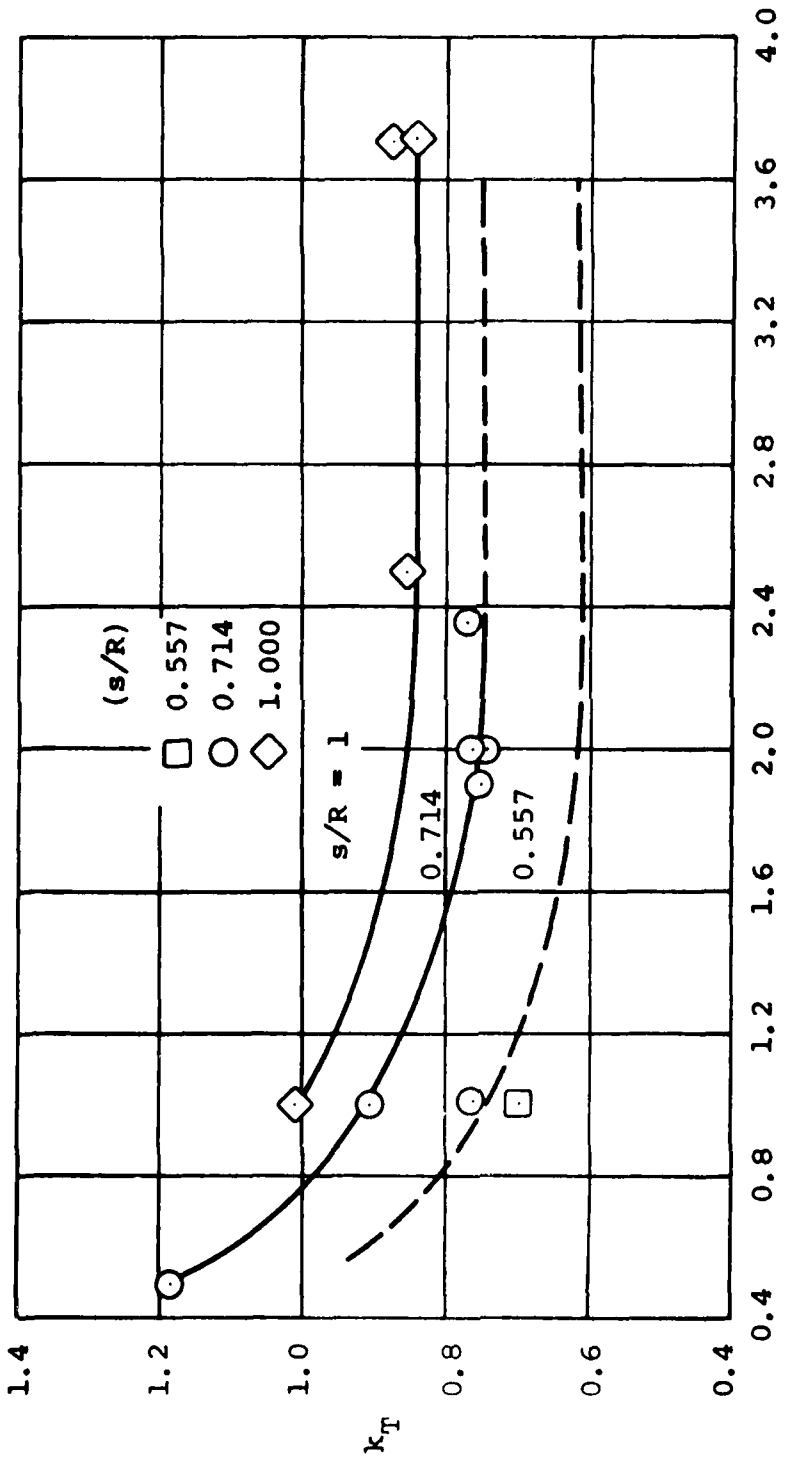

FIGURE 15. CORRELATION OF WING-BODY INTERFERENCE FACTOR k_T FOR VARIOUS FINS MOUNTED ON CONICAL BOATTAIL

TABLE 3

EXPERIMENTAL VALUES OF k_T

Fin	$\left(\frac{dC_N}{d\delta}\right)_{T(B)}$	$\left(\frac{dC_L}{d\alpha}\right)_{DAT}$	k_T
T9	0.0309	0.0401	0.771
T12	0.0335	0.0447	0.749
T2	0.0177	0.0253	0.700
T14	0.0234	0.0259	0.903
T11	0.0194	0.0253	0.767
T13	0.0160	0.0137	1.168
T5	0.0257	0.0253	1.016
T15	0.0331	0.0439	0.754
T20	0.0387	0.0501	0.772
T19	0.0446	0.0520	0.858
T24	0.0567	0.0652	0.870

This result is possible because of increased dynamic pressure. For high aspect ratios, losses of fin normal force up to 25 percent are due to fin-body interference.

It would be of interest to have data on the effect of s/R at $\mathcal{R}$ = 0.5 and $\mathcal{R}$ = 3-4, but in lieu thereof we must extrapolate with extreme caution.

5.1.3 Prediction Method

1. The first step in the prediction method is to determine the fin alone lift-curve slope by the DATCOM method using Equation (5). For this purpose the fin alone values of $\mathcal{R}$ and tan $\Lambda_{c/2}$ are required. In this calculation the fin alone planform area is the reference area. The fin in the presence of the body has the same lift-curve slope based on its planform area.

2. The second step in the method is to determine k_T with the help of the following relationship

$$k_T = k_T^* F(s/R) \qquad (6)$$

Here k_T^* is the value of k_T from Figure 15 for s/R = 0.714 and F(s/R) is an empirical factor to account for changes in s/R.

Approximate values of F(s/R) are given in Figure 16 as deduced from the faired data of Figure 15. These values will be used for the aspect ratio range $1 \leq AR \leq 3.5$. For $AR \leq 1.0$, values of F(s/R) greater than unity are to be conservatively set equal to unity until more data are available to make extrapolation unnecessary.

3. The third step in the method is to obtain the fin normal force due to fin deflection by the following formula.

$$(C_N)_{T(B)} = \left(\frac{dC_L}{d\alpha}\right)_{DAT} \cdot k_T \cdot \delta \qquad (7)$$

5.1.4 Nonlinear Effects on Fin Normal Force

The curves of $(C_N)_{T(B)}$ versus δ exhibit nonlinearities which we have attempted to quantify. For each fin on the body, the data have been fitted to the following equation by the method of least squares.

$$(C_N)_{T(B)} = b_0 + b_1\delta + b_2\delta|\delta|; \quad \delta \text{ in degrees} \qquad (8)$$

The constant b_0 is a tare which is not used. The values of b_1 are the linear normal-force curve slopes which have been discussed previously. The values of b_2 are listed in Table 4.

TABLE 4

EXPERIMENTAL VALUES OF b_2

Fin	AR	λ	s	b_2		
				Fin 2	Fin 4	Ave.
9	2.000	0	2.50	-0.000027		
15	1.905	1.000	2.50	-0.000165		
20	2.352	0.523	2.50	-0.000223	-0.000149	-0.000231
12	2.000	0.500	2.50	-0.000359	0.000053	-0.000153
2	1.000	0.500	1.95	0.000237	0.000197	0.000217
14	1.000	1.000	2.50		-0.000034	
24	3.733	0.526	3.50		-0.000568	
11	1.000	0.500	2.50	0.000259	0.000222	0.000241
19	2.500	0.500	3.50	-0.000116	-0.000525	-0.000335
13	0.500	1.000	2.50	0.000275	0.000124	0.000199
5	1.000	0.500	3.50	-0.000015	-0.000146	-0.000080

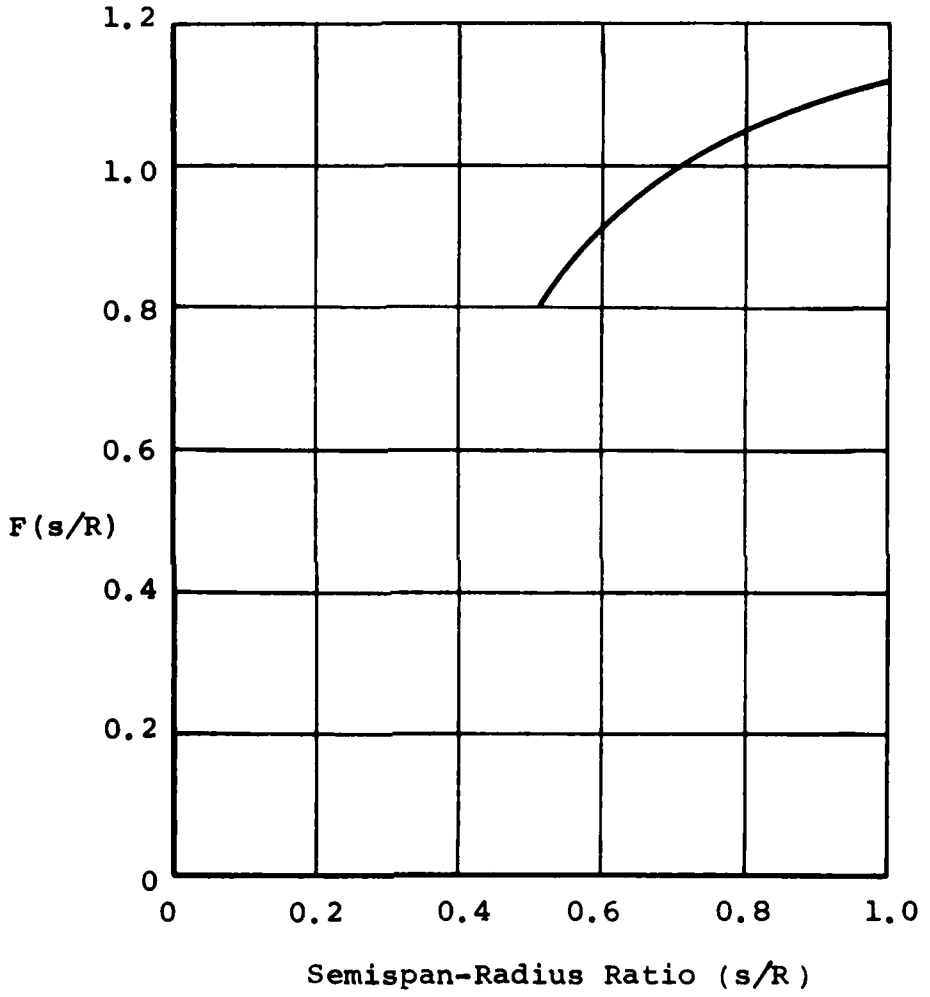

FIGURE 16. VARIATION OF F(s/R) WITH (s/R)

Fin 2 is the right fin and fin 4 the left fin as shown in Figure 9. The average column used the average of the fin 2 and fin 4 data in the least squares fit.

In the case of certain fins, it was not meaningful to fit the average data because of its scatter. In these instances b_2 is based on one fin. The repeatability of b_2 from the left to the right fin is not very good, and the average column is used in the correlation which follows.

In Figure 17 the value of b_2 is plotted versus fin aspect ratio for the 11 fins tested. For seven of these fins, the variation in b_2 from left to right is indicated by vertical lines. At $AR = 1$ three point with different values of s/R are shown which exhibit the effect of this parameter. Also a dashed line through the three triangular points compared with the faired curve exhibit the decreasing effect of s/R as AR increases. The three points in the range $1.9 \leq AR \leq 2.0$ exhibit the effect of taper ratio, but the uncertainty between left and right fins obscures the effect. For estimation purposes, we have faired a solid straight line through the data for s/R = 0.714. In addition two dashed lines are drawn to represent the approximate effects of s/R as estimated from the data.

It is of interest to see how important the nonlinear effect of δ is on $(C_N)_{T(B)}$. For this purpose we might form the ratio of the nonlinear term to the linear term at $\delta = 20$ degrees. The ratio of the nonlinear term to the linear term in Equation (8) is given by $\frac{b_2|\delta|}{b_1}$. Table 5 gives the ratio for the fins tested. It is clear that the nonlinear effect can be as much as 20 to 25 percent of the linear term in many cases. We will include the nonlinear effect in the prediction method by adding the $b_2\delta|\delta|$ term to Equation (7).

The problem of nonlinearities can also arise in prediction of the fin hinge moment and bending moment as well as the loading on the body due to fin deflection. It is possible to handle these nonlinearities in connection with the other quantities by using center-of-pressure locations and normal force ratios.

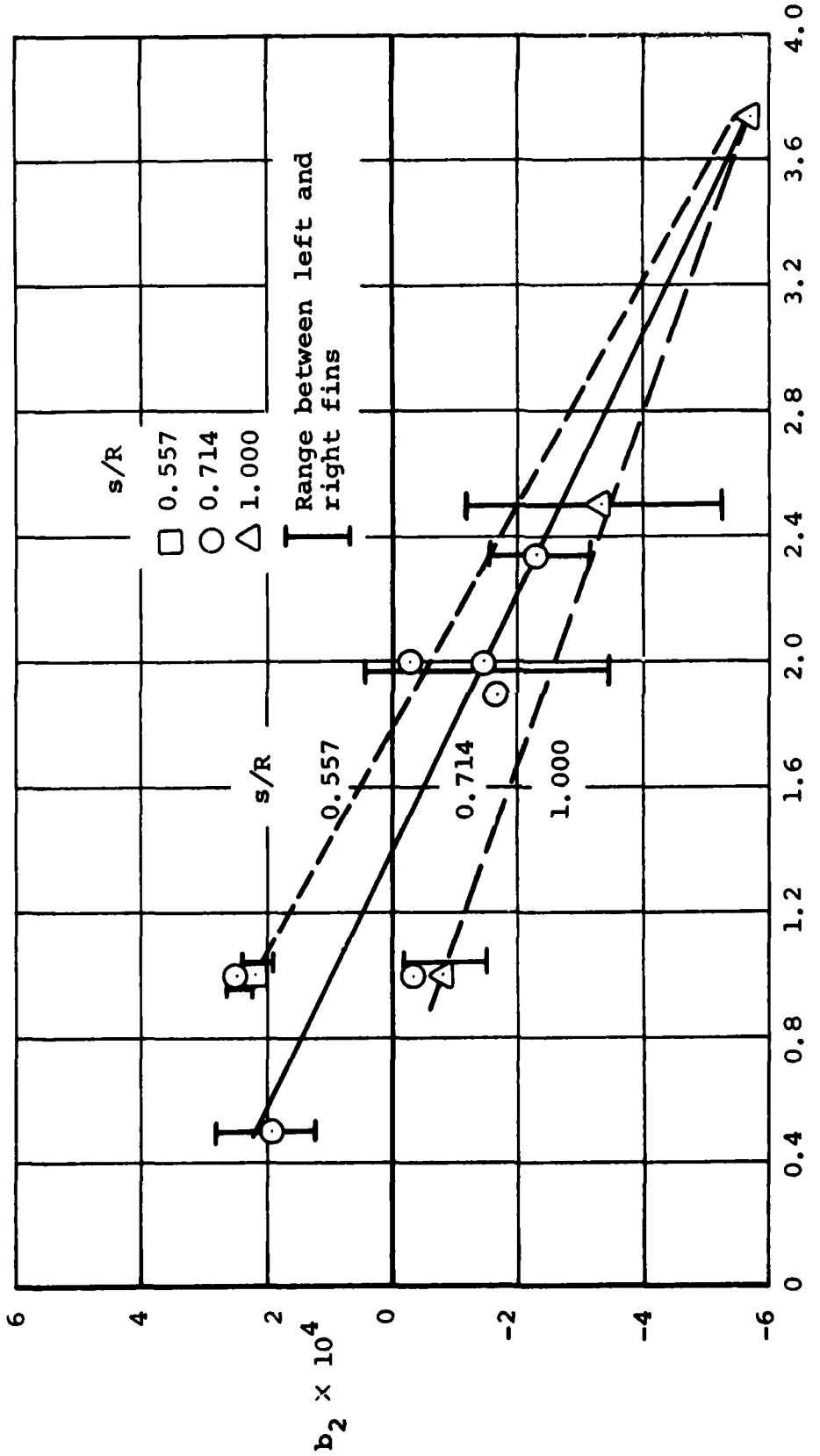

FIGURE 17. VALUE OF b_2 FOR OBTAINING NONLINEAR COMPONENT OF FIN NORMAL FORCE IN PRESENCE OF CONICAL BOATTAIL

TABLE 5

IMPORTANCE OF NONLINEAR EFFECTS ON NORMAL FORCE CURVE SLOPE AT $\delta=20°$

Fin	b_1	$b_2 \times 10^4$	$\frac{b_2\|\delta\|}{b_1}$
T9	0.0309	-0.27	-0.017
T15	0.0331	-1.65	-0.100
T20	0.0387	-2.31	-0.119
T12	0.0335	-1.53	-0.091
T2	0.0177	2.17	0.245
T14	0.0234	-0.34	0.029
T24	0.0567	-5.68	-0.200
T11	0.0194	2.41	0.248
T19	0.0446	-3.35	-0.150
T13	0.0160	1.99	0.249
T5	0.0257	-0.80	-0.062

5.2 CHORDWISE CENTER-OF-PRESSURE LOCATION ON DEFLECTED FIN ON CONICAL BOATTAIL (HINGE MOMENT)

5.2.1 Preliminary Remarks

The chordwise center of pressure position is given by the distance x_{cp} behind the leading edge of the root chord

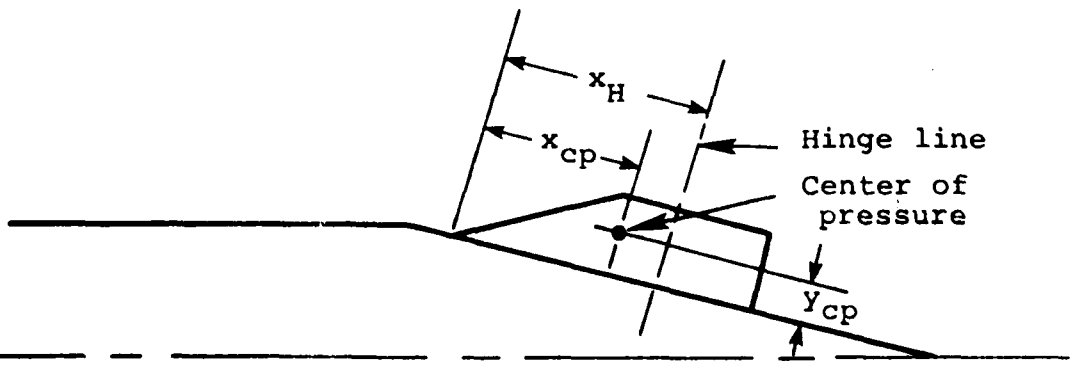

measured parallel to the root chord as shown in the sketch. The hinge-moment coefficient, C_H, is given by

$$C_H = (C_N)_{T(B)} \frac{(x_H - x_{cp})}{c_r} \qquad (9)$$

where c_r is the fin root chord and is the reference length for C_H, and C_H and C_N are based on the same reference area. From the values of C_N calculated as described in the previous section and the value of the center-of-pressure position as calculated as described in this section, the hinge-monent coefficient can be calculated for any hinge-line position.

It is of interest to know what fin-body interference does to the fin center-of-pressure position for a fin mounted on a circular cylindrical body. According to slender-body theory the change in position for the fin in the presence of the body relative to that for the fin alone depends on the ratio of body diameter to fin total span as mounted on the body. In terms of $(x_{cp}/c_r)_{T(B)}$ for a delta fin the maximum difference is 0.006 (Reference 2, p. 218). Accordingly, in much preliminary design work, the center-of-pressure of the fin due to deflection is taken equal to that for the fin alone. Fin taper ratio has a large effect on the center-of-pressure position of the fin alone in the form $(x_{cp}/c_r)_T$.

5.2.2 Comparison Between Prediction and Data

Since it is our intention to compare the theoretical fin alone center-of-pressure positions with the experimental ones for the fin due to deflection, let us first see how the theory and experiment compare for the fin alone. Figure 18 presents a comparison of fin-alone measurements reported in Reference 1 with theoretical predictions obtained from the charts of Reference 4. This comparison shows us two interesting things. First our wings, which have airfoil sections which are flat plates with rounded edges, give results in good agreement with linear lifting-line theory. Second, the predictions are within 3 to 4 percent of the root chord in the extreme cases.

---

(1)
(2) ibid.
(4) ibid.
Pitts, William C., Nielsen, Jack N., and Kaattari, George E.: Lift and Center of Pressure of Wing-Body-Tail Combinations at Subsonic, Transonic, and Supersonic Speeds. NACA TR 1307, 1957

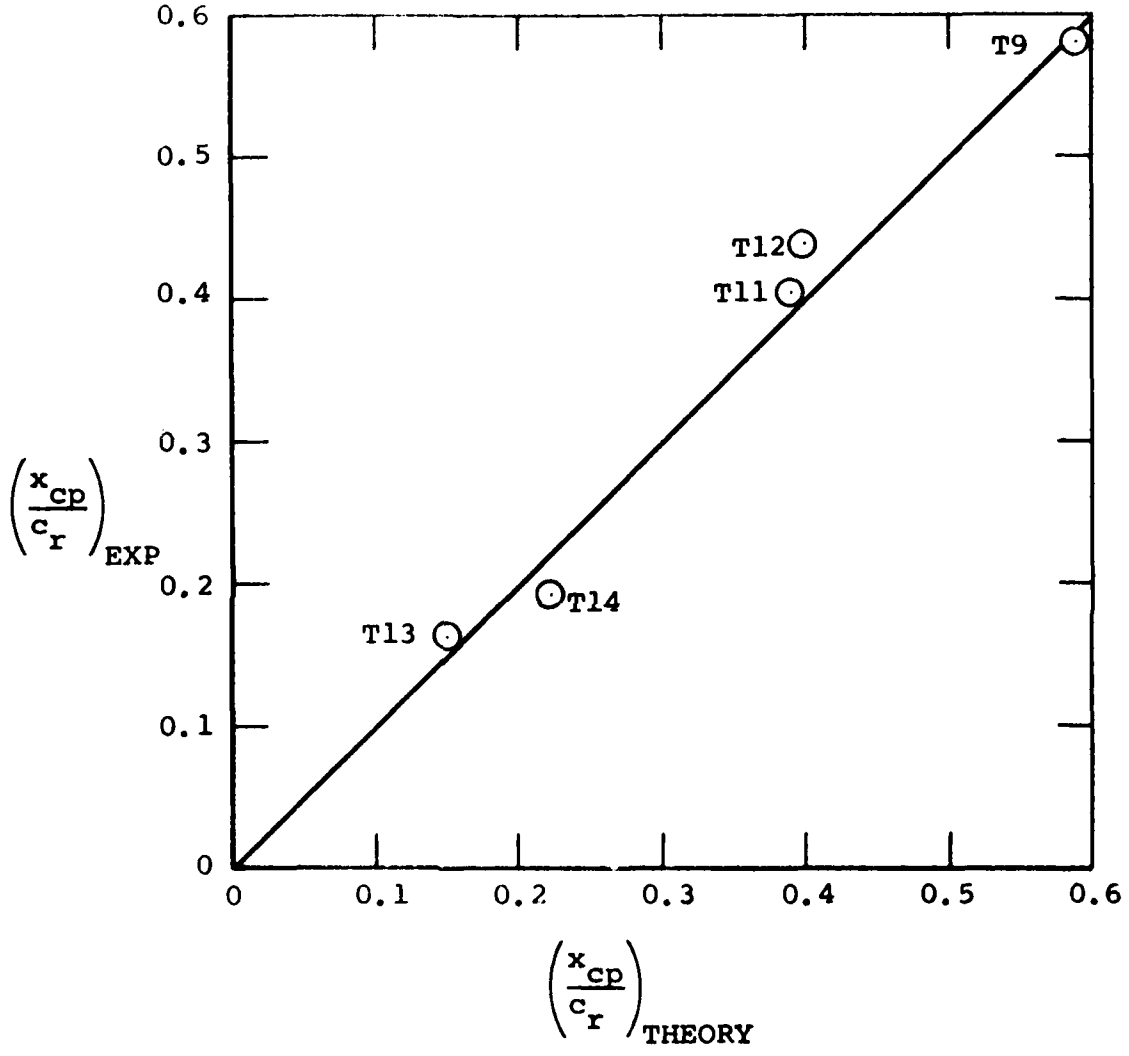

FIGURE 18. COMPARISON OF EXPERIMENTAL AND THEORETICAL CENTER-OF-PRESSURE POSITIONS FOR FINS ALONE

It is natural to try to correlate the data using the existing rule of thumb that the center-of-pressure location due to control deflection, $(x_{cp}/c_r)_{T(B)}$, is equal to that for the fin alone, $(x_{cp}/c_r)_T$. Plots of $(C_H)_{T(B)}$ versus $(C_N)_{T(B)}$ are essentially linear between δ = -12 degrees and δ = 20 degrees and up to δ = 30 degrees in some cases for both left and right fins. The average slope of these curves for the two fins is $(X_{cp}/c_r)_{T(B)}$ This quantity does not differ more than 0.02 between the left and right fins except in one case. Table 6 gives the values of these quantities for the fins tested.

TABLE 6

EXPERIMENTAL VALUES OF $(x_{cp}/c_r)_{T(B)}$

Fin	$(x_{cp}/c_r)_{T(B)}$ (data)	$(x_{cp}/c_r)_T$ (theory)	λ	AR
T2	0.384	0.39	0.500	1.000
T5	0.430	0.39	0.500	1.000
T9	0.550	0.56	0.000	2.000
T11	0.413	0.39	0.500	1.000
T12	0.419	0.41	0.500	2.000
T13	0.293	0.15	1.000	0.500
T14	0.224	0.22	1.000	1.000
T15	0.210	0.25	1.000	1.905
T19	0.419	0.41	0.500	2.500
T20	0.397	0.41	0.523	2.352
T24	0.420	0.41	0.526	3.733

These values have been plotted in Figure 19, and the 45 degree line correlates all the data except for the AR = 0.5 fin very well. The AR = 0.5 fin gave a very large value of k_T as well as a very rearward $(x_{cp}/c_r)_{T(B)}$. This behavior suggested that some special aerodynamic phenomenon may be occurring for this fin. Since we have only one AR = 0.5 fin in the data base, it is thus not appropriate to try to generalize the prediction method for aspect ratios less than unity until data for other λ and s/R are available in the low aspect ratio range.

The effect of s/R as shown by the different symbols is systematic but small for fins T2, T4, and T11. It is not

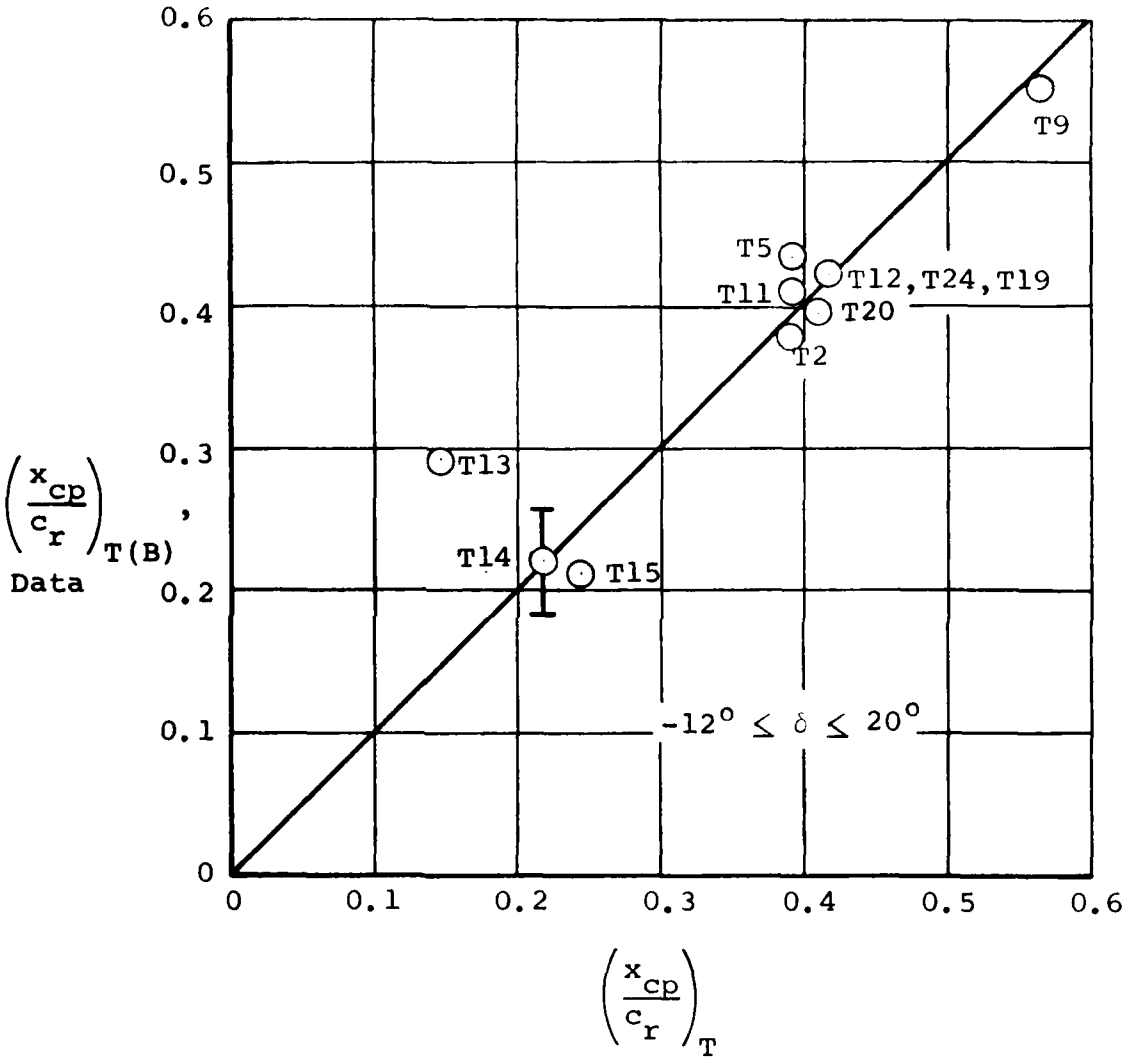

FIGURE 19. CENTER-OF-PRESSURE POSITION OF FIN ON BOAT-TAIL BASE CORRELATED AS FUNCTION OF FIN ALONE POSITIONS

systematic for the other fins. Accordingly no account of s/R on $(x_{cp}/c_r)_{T(B)}$ is considered as it was for k_T.

5.2.3 Prediction Method

The objective of the prediction method is the determination of the fin hinge-moment coefficient when mounted on a conical boattail of 14 degrees half-angle. The following quantities are presumed known.

$$\begin{aligned} AR: &\quad 1 \leq AR \leq 3.8 \\ \lambda: &\quad 0 \leq \lambda \leq 1.0 \\ s/R: &\quad 0.5 \leq s/R \leq 1.0 \\ \delta: &\quad -20 < \delta < +20 \\ \Lambda_{te}: &\quad 0°;\ c_r;\ x_H \end{aligned}$$

1. Determine $(C_N)_{T(B)}$ based on fin planform and using the method of Section 5.1.

2. Find $(x_{cp}/c_r)_T$ from the charts of Figure 20 taken from Reference 4.

3. Assume that $(x_{cp}/c_r)_{T(B)}$ is equal to $(x_{cp}/c_r)_T$.

4. Calculate C_H using Equation (10).

$$C_H = (C_N)_{T(B)} \left[\frac{x_H}{c_r} - \left(\frac{x_{cp}}{c_r} \right)_{T(B)} \right] \tag{10}$$

5.3 SPANWISE CENTER-OF-PRESSURE LOCATION OF DEFLECTED FIN ON CONICAL BOATTAIL (ROOT-BENDING MOMENT)

5.3.1 Preliminary Remarks

The spanwise location of the deflected fin center-of-pressure is of interest for obtaining the fin root-bending moment. The root-bending moment coefficient is given by

$$C_B = (C_N)_{T(B)} \cdot \left(\frac{y_{cp}}{s} \right)_{T(B)} \tag{11}$$

wherein s, the exposed fin span, is the reference length for C_B. The sketch in Section 5.2.1 illustrates the geometry.

---

(4) ibid.

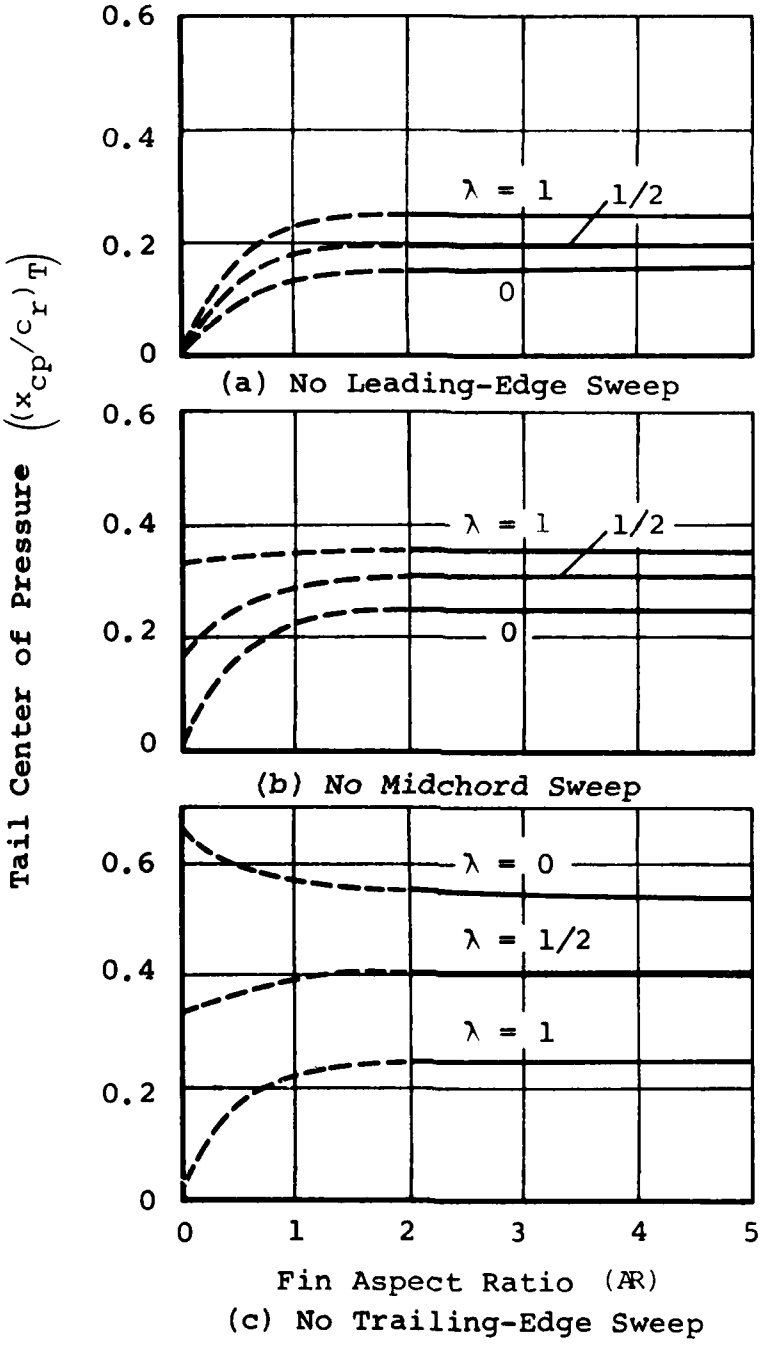

FIGURE 20. CHARTS FOR TAIL-ALONE CENTER OF PRESSURE AT SUBSONIC SPEEDS AS DETERMINED BY LIFTING-LINE THEORY

It is of interest to consider the known effects of wing-body interference on lateral center-of-pressure position for a slender fin mounted on a cylindrical body. The lateral location of the center-of-pressure as a fraction of the exposed fin span for a deflected fin on a body is not expected to change much relative to its position for the fin alone. As a result the rule of thumb is to take the fin center-of-pressure approximately equal to that for the fin alone provided vortex interference is not present. For the fins alone tested in Reference 1, $(y_{cp}/s)_T$ varies from 0.414 to 0.431 so it is not to be expected that fin planform will have much effect on $(y_{cp}/s)_{T(B)}$, even for a fin on a concial boattail.

5.3.2 Comparison Between Prediction and Data

The first prediction of interest is how close the fin-alone lateral center-of-pressure position is predicted by DATCOM. It turns out that we will not use $(y_{cp}/s)_T$ as a correlation parameter because it exhibits such little change with fin alone planform. Table 7 shows comparisons between data and DATCOM predictions for the fins alone.

TABLE 7

COMPARISON OF PREDICTED AND MEASURED VALUES OF TAIL-ALONE LATERAL CENTER-OF-PRESSURE POSITION

Fin	$(y_{cp}/s)_T$	
	Data	DATCOM
T9	0.40	0.414
T12	0.43	0.428
T14	0.43	0.426
T11	0.44	0.426
T13	0.45	-----

The data show small variability among the fins in $(y_{cp}/s)_T$ in conformity with the predictions.

It is not expected that the experimental values of $(y_{cp}/s)_{T(B)}$ would correlate with $(y_{cp}/s)_T$ because of the small variability of the latter quantity unless the effects of

(1) ibid.

fin-body interference are negligible. In fact, it is found that the principal correlation parameter is fin aspect ratio as shown in Figure 21. The results for $\lambda = 0$ and 0.5 are well represented by the lower line and the results for $\lambda = 1.0$ by the upper line. The $\lambda = 1.0$ results are more outboard than those for $\lambda = 0$ and 0.5 as might be expected. At $AR = 1$ and $\lambda = 0.5$ the three points show the effect of s/R to be small enough to neglect as does comparison of the $AR = 2.35$ and $AR = 2.5$ points. The two $AR = 2$ points show small effect of taper ratio between 0.5 and 0. These curves provide the basis for the bending-moment prediction method.

5.3.3 Prediction Method

The following input quantities are needed for the root bending-moment prediction method for a deflected fin on a conical boattail. The following quantities are given:

$$AR: \quad 1 \leq AR \leq 4.0$$

$$\lambda: \quad 0 \leq \lambda \leq 1.0$$

$$s/R: \quad 0.5 \leq s/R \leq 1.0$$

$$\delta: \quad -20 \leq \delta \leq 20°$$

$$\Lambda_{te}: \quad 0°; \ s \ .$$

1. Determine $(C_N)_{T(B)}$ based on fin planform area from method of Section 5.1.

2. Find $(y_{cp}/s)_{T(B)}$ from Figure 21.

3. Calculate the root bending moment from

$$C_B = (C_N)_{T(B)} \cdot \left(\frac{y_{cp}}{s}\right)_{T(B)} \tag{12}$$

5.4 LIFT CARRYOVER ONTO CONICAL BOATTAIL DUE TO DEFLECTED FINS

5.4.1 Preliminary Remarks

Lift is carried over from the fins onto the body since the body does not present a vertical reflection plane to the fins. Such body lift carryover is usually thought of as being proportional to the amount of lift or normal force on the fin $(C_N)_{T(B)}$. Similar to an interference factor, k_T, defined based on the normal force on the fin due to control deflection, we can define a factor, k_B, to define the body lift carryover.

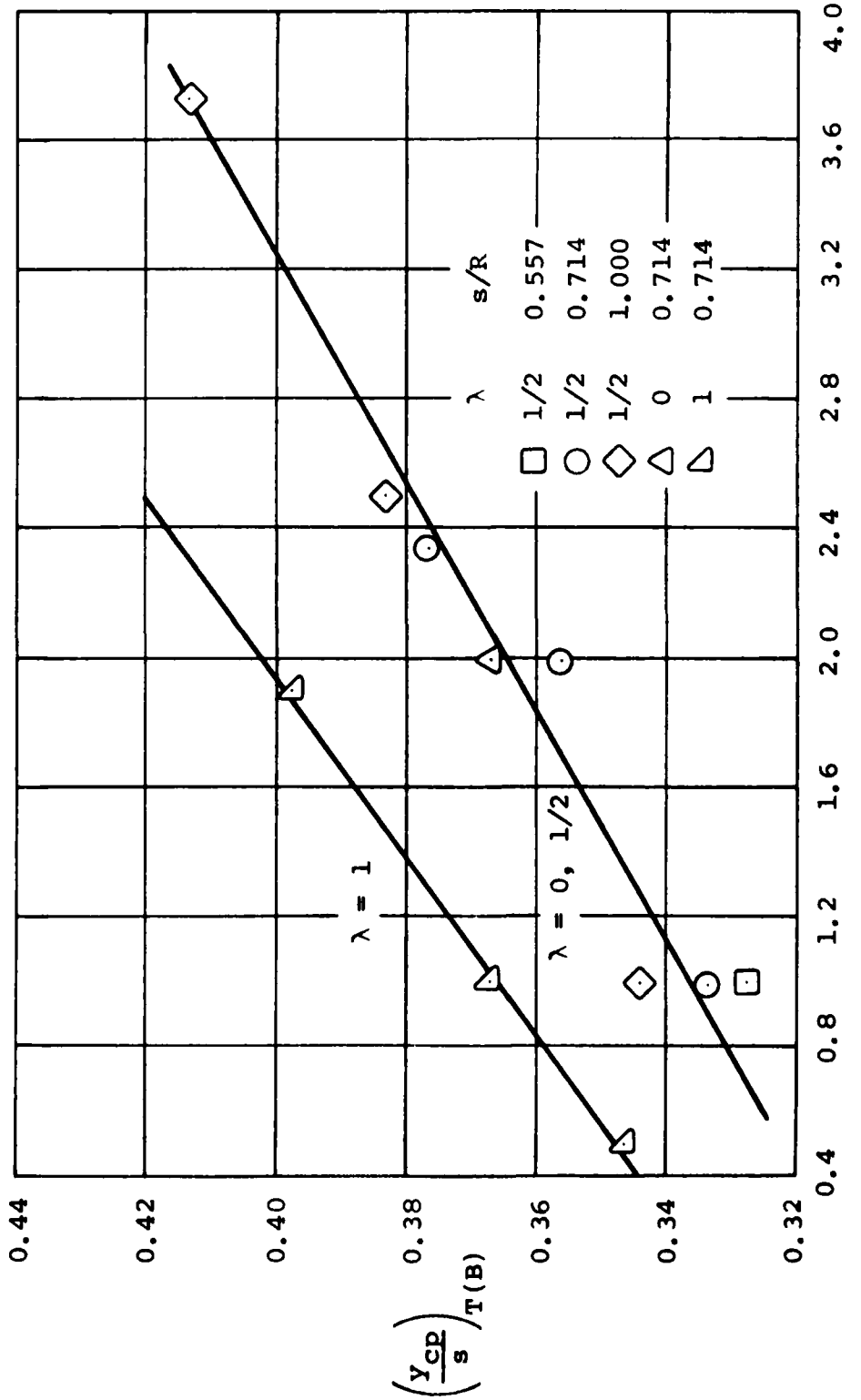

FIGURE 21. CORRELATION OF LATERAL CENTER-OF-PRESSURE POSITION OF DEFLECTED FIN ON CONICAL BOATTAIL

$$k_B = \frac{\text{normal force on body due to deflected fin at } \delta}{\text{1/2 normal force on fin alone at } \alpha = \delta} = \frac{N_{B(T)}}{N_T} \quad . \tag{13}$$

If we normalize k_B by k_T, we have

$$\frac{k_B}{K_T} = \frac{N_{B(T)}}{N_{T(B)}} = \frac{(C_N)_{B(T)}}{(C_N)_{T(B)}} \tag{14}$$

The quantity $N_{B(T)}$ is usually not normally measured directly since it requires a pressure distribution model. It is usually obtained by subtracting the fin forces normal to the body from the body-tail combination normal force.

The values of k_B and k_T for a cylindrical body with slender fins mounted on it depend on the ratio of body diameter to the total span of the fins mounted on the body. To a close approximation

$$\frac{k_B}{k_T} = \frac{\text{body diameter}}{\text{total body-tail span}} \tag{15}$$

for such configurations. We can thus expect this ratio to increase for our case as s/R decreases. The actual values of k_B and k_T can depend on the control deflection angle since the geometry changes with control deflection.

5.4.2 Correlation of Lift Carryover Data

The precise method of extracting $(C_N)_{B(T)}$ from the data is embodied by the following equation

$$(C_N)_{B(T)} = \frac{1}{2}\left[\frac{S_R}{S_T}(C_N)_{BT} - 2 \cos \delta \ (C_N)_{T(B)}\right] \tag{16}$$

where $(C_N)_{B(T)}$ = the normal-force carryover onto the body due to one tail; $N_{B(T)}/q_\infty S_T$

S_R = the body frontal area; 38.4845 in.^{2}

S_T = the area of one fin; in.^{2}

$(C_N)_{BT}$ = the total normal force measured on the body-tail combination; $N_{BT}/q_\infty S_R$

δ = the tail deflection angle in degrees

$(C_N)_{T(B)}$ = the normal force measured on one tail; $N_{T(B)}/q_\infty S_T$.

It should be mentioned that with two fins, $(C_N)_{T(B)}$ is not exactly the same for each fin, and the average was used in the calculation.

In order to extract the ratio k_B/k_T from the data, it is necessary to plot $(C_N)_{B(T)}$ versus $(C_N)_{T(B)}$ since the support strut on the body in the wind tunnel causes nonzero values of both quantities at δ = 0 degrees. Figure 22 exhibits the fact that a basically linear relationship exists between these quantities except in a few cases of extreme deflection. The prediction method will assume a linear relationship. This assumption implies that the lift carryover onto the body is a certain fraction of the fin normal force even though the latter quantity is nonlinear in δ.

The values of k_B/k_T are given in Table 8.

TABLE 8

EXPERIMENTAL VALUES OF k_B/k_T

Fin	k_B/k_T
T9	1.030
T15	0.970
T20	0.930
T12	0.810
T2	1.215
T14	1.110
T24	0.685
T11	1.010
T19	0.750
T13	0.900
T5	0.735

The parameter k_B/k_T is expected to vary with s/R on the basis of the previous discussion. Table 9 presents single parameter variations which illustrate the effects of s/R, AR, and λ.

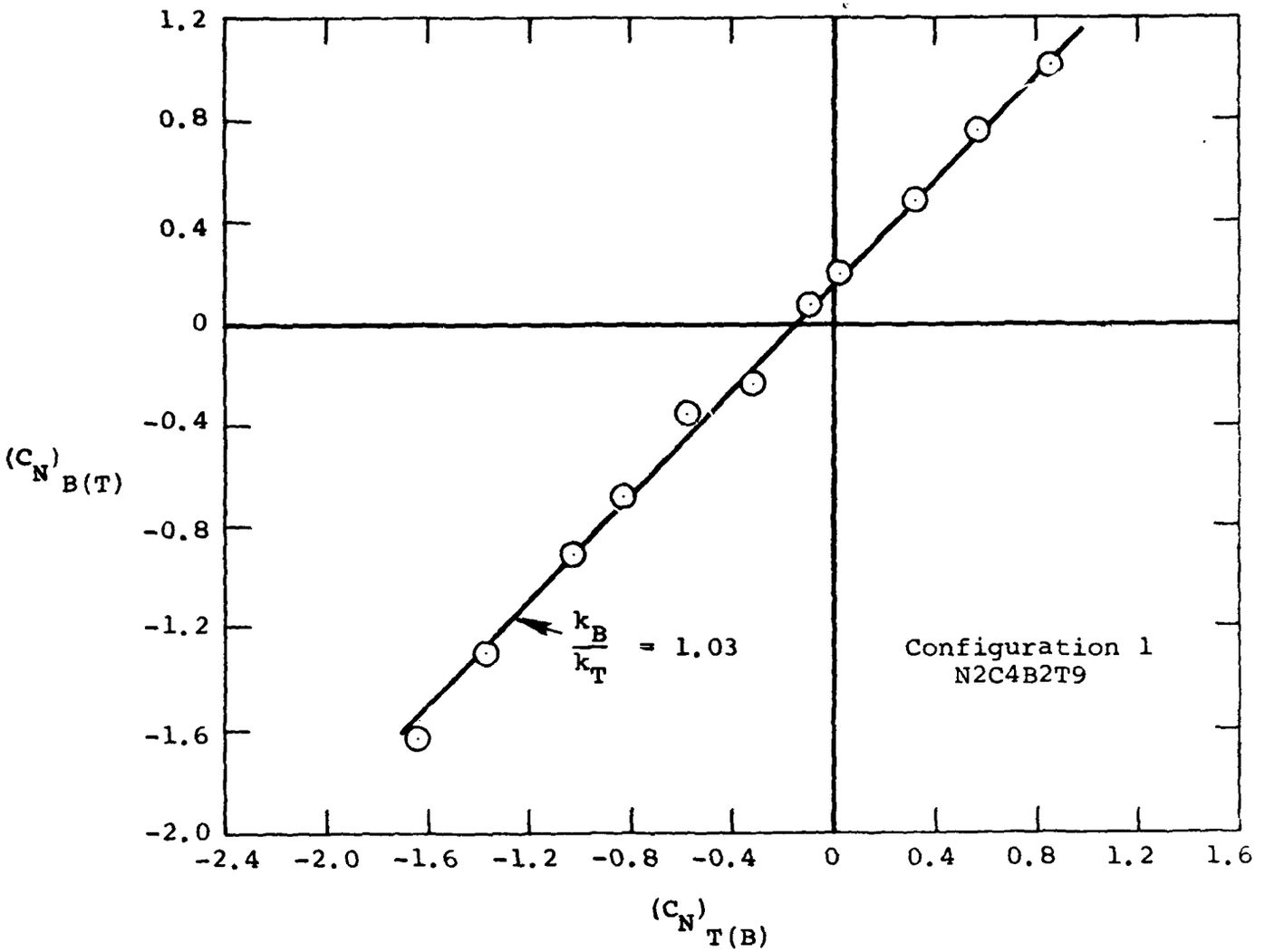

(a) Fin T9

FIGURE 22. PLOTS OF NORMAL FORCE ON BODY VERSUS NORMAL FORCE ON FIN MOUNTED ON BOATTAIL

(Sheet 1 of 11)

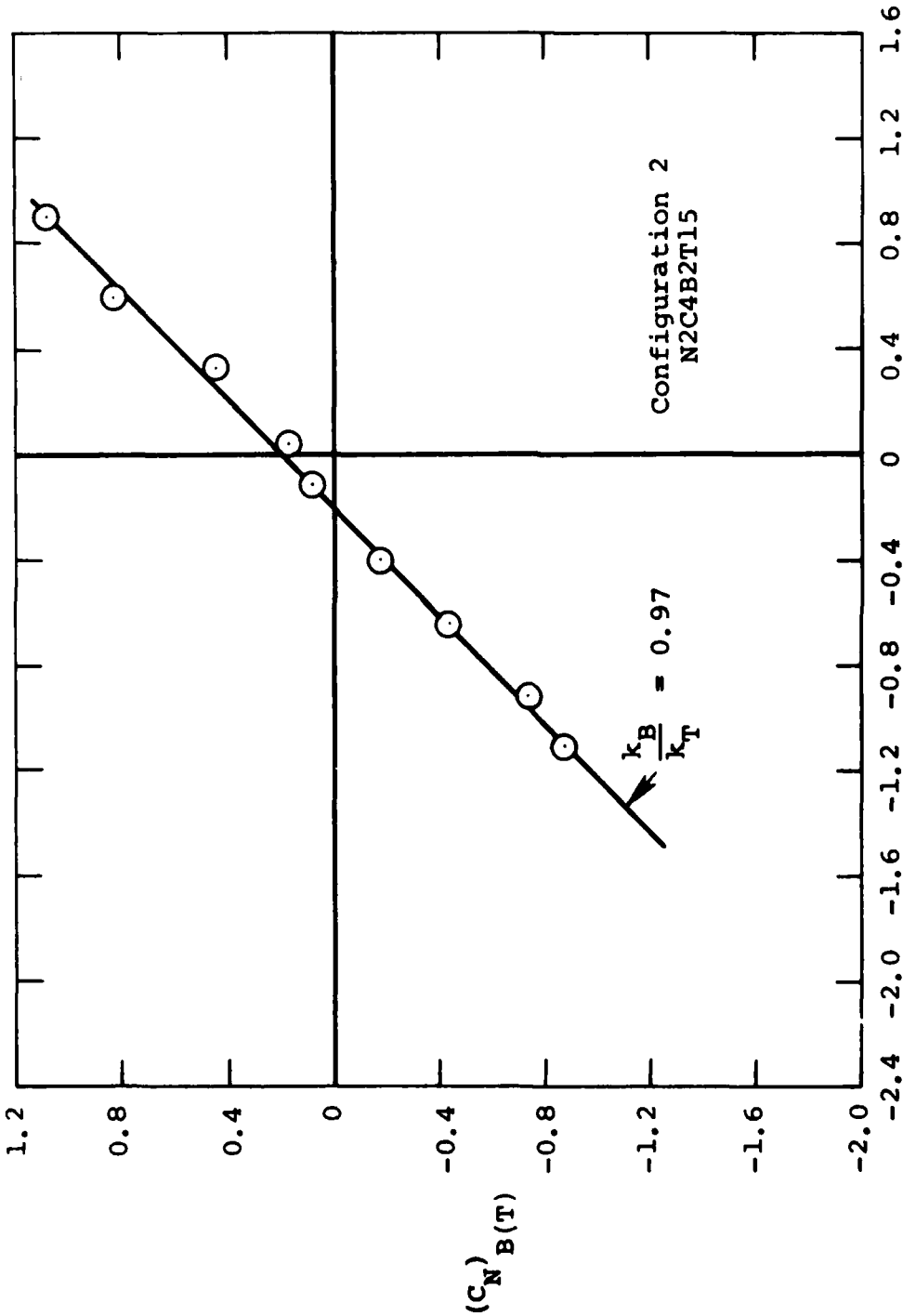

(b) Fin T15

FIGURE 22. (Sheet 2 of 11)

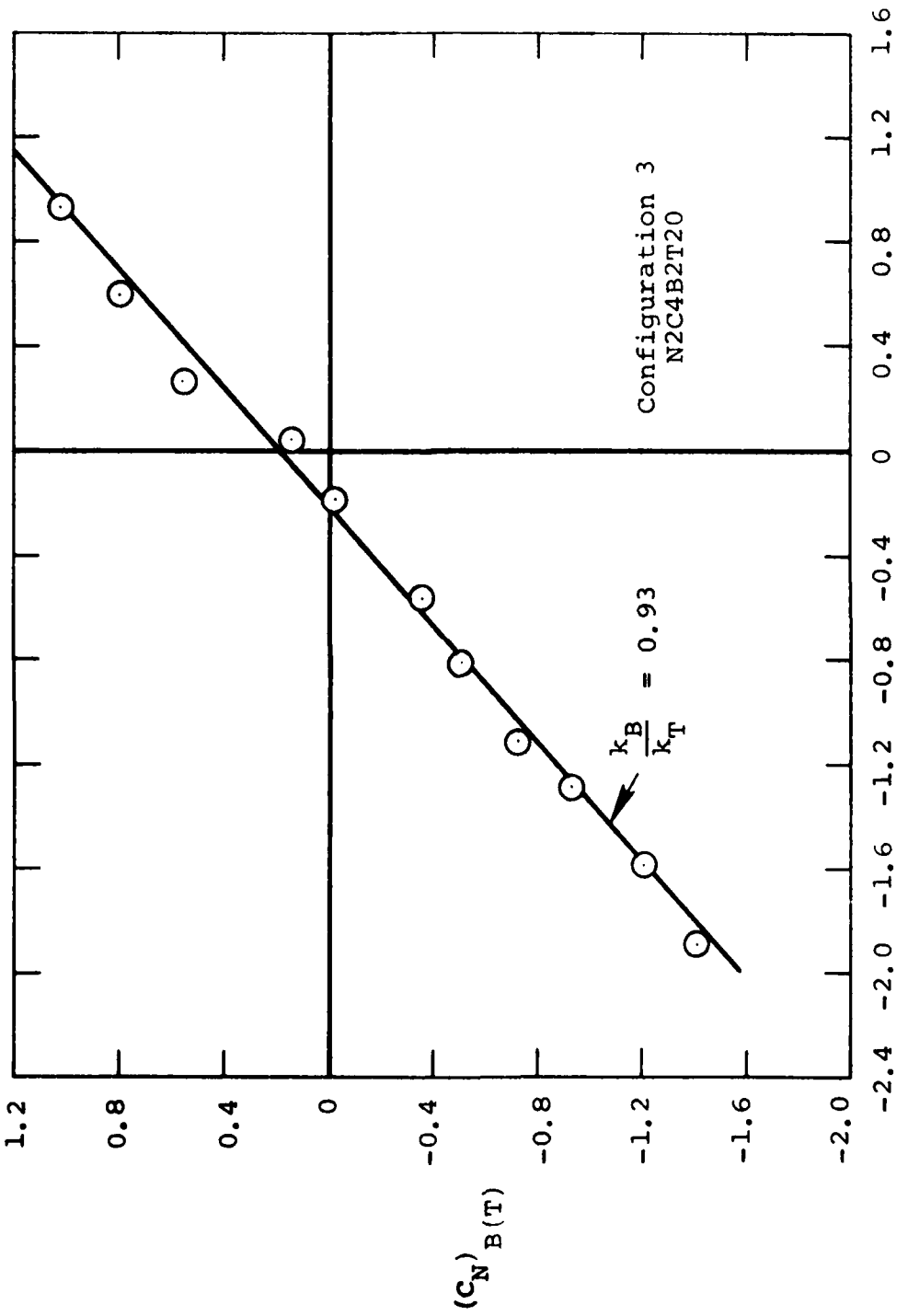

(c) Fin T20

FIGURE 22. (Sheet 3 of 11)

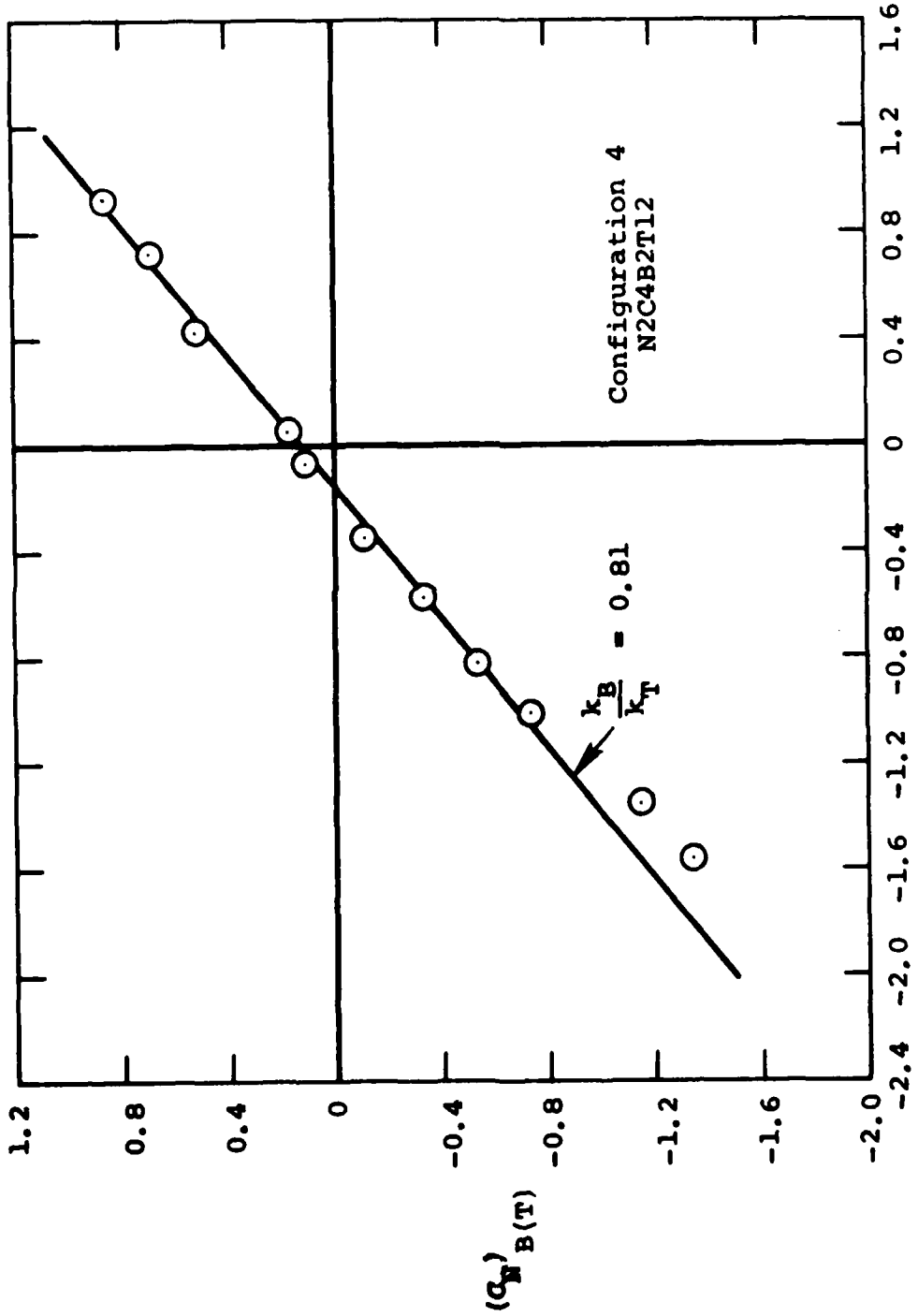

(d) Fin T12

FIGURE 22. (Sheet 4 of 11)

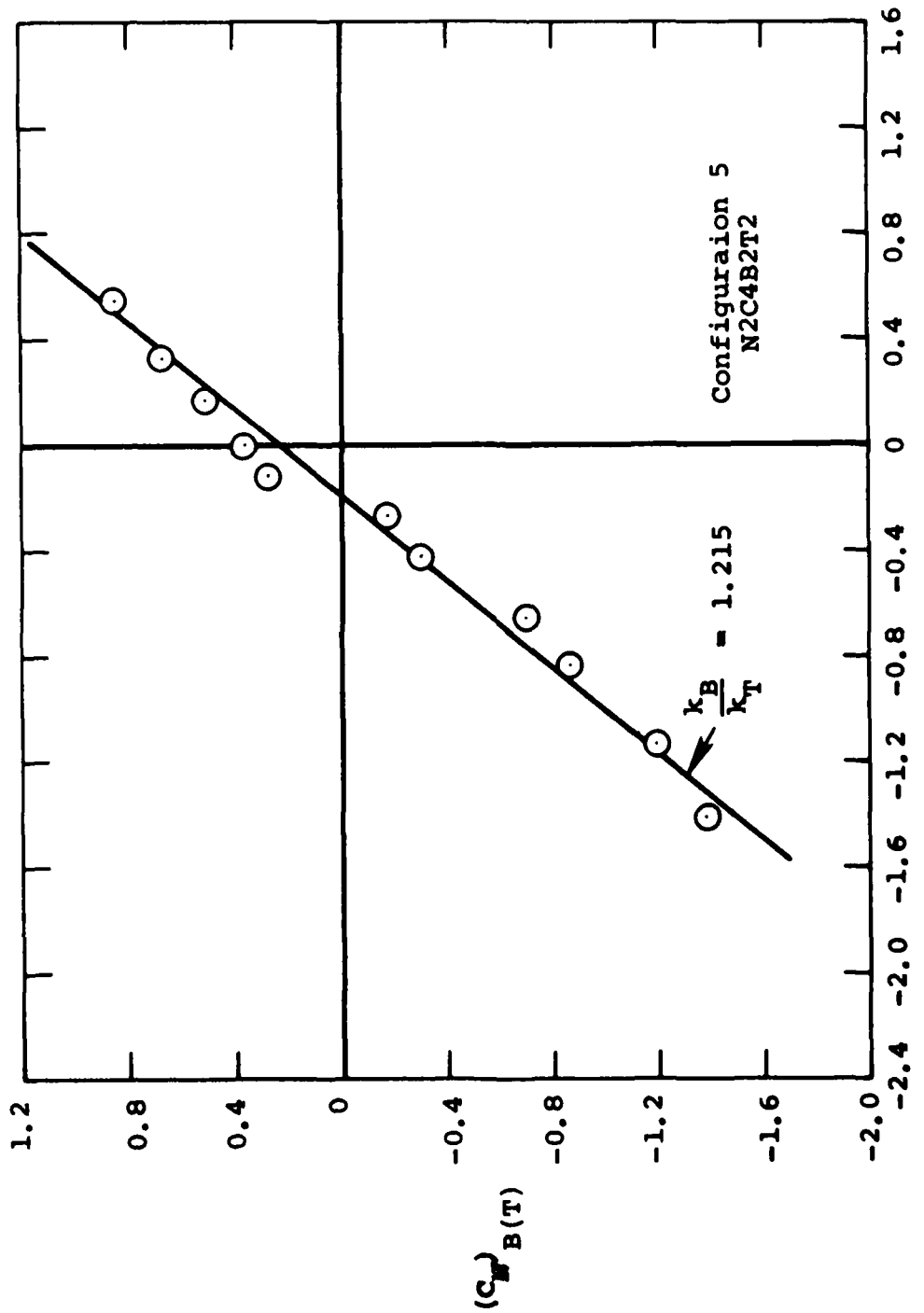

(e) Fin T2

FIGURE 22. (Sheet 5 of 11)

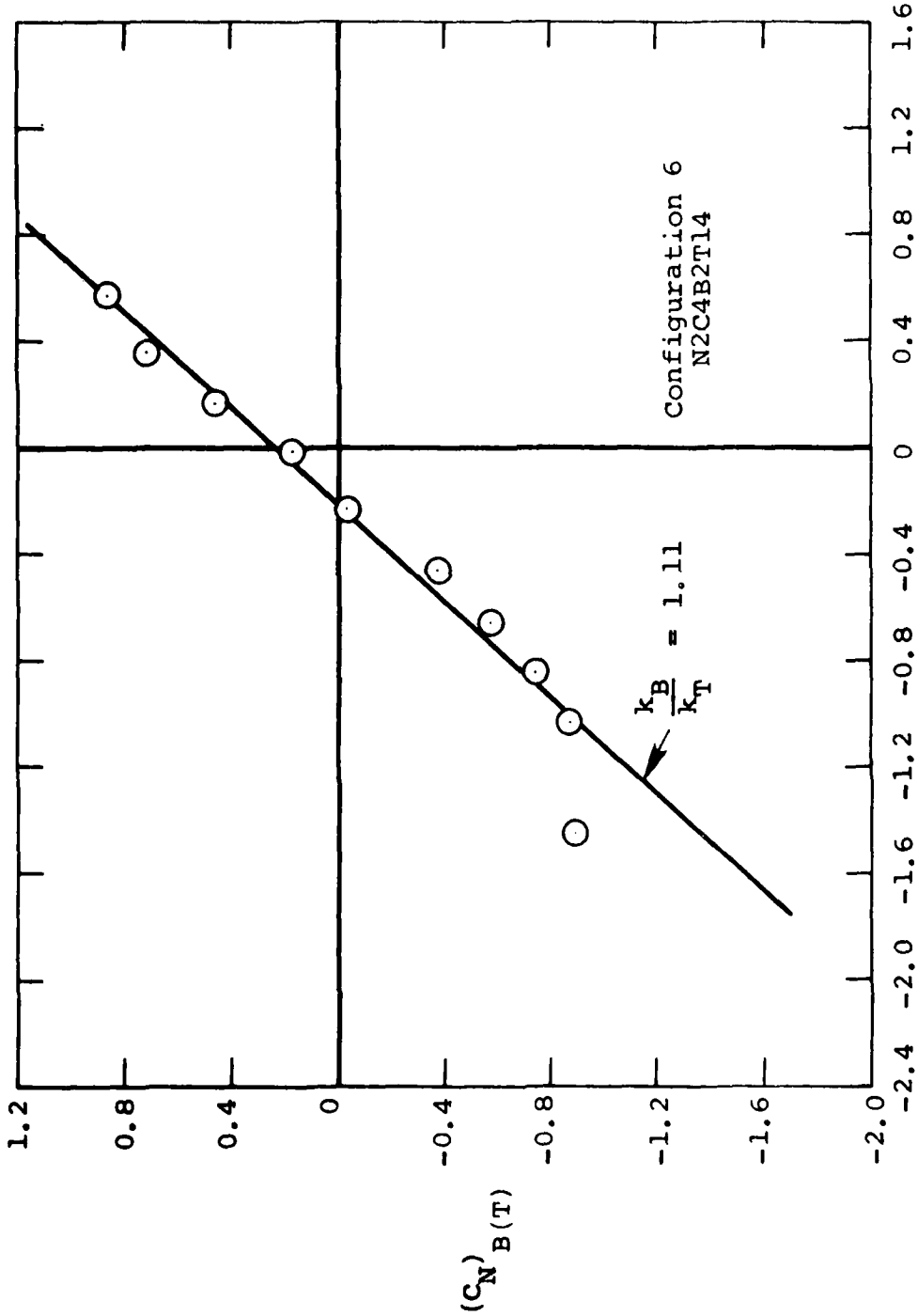

FIGURE 22. (Sheet 6 of 11)

(f) Fin T14

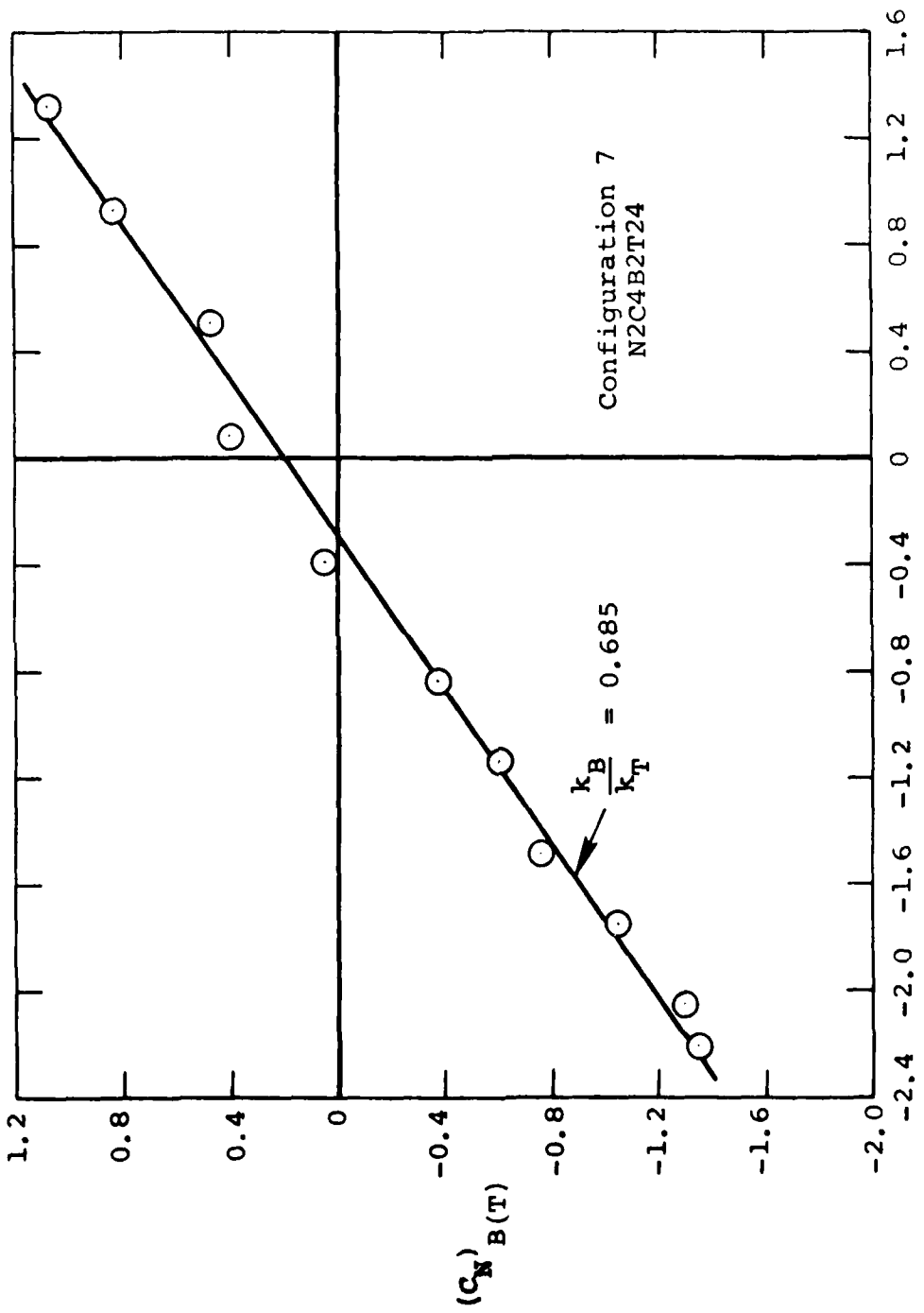

(g) Fin T24

FIGURE 22. (Sheet 7 of 11)

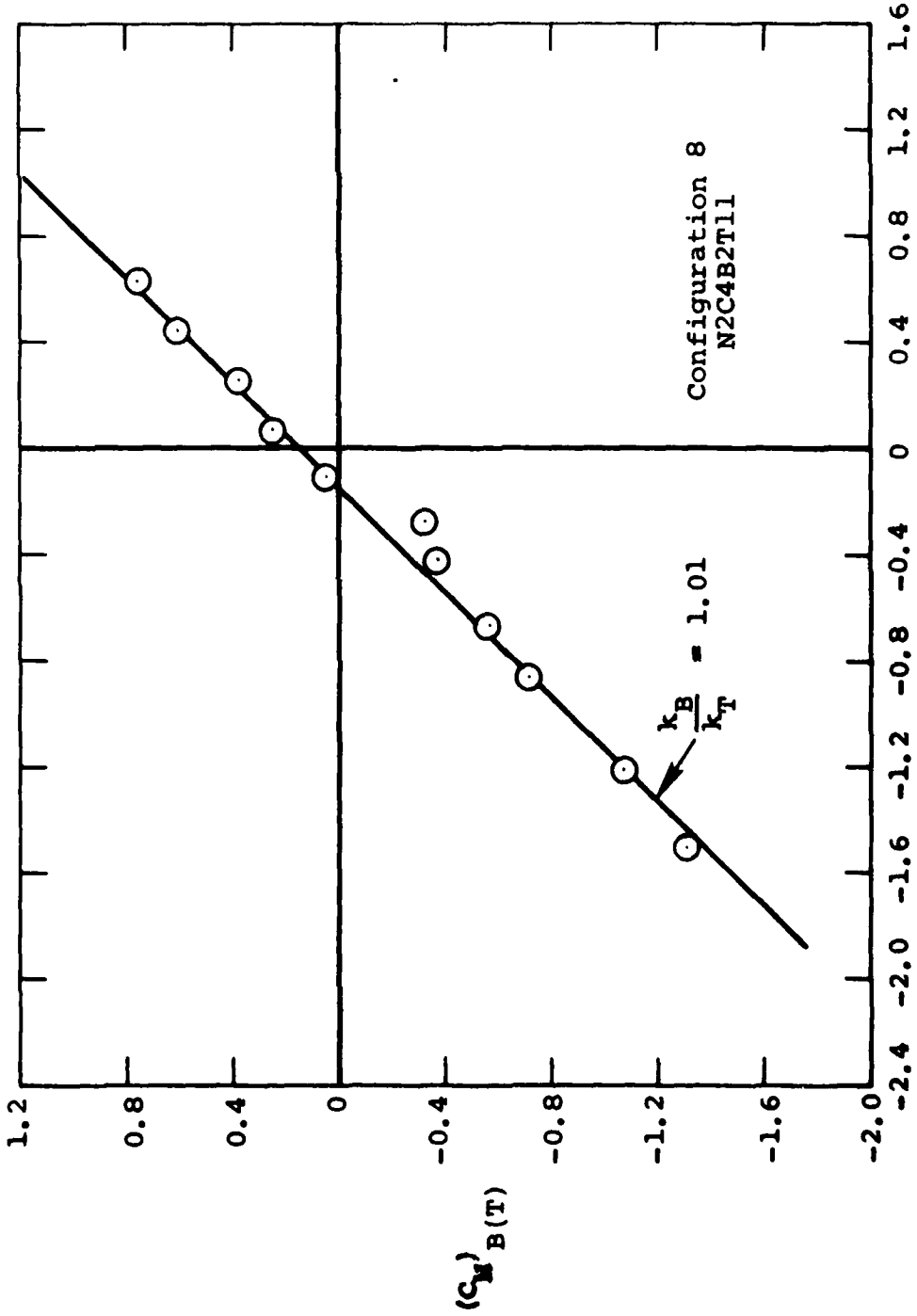

(h) Fin T11

FIGURE 22. (Sheet 8 of 11)

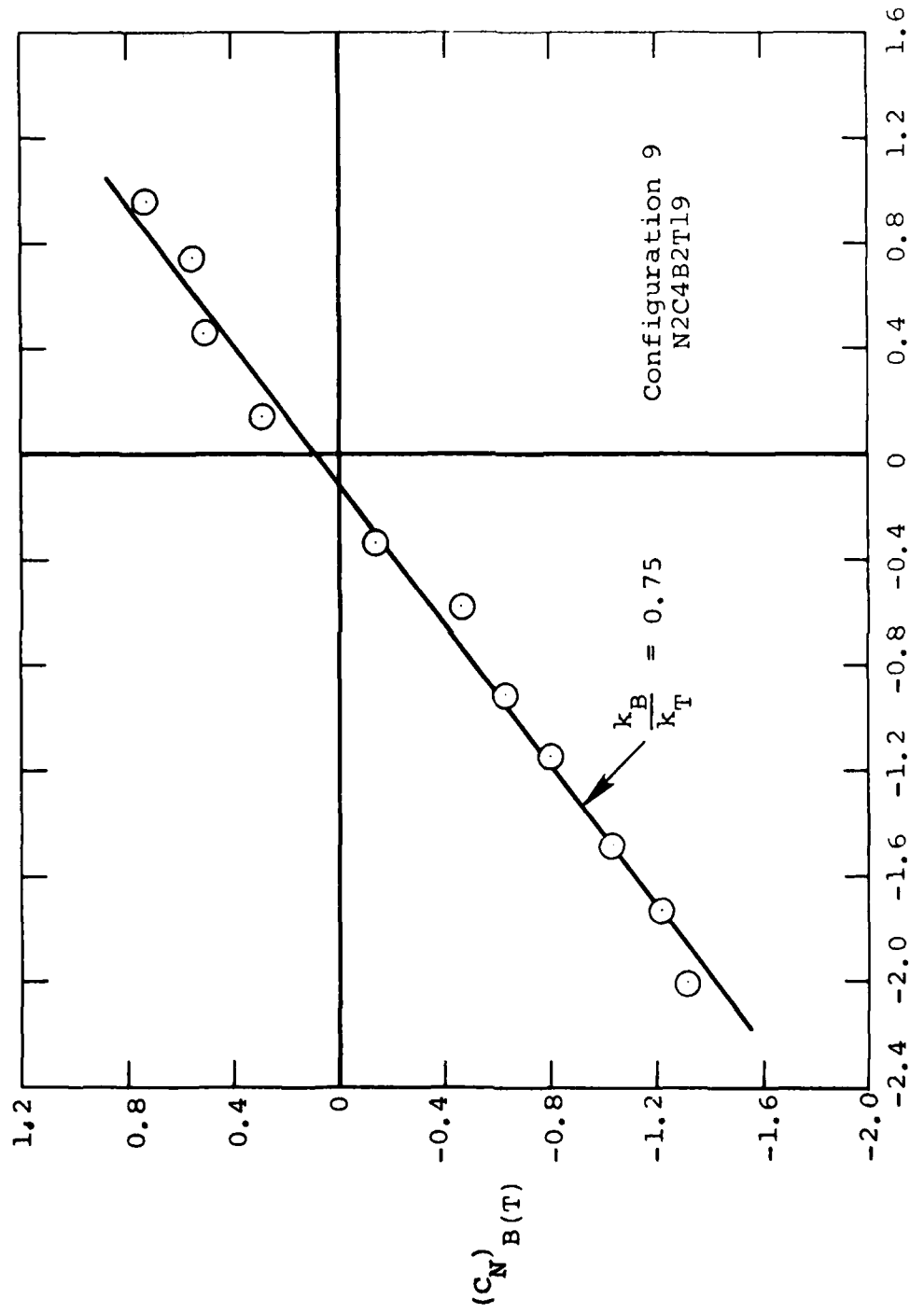

(i) Fin T19

FIGURE 22. (Sheet 9 of 11)

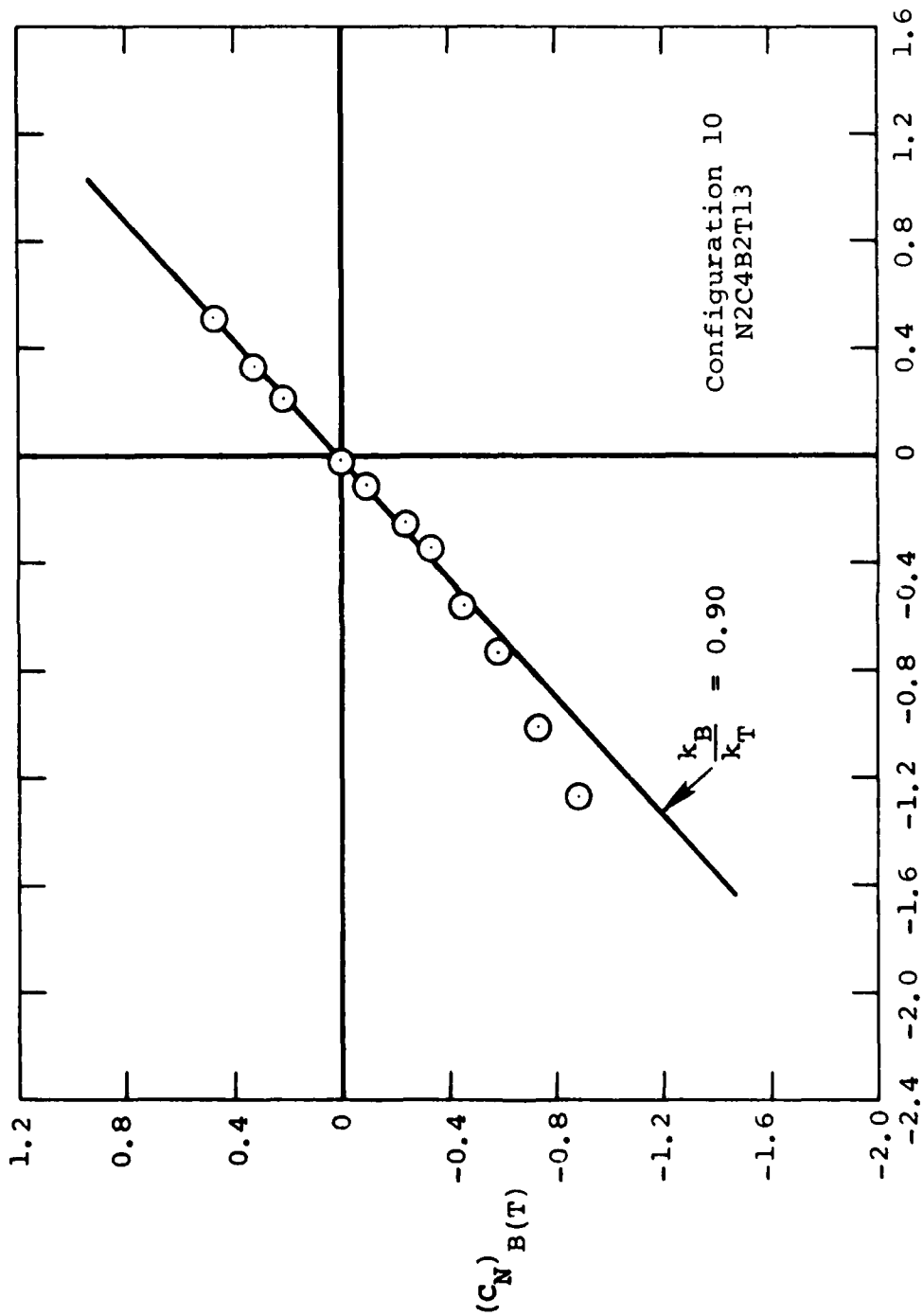

(j) Fin T13

FIGURE 22. (Sheet 10 of 11)

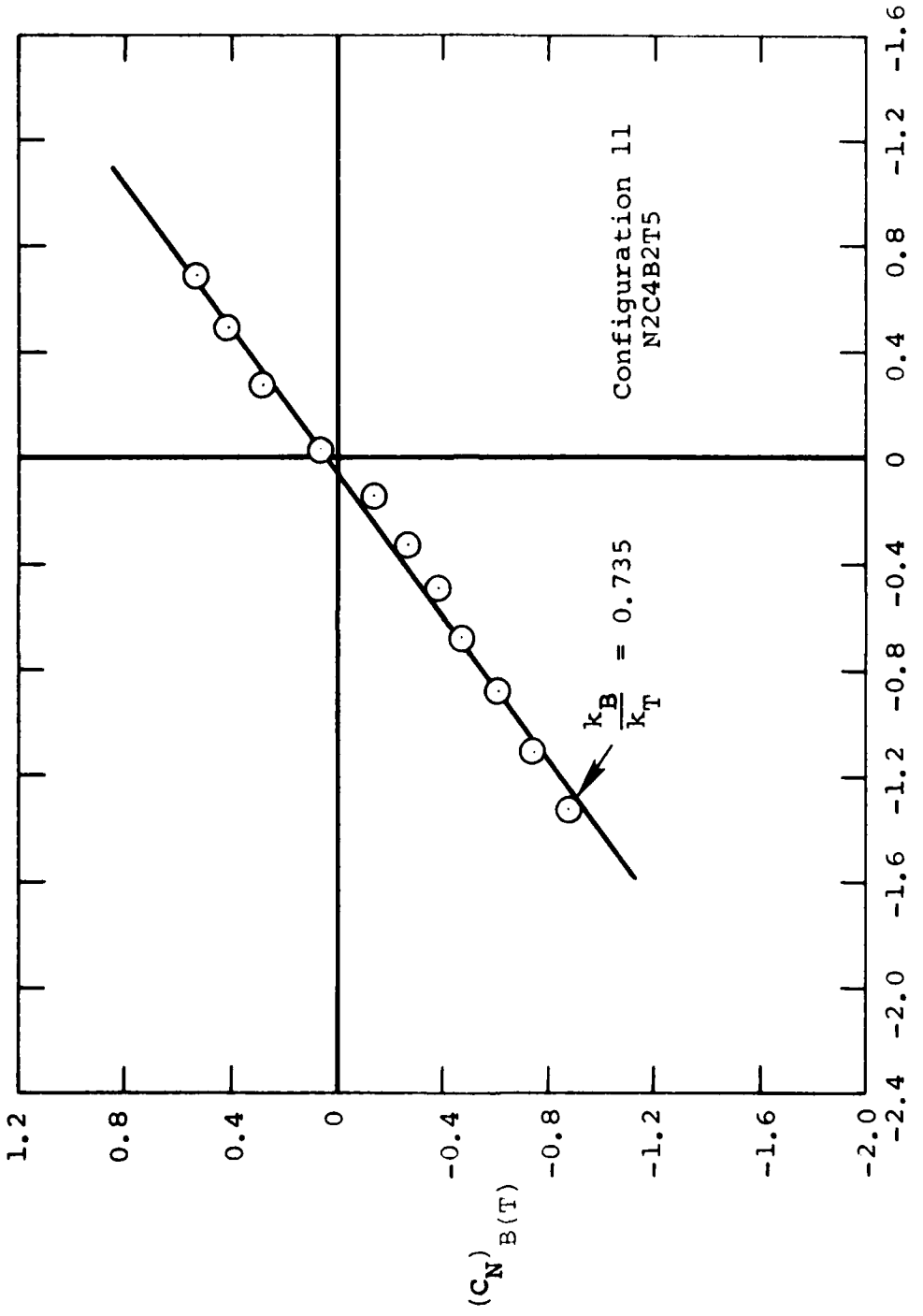

FIGURE 22. (Sheet 11 of 11)

(k) Fin T5

The significant variable is s/R. The three aspect-ratio series shows no systematic effect of AR. We plot k_B/k_T versus s/R in Figure 23. An Average curve has been faired through the points. The correlation generally gives the ratio k_B/k_T within about ±15 percent. Since the lift carryover is the difference of two measured quantities, its accuracy of determination is not so good as $(C_N)_{T(B)}$ which is measured directly. The accuracy of the correlation may thus be better than ±15 percent.

TABLE 9

EXPERIMENTAL VALUES OF k_B/k_T AND $(x_{cp}/c_r)_{B(T)}$ FOR SYSTEMATIC FAMILIES OF TAIL FINS

a. Effect of s/R at AR = 1, λ = 0.5:

Fin	AR	λ	s	k_B/k_T	$\frac{x_{cp}}{c_r}_{B(T)}$
T2	1.000	0.500	1.95	1.215	0.325
T11	1.000	0.500	2.50	1.010	0.020
T5	1.000	0.500	3.50	0.735	0.050

b. Effect of AR at λ = 1, s = 2.5:

T13	0.500	1.000	2.50	0.900	0.100
T14	1.000	1.000	2.50	1.110	-0.080
T15	1.905	1.000	2.50	0.970	-0.430

c. Effect of AR at λ = 0.5, s = 2.5:

T11	1.000	0.500	2.50	1.010	0.020
T12	2.000	0.500	2.50	0.810	0.020
T20	2.350	0.523	2.50	0.930	0.020

d. Effect of λ at AR = 2, s = 2.5:

T9	2.000	0	2.50	1.030	0.460
T12	2.000	0.500	2.50	0.810	0.020
T15	1.905	1.000	2.50	0.970	-0.430

e. Effect of AR at λ = 0.5, s = 3.5:

T5	1.000	0.500	3.50	0.735	0.050
T19	2.500	0.500	3.50	0.750	-0.170
T24	3.730	0.526	3.50	0.685	-0.360

5.4.3 Prediction Method

As input data for the calculation of $(C_N)_{B(T)}$, the following information is needed.

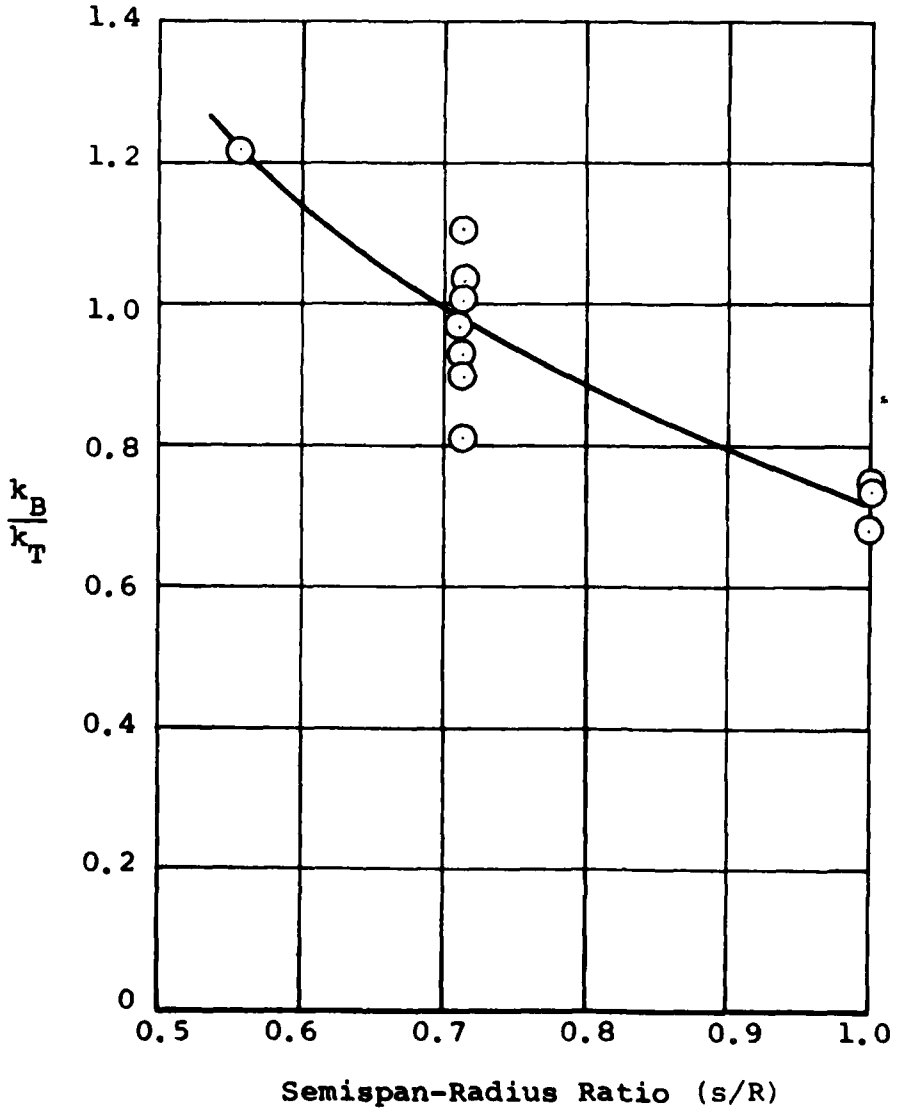

FIGURE 23. CORRELATION OF k_B/k_T WITH s/R

$$\text{AR:} \quad 1 \leq AR \leq 4.0$$
$$\lambda: \quad 0 \leq \lambda \leq 1.0$$
$$s/R: \quad 0.5 \leq s/R \leq 1.0 \quad .$$

1. From the fin aspect ratio, AR, and the ratio s/R obtain the value of k_B/k_T from Figure 23 .

2. Obtain $(C_N)_{T(B)}$ from Section 5.1.

3. Obtain $(C_N)_{B(T)}$ based on S_T as follows:

$$(C_N)_{B(T)} = \left(\frac{k_B}{k_T}\right)(C_N)_{T(B)} \tag{17}$$

5.5 CENTER-OF-PRESSURE POSITION OF LOADING ON CONICAL AFTERBODY DUE TO FIN DEFLECTION

5.5.1 Preliminary Remarks

The deflected fin causes a force to appear on a cylindrical body normal to its longitudinal axis. For a boattail body a net axial force can be produced which can also contribute to the pitching moment. We designate the pitching-moment coefficient caused by the load on the body due to fin deflection of one fin as $(C_m)_{B(T)}$ given as follows:

$$(C_m)_{B(T)} = \frac{M_{B(T)}}{q_\infty S_T c_r} \tag{18}$$

where $M_{B(T)}$ = pitching moment about center of moments due to load on body caused by deflection of one fin.

Let X measure the axial position aft of the center of moments. Then the position of the effective center-of-pressure due to $(C_N)_{B(T)}$ is given by

$$\left(\frac{\bar{X}}{D}\right)_{B(T)} = -\left(\frac{C_m}{C_N}\right)_{B(T)} \cdot \left(\frac{c_r}{D}\right) \tag{19}$$

$(\bar{X})_{B(T)}$ = center-of-pressure position of loading on conical boattail due to fin deflection measured positive aft of center-of-moment reference.

This center-of-pressure position includes any moments associated with boattail axial force due to fin deflection.

We will want to refer $(\bar{X})_{B(T)}$ to the fin coordinate system and we let $(x_{cp})_{B(T)}$ be the distance measured along the fin root chord from its leading edge to the station which corresponds to the axial position $\bar{X}_{B(T)}$. The value of $(x_{cp})_{B(T)}$ will depend on fin deflection angle δ to a slight degree. The two quantities are related by the following equation

$$\left(\frac{x_{cp}}{c_r}\right)_{B(T)} = \frac{1}{\cos\gamma\cos\delta}\left[\frac{D}{c_r}\left(\frac{\bar{X}}{D}\right)_{B(T)} - \frac{1}{c_r}(x_s + x_B\cos\gamma - x_H\cos\gamma\cos\delta)\right] . \quad (20)$$

No simple method exists for predicting $(x_{cp}/c_r)_{B(T)}$ for a fin mounted on a conical boattail. For fins on a cylindrical body, a simple lifting-line model is shown in the following sketch.

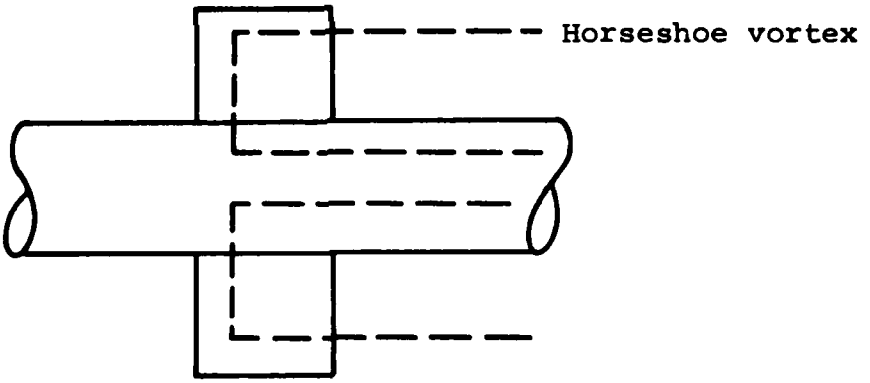

In this case the lifting line goes into the body up to the image point of the external trailing vortex. The part of the lifting line inside the body represents the normal force on the body due to the carryover from the fin as well as its center-of-pressure position. However for a conical boattail, the model is more complex.

5.5.2 Correlation of Center-of-Pressure Position of Body Loading

The quantity $(C_m)_{B(T)}$ is needed in Equation (19) to calculate $(\bar{X}/D)_{B(T)}$. This quantity is determined from the following equation.

$$(C_m)_{B(T)} = \frac{1}{2}\frac{S_R D}{S_T c_r}\left[(C_m)_{BT} - (C_m)_B\right] - (C_m)_{T(B)} \quad . \quad (21)$$

The coefficients $(C_m)_{B(T)}$ and $(C_m)_{T(B)}$ refer to moments due to one fin about the center-of-moments axis with S_T and c_r as reference area and reference length, respectively. The coefficients $(C_m)_{BT}$ and $(C_m)_B$ refer to moments about the center-of-moments axis with S_R and D as reference area and reference length. While $(C_m)_B$ should be zero at α = 0 degrees, it is not because of the influence of the support strut. Its inclusion in the above formula is an attempt to reduce this component of strut interference. Also for δ = 0 degrees, $(C_m)_{BT}$ should be zero. Since it is generally different from $(C_m)_B$, there is also some support interference on the fins at δ = 0 degrees, α = 0 degrees. We will plot $(C_m)_{B(T)}$ versus $(C_N)_{B(T)}$ and take the slope of the curve to determine $(\bar{X}/D)_{B(T)}$ in accordance with Equation (19), thereby circumventing the strut tare problem.

The quantity $(C_m)_{T(B)}$ was not measured directly in the experiment. However the hinge-moment coefficient and root-bending coefficient of each fin were measured individually. In Appendix A, these moment coefficients are properly resolved and transferred to a lateral axis through the center-of-moment reference point to obtain $(C_m)_{T(B)}$. The derived result is

$$(C_m)_{T(B)} = (C_N)_{T(B)}\left\{\left[\frac{x_H}{c_r} - \left(\frac{x_{cp}}{c_r}\right)_{T(B)}\right]\cos\gamma - \left(\frac{y_{cp}}{c_r}\right)_{T(B)}\cos\delta\cos\gamma - \frac{(x_s + x_B\cos\gamma)}{c_r}\cos\delta\right\} \quad . \quad (22)$$

It is to be expected that the center-of-pressure position of the body loading due to fin deflection should bear a relatively fixed position with respect to the fin as long as the fin is well forward on the conical boattail for small boattail angles. Accordingly we will try to correlate $(x_{cp}/c_r)_{B(T)}$ rather than $(\bar{X}/D)_{B(T)}$, thereby elminiating hinge-line position as a parameter in the correlation.

The values of $(C_m)_{B(T)}$ calculated using Equation (21) have been plotted versus $(C_N)_{B(T)}$ in Figure 24 for all 11 fins.

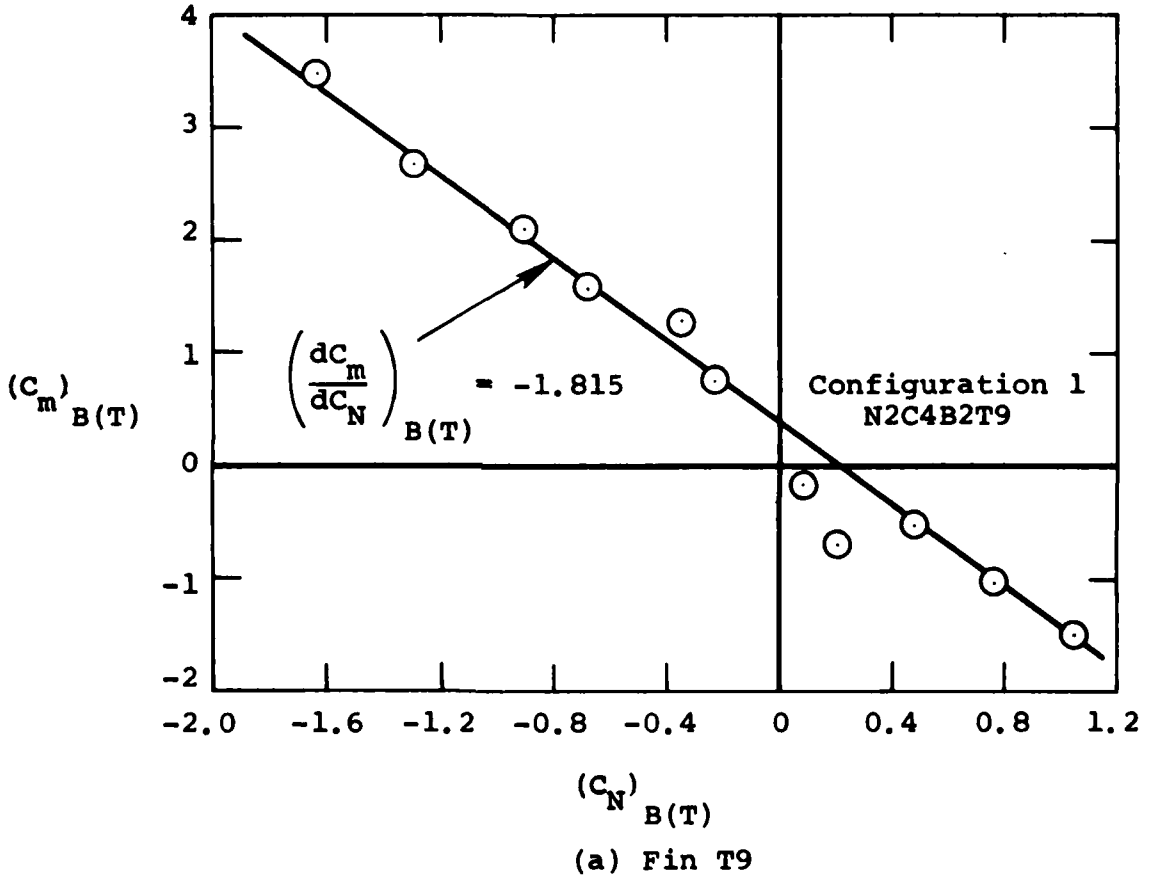

(a) Fin T9

FIGURE 24. PLOTS FOR DETERMINING CENTER-OF-PRESSURE LOCATION OF LOADING ON BODY DUE TO FIN DEFLECTIONS

(Sheet 1 of 11)

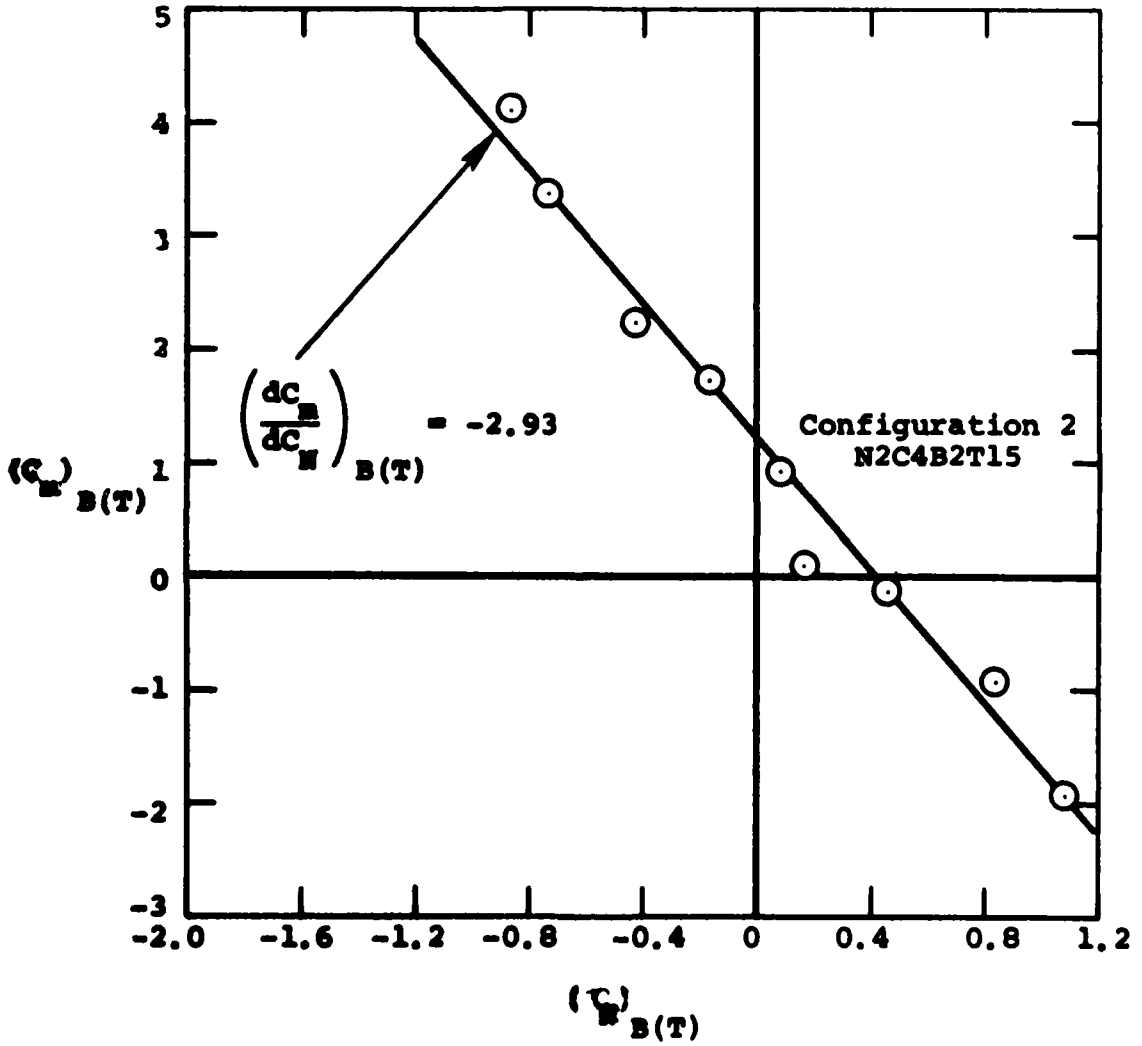

(b) Fin T15

FIGURE 24. (Sheet 2 of 11)

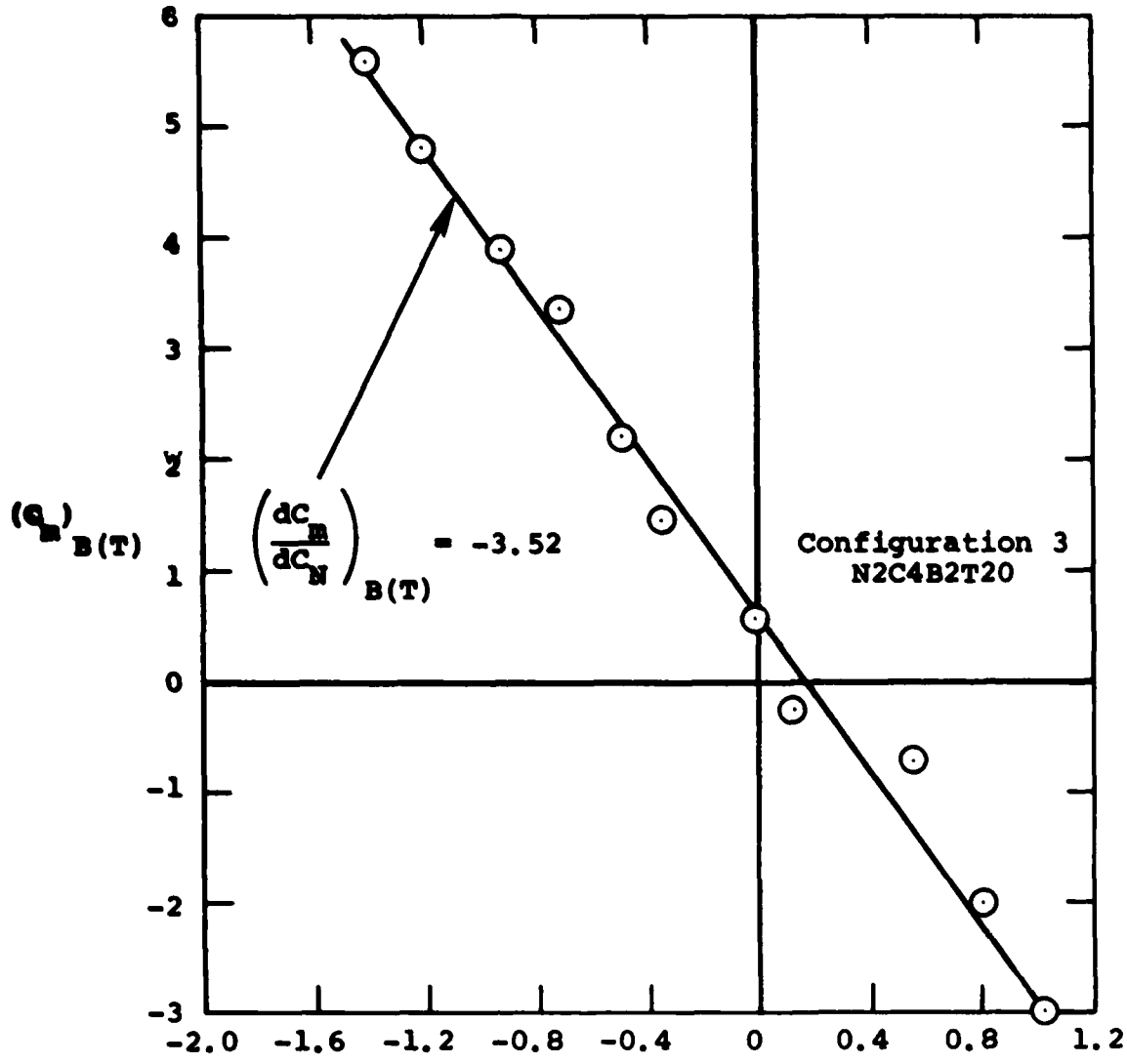

(c) Fin T20

FIGURE 24. (Sheet 3 of 11)

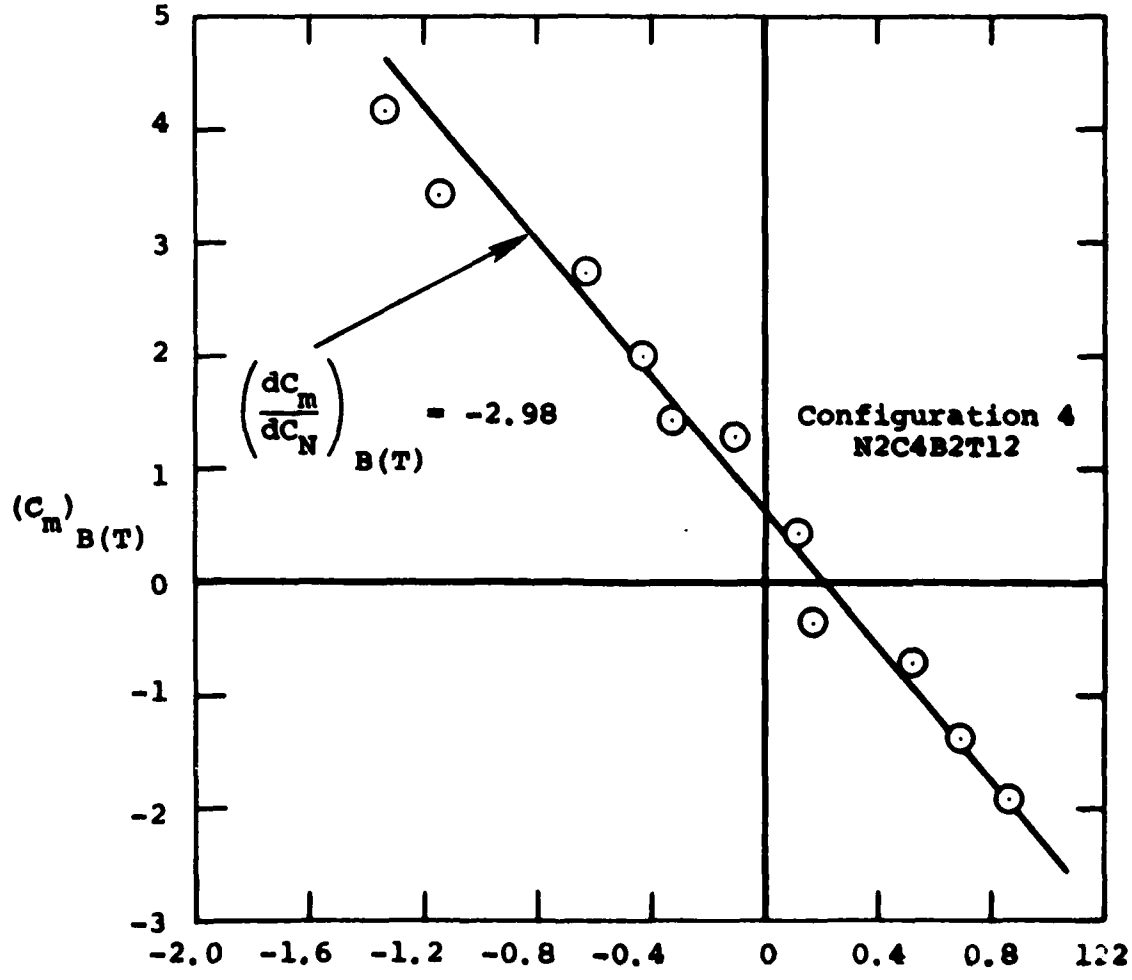

(d) Fin T12

FIGURE 24. (Sheet 4 of 11)

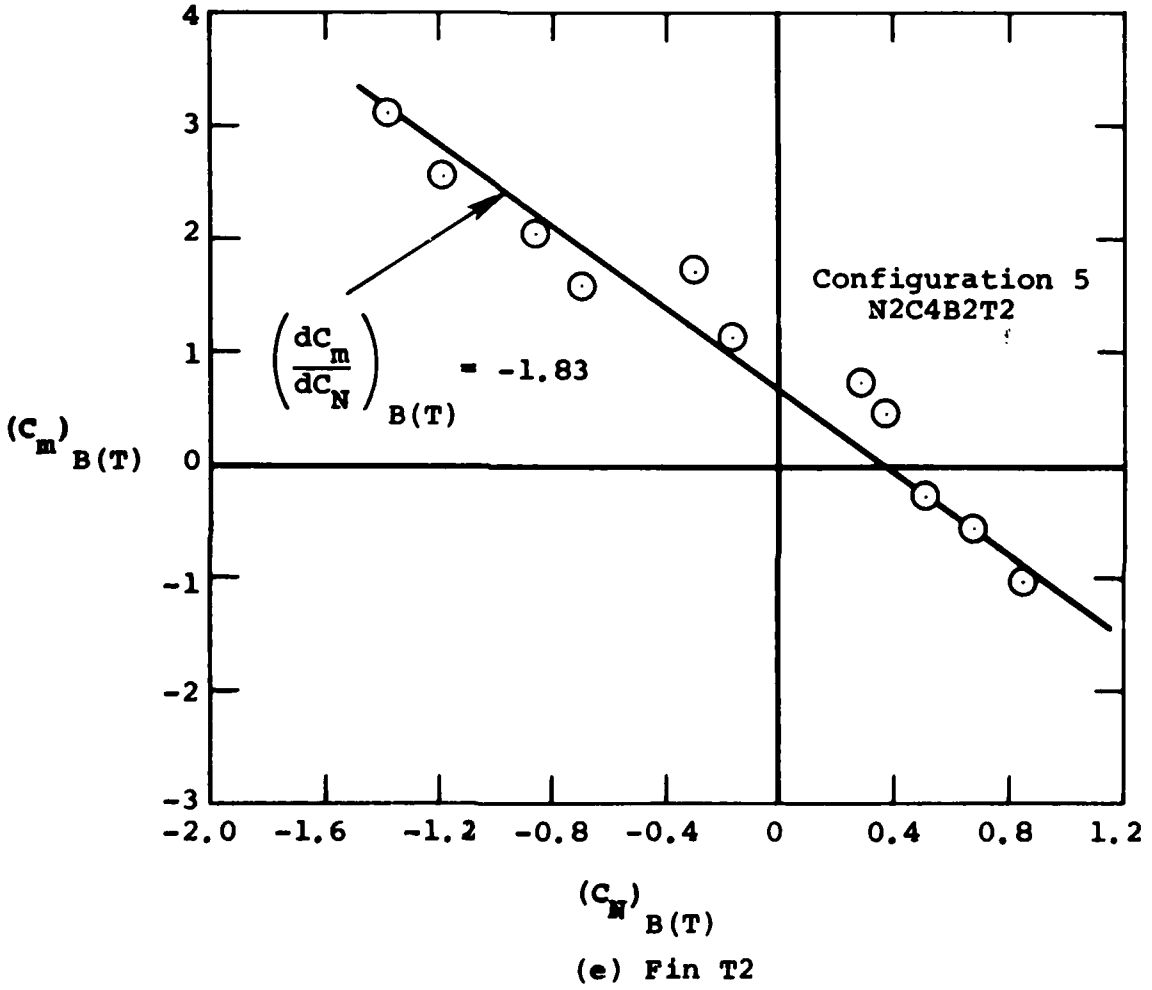

(e) Fin T2

FIGURE 24. (Sheet 5 of 11)

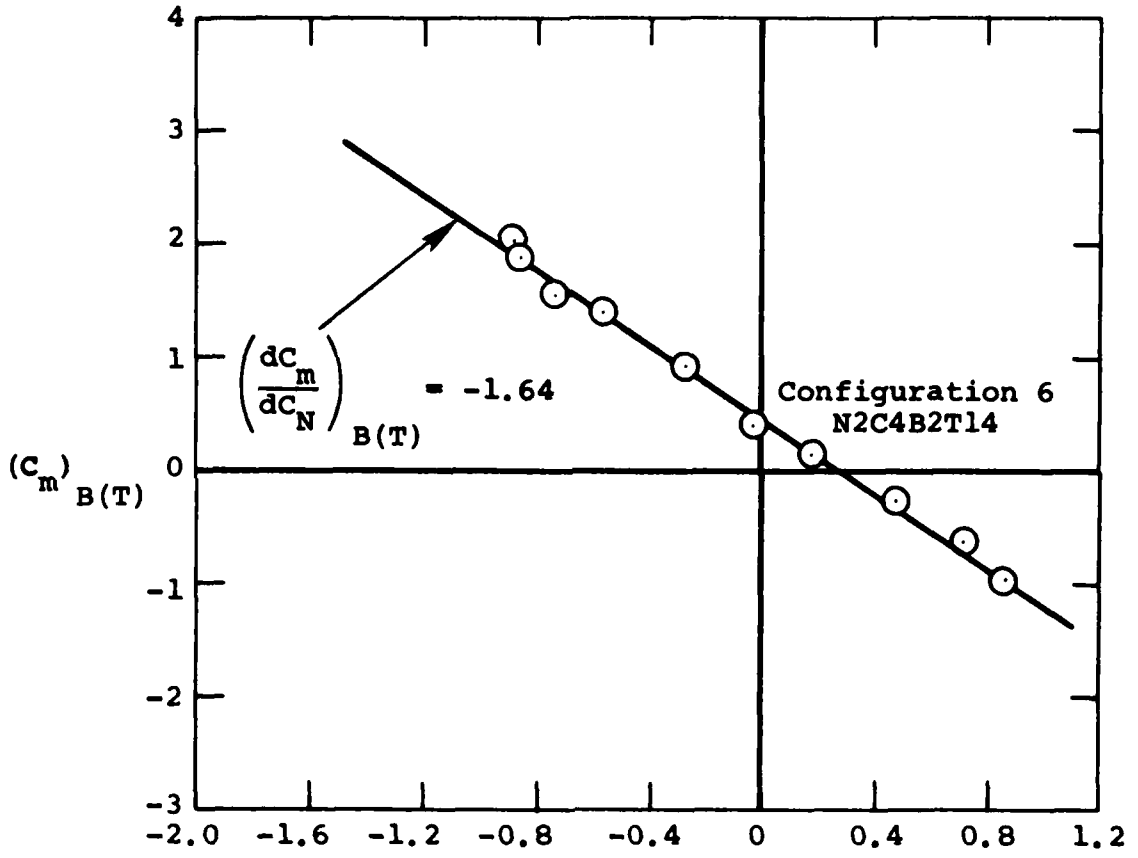

(f) Fin T14

FIGURE 24. (Sheet 6 of 11)

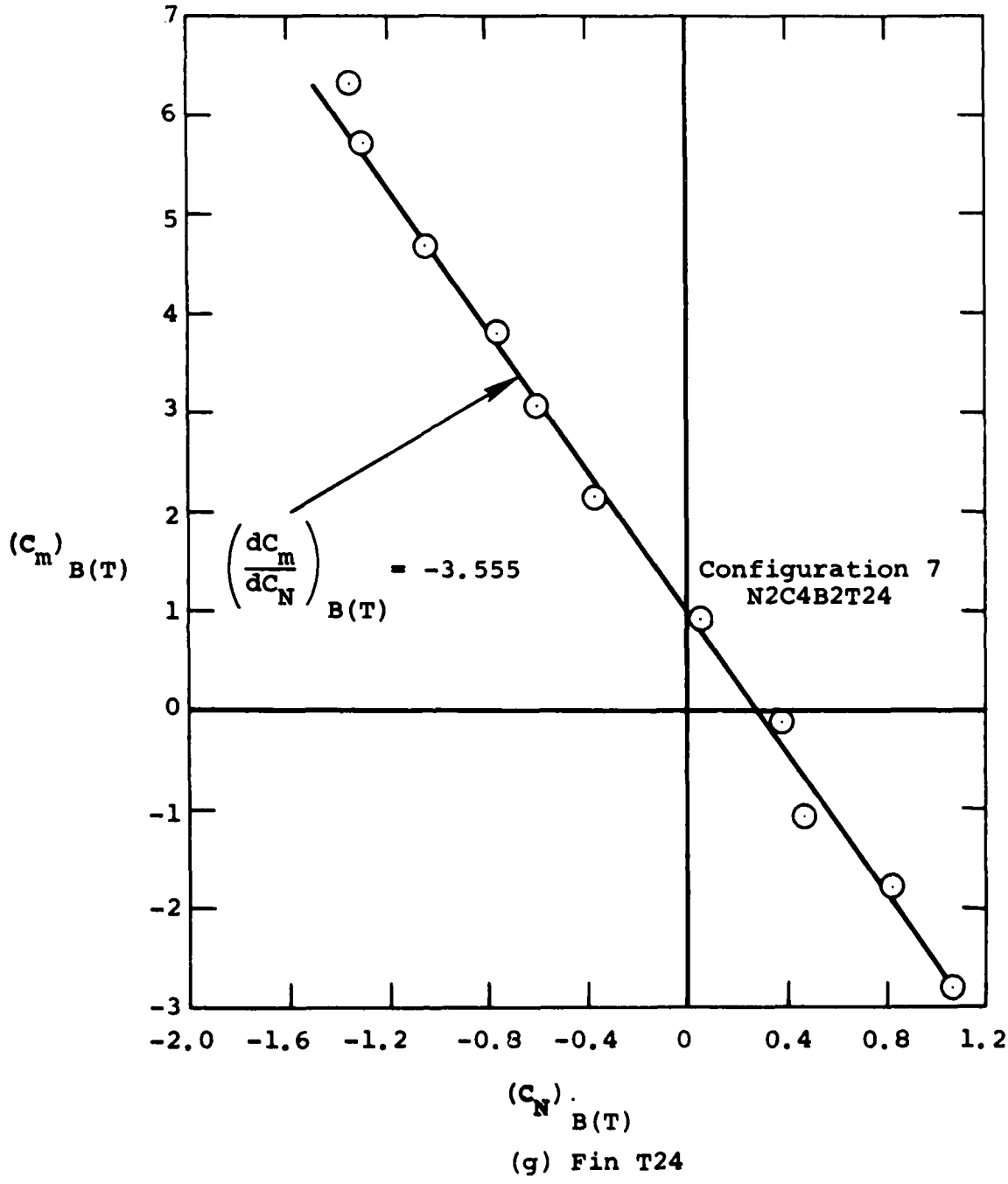

(g) Fin T24

FIGURE 24. (Sheet 7 of 11)

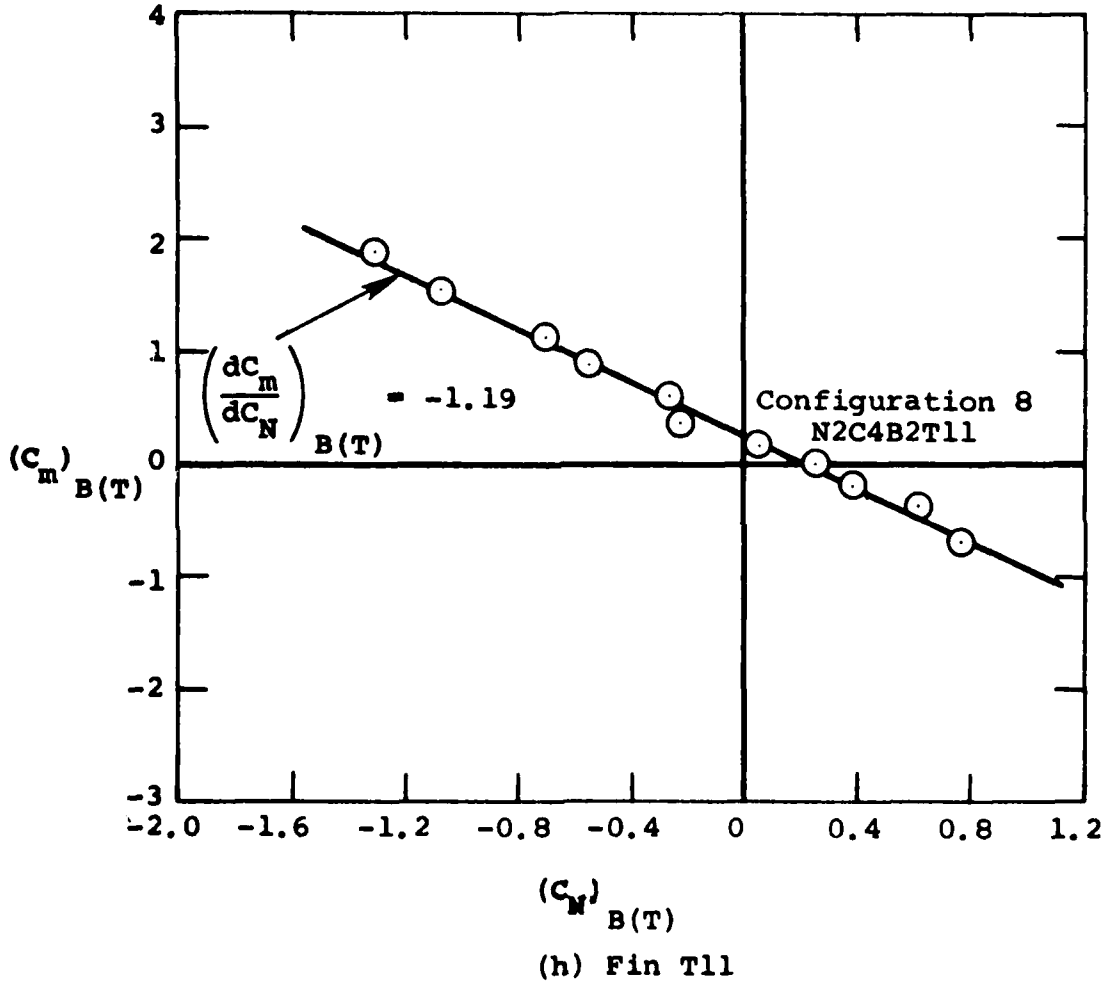

(h) Fin T11

FIGURE 24. (Sheet 8 of 11)

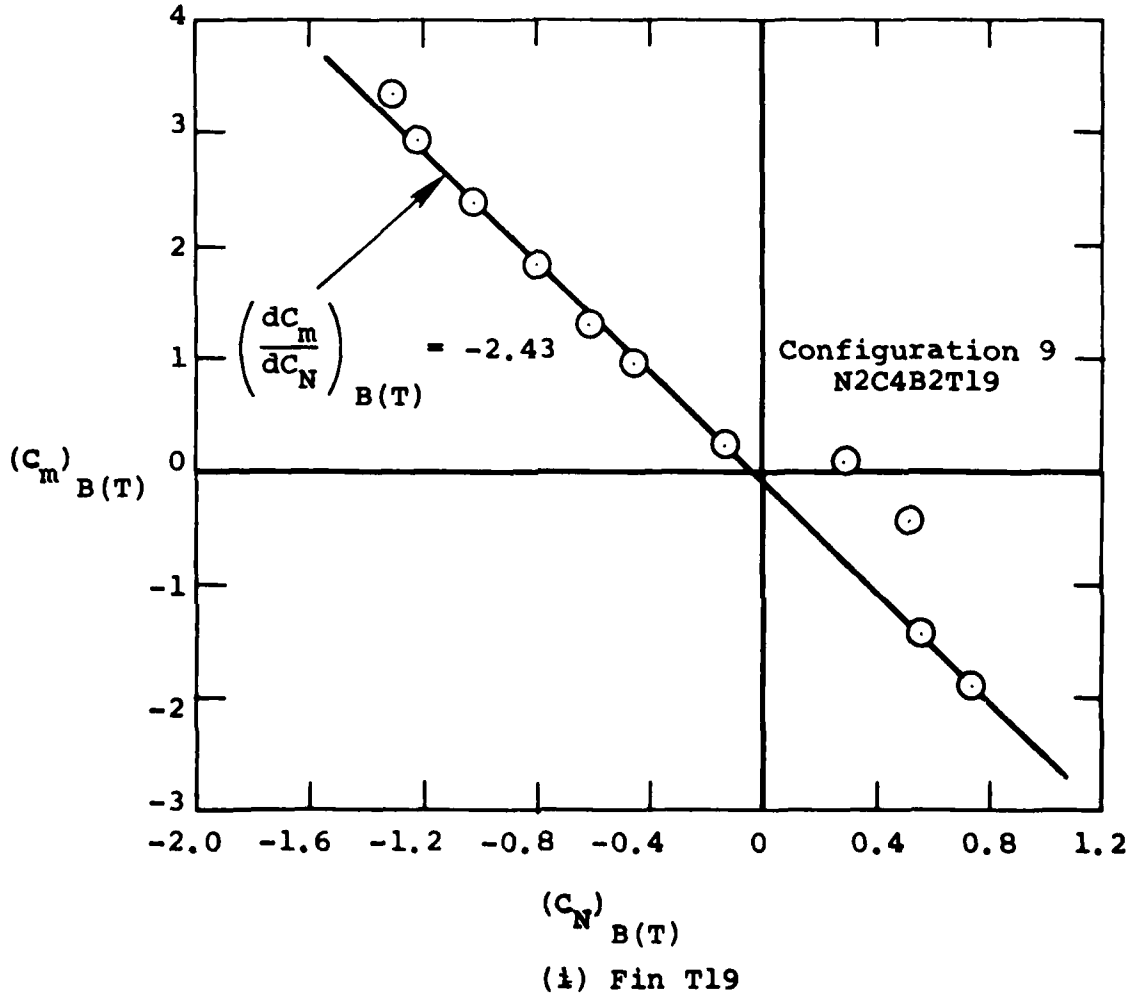

(i) Fin T19

FIGURE 24. (Sheet 9 of 11)

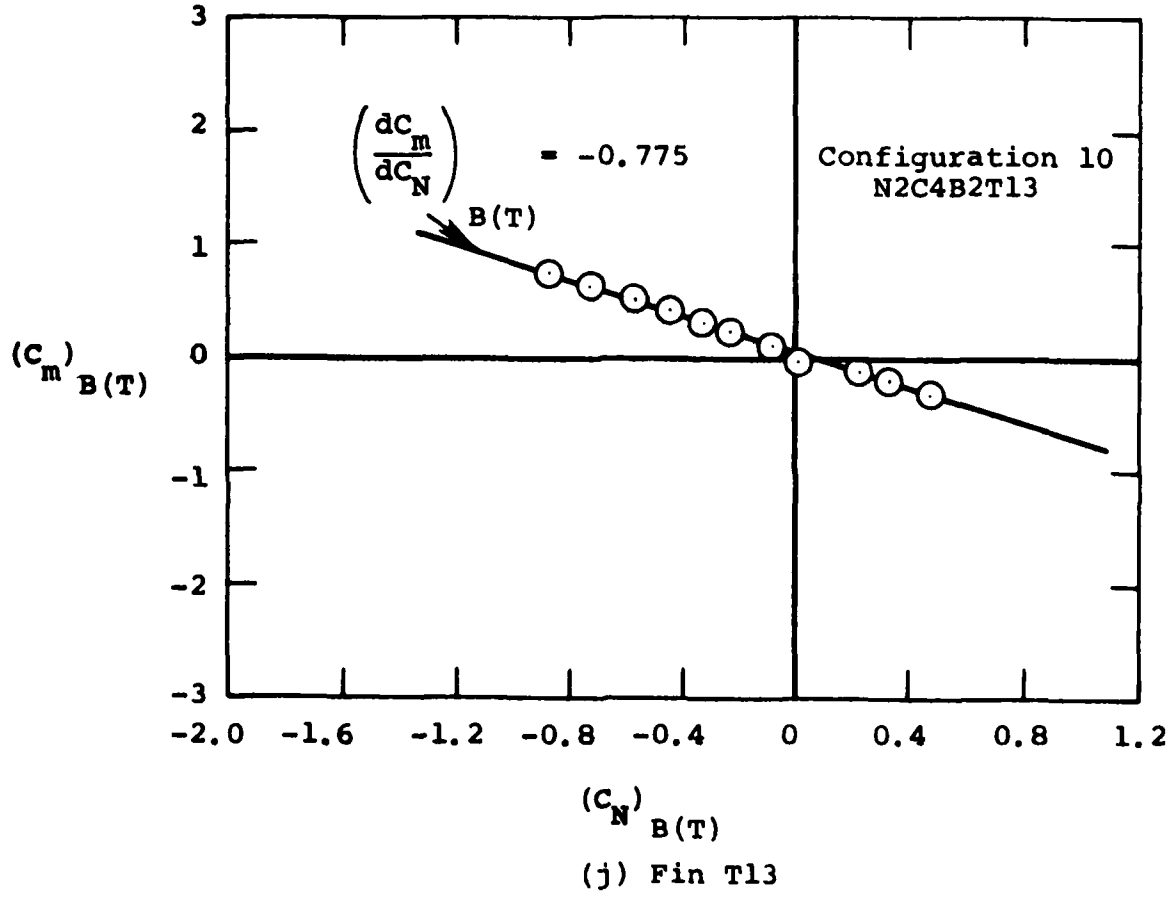

(j) Fin T13

FIGURE 24. (Sheet 10 of 11)

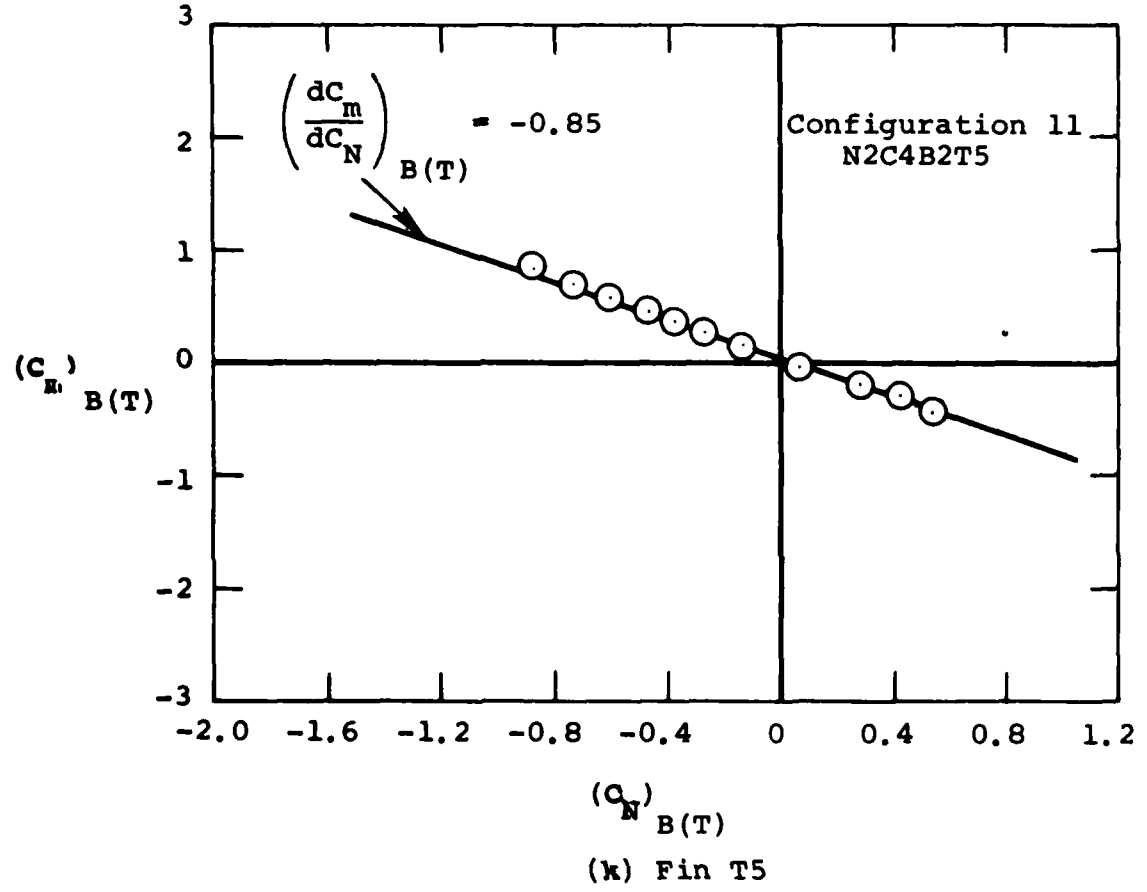

(k) Fin T5

FIGURE 24. (Sheet 11 of 11)

Straignt lines can be faired through the data for each configuration within the scatter of the data except for a few wild points. Accordingly we can characterize each configuration with a constant center-of-pressure position over the test range of fin deflection.

There is a degree of uncertainty in the slope of the lines to be faired through the data which can result in values of $(x_{cp}/c_r)_{B(T)}$ which vary by about ±0.10. In order to study the dependence of this quantity on s/R, λ, and AR the data points and their ranges of uncertainty were plotted against s/R, λ, and AR for the five systematic families listed in Section 5.4.2. For the three aspect-ratio families and the taper-ratio family, it was found that straight lines could be made to fit the data within the scatter bands with good accuracy. However, it was found that the s/R family exhibited quadratic behavior. Such a curve was faired through the scatter bands for this case. The resulting values of $(x_{cp}/c_r)_{B(T)}$ have been listed in Table 9 of Section 5.4.2 for examination. The results are also listed systematically in Table 10.

TABLE 10

EXPERIMENTAL VALUES OF $(x_{cp}/c_r)_{B(T)}$

Conf.	Fin	$\left(\frac{\bar{X}}{D}\right)_{B(T)}$	$\left(\frac{x_{cp}}{c_r}\right)_{B(T)}$
1	T9	1.296	0.460
2	T15	1.099	-0.430
3	T20	1.404	0.020
4	T12	1.418	0.020
5	T2	1.356	0.325
6	T14	1.171	-0.080
7	T24	1.248	-0.360
8	T11	1.133	0.020
9	T19	1.296	-0.170
10	T13	1.107	0.100
11	T5	1.130	0.050

One effect exhibited by Table 10 is the tendency of the center-of-pressure to be forward of the fin in a few instances. These cases occur for s/R = 1 or λ = 1.

The quantity $(x_{cp}/c_r)_{B(T)}$ is a complicated function of all three parameters, and a simple correlation was not found. The correlation means adopted was to fit a Taylor series to the data by means of least squares. Accordingly a series of the following type was selected.

$$\left(\frac{x_{cp}}{c_r}\right)_{B(T)} = A_1 + A_2(s/R) + A_3(\lambda) + A_4(\text{Æ}R) + A_5(s/R)^2 + A_6(\lambda \text{Æ}R) + A_7(\lambda s/R) + A_8(\text{Æ}Rs/R) \quad (23)$$

Quadratic terms in λ and ÆR were excluded on the grounds that only (s/R) showed any quadratic variation. With eight unknowns and 11 data point, the following results were obtained.

$$A_1 = 4.993$$

$$A_2 = -10.818$$

$$A_3 = -4.053$$

$$A_4 = 0.758$$

$$A_5 = 4.823$$

$$A_6 = -0.736$$

$$A_7 = 6.450$$

$$A_8 = -0.537$$

The standard deviation between the predicted quantities and the measured quantities is 0.01.

The degree of fit of Equation (23) to the data is shown in Figure 25 for each of the five systematic families. The fit is excellent. No independent data out of the range of the data used in determining the correlation are available. Accordingly, use of Equation (23) out of the range of the data is considered risky.

5.5.3 Prediction Method

1. There is only one step in the prediction method for $(x_{cp}/c_r)_{B(T)}$ and that is to calculate the quantity from Equation (23) from the known values of ÆR, λ, and s/R.

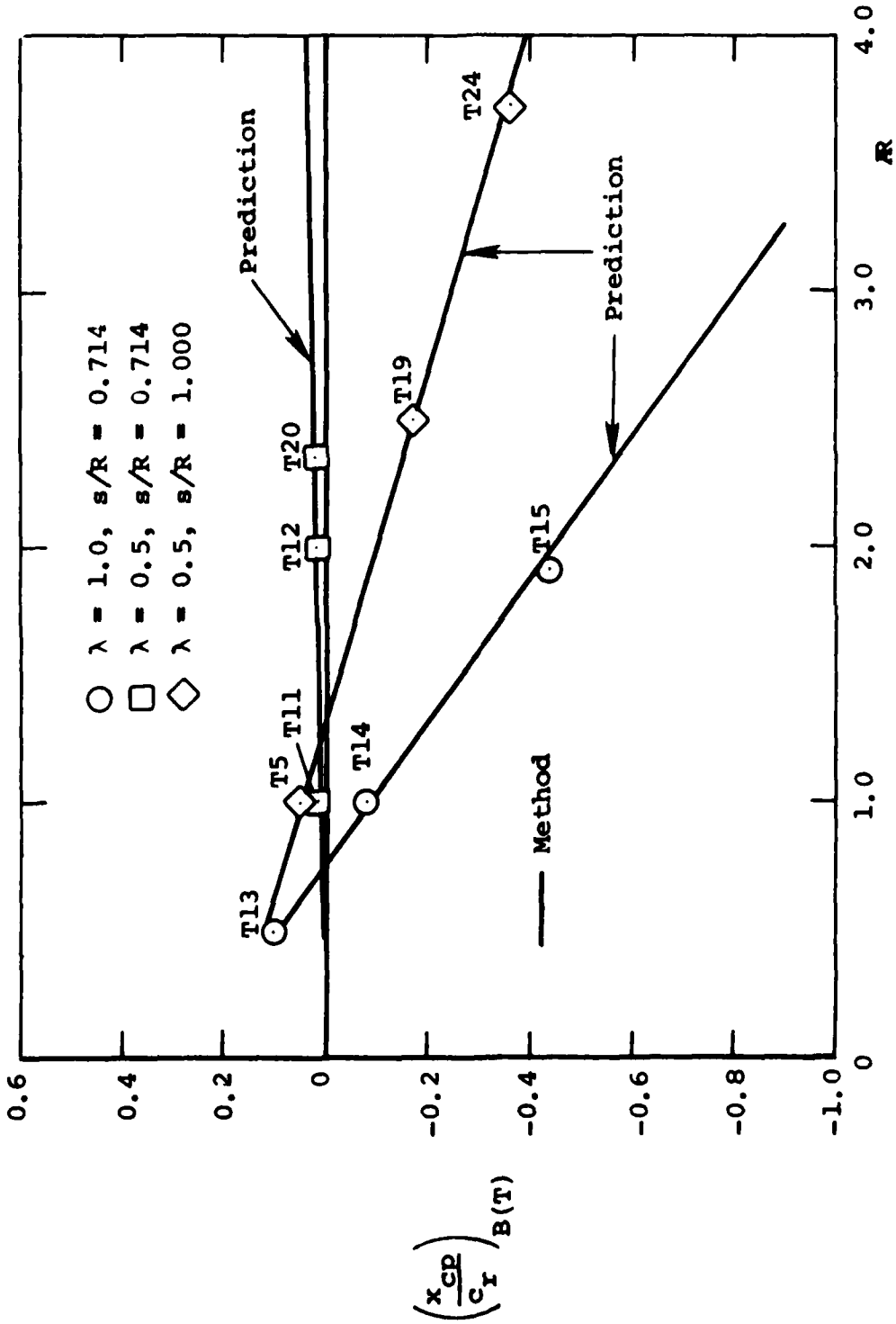

(a) Fin Aspect Ratio (AR)

FIGURE 25. COMPARISON BETWEEN EXPERIMENTAL AND PREDICTED VALUES OF $\left(\frac{x_{cp}}{c_r}\right)_{B(T)}$

(Sheet 1 of 3)

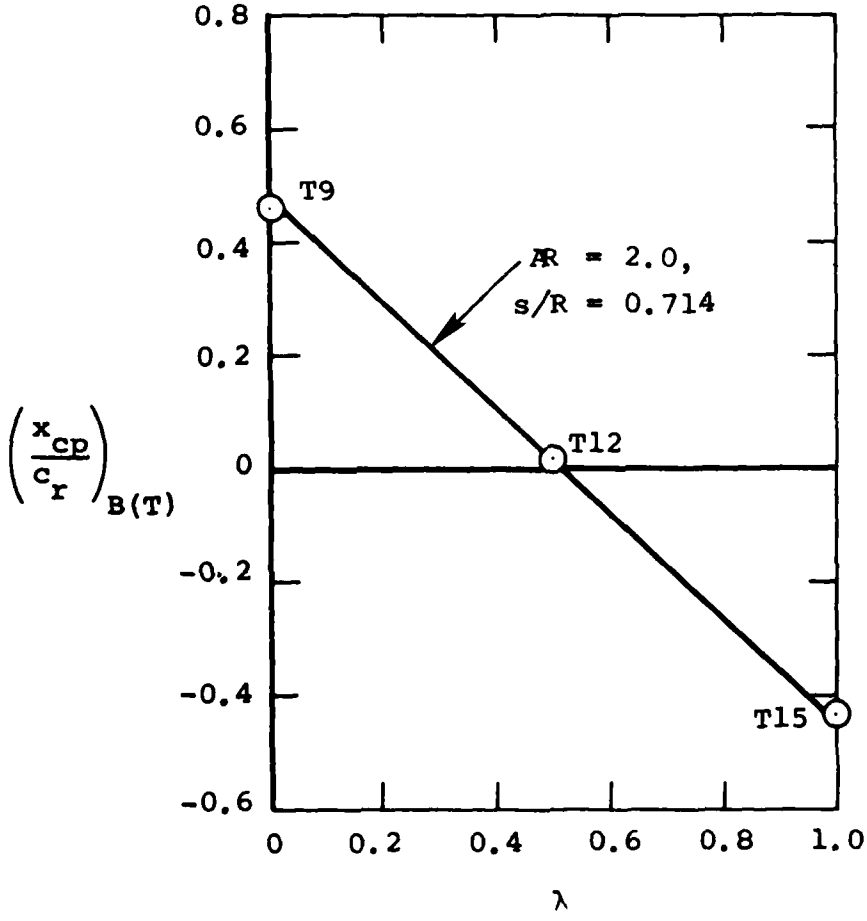

(b) Fin Taper Ratio (λ)

FIGURE 25. (Sheet 2 of 3)

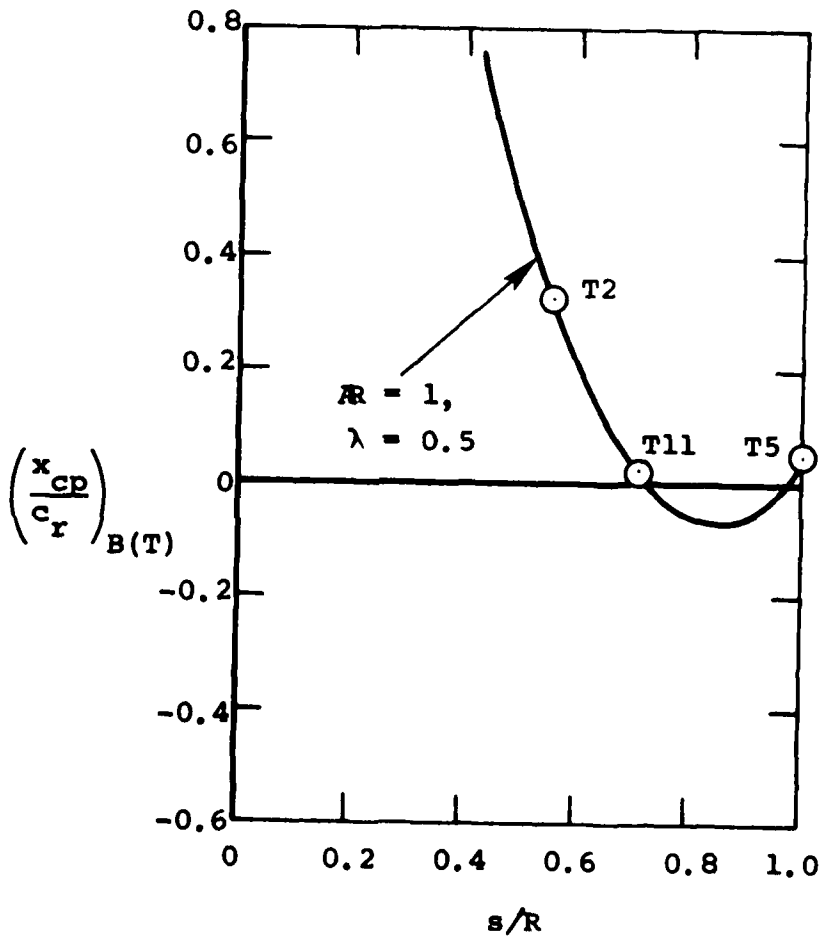

(c) Semispan-Radius Ratio (s/R)

FIGURE 25. (Sheet 3 of 3)

5.6 CHARACTERISTICS OF COMPLETE CONFIGURATION

5.6.1 Preliminary Remarks

From the quantities covered so far it is possible to determine the normal force and pitching moment for the body-tail combination. In what follows, the coefficients $(C_N)_{T(B)}$, $(C_m)_{T(B)}$, $(C_N)_{B(T)}$, and $(C_m)_{B(T)}$ are based on S_T as reference area and c_r as reference length and are the contributions of one fin. The quantities $(C_N)_{BT}$ and $(C_m)_{BT}$ are based on S_R as reference area and D as reference length.

5.6.2 Method of Calculation

In determining $(C_N)_{BT}$ we must account for the facts that $(C_N)_{T(B)}$ is normal to the fin, that there are two fins, and that there is a change in reference area. These considerations lead to the equation

$$(C_N)_{BT} = \frac{2S_T}{S_R}\left[(C_N)_{B(T)} + \cos\delta\ (C_N)_{T(B)}\right] \quad . \tag{24}$$

Determination of the quantity $(C_m)_{BT}$ requires a number of steps. The first step is to determine the pitching-moment coefficient of the fin about a lateral axis Y' through the hinge line intersection with the conical boattail. Using the measured hinge moment C_H and the bending moment C_B, and adopting c_r as the reference length.

$$C_{m_{Y'}} = C_H \cos\gamma - C_B \sin\gamma \cos\delta \left(\frac{s}{c_r}\right) \tag{25}$$

The second step is to transfer this moment to a lateral axis Y" through the center of moments by the parallel axis theorem.

$$C_{m_{Y''}} = C_{m_{Y'}} - (C_N)_{T(B)} \left(\frac{x_s + x_B \cos\gamma}{c_r}\right) \cos\delta \tag{26}$$

The third step is to transfer the $(x_{cp}/c_r)_{B(T)}$ location to the X coordinate measured rearward from the center-of-moment position.

$$\left(\frac{\bar{X}}{c_r}\right)_{B(T)} = \cos\gamma \cos\delta \left(x_{cp}/c_r\right)_{B(T)} + \frac{1}{c_r}\left(x_s + x_B\cos\gamma - x_H\cos\gamma \cos\delta\right) \quad (27)$$

Also we obtain the quantity $(C_m)_{B(T)}$

$$(C_m)_{B(T)} = -(C_N)_{B(T)}\left(\frac{\bar{X}}{c_r}\right)_{B(T)} \quad . \quad (28)$$

The final step is to determine the total body-tail pitching-moment coefficient changing the reference area from S_T to S_R and the reference length from c_r to D.

$$(C_m)_{BT} = 2\left[C_{m_{Y''}} + (C_m)_{B(T)}\right]\left(\frac{c_r}{D}\right)\frac{S_T}{S_R} \quad (29)$$

6. USE OF METHODS TO PREDICT CHARACTERISTICS OF COMPLETE CONFIGURATIONS

6.1 INTRODUCTORY REMARKS

The purpose of this section is to provide an example in the use of the methods for predicting the force and moment characteristics of a tail-body combination at zero angle of attack as a function of control deflection angle. For this purpose we will use one of the configurations tested during this investigation since we have no independent data not used in developing the method. The comparisons we will make between the measured and predicted quantities will thus be a measure of how well we have been able to correlate the data.

6.2 EXAMPLE CONFIGURATION

For the example configuration N2C4B2T11, the nose is designated N2, the centerbody C4, the base B2, and the fins T11. The basic body without fins is shown in Figure 1. The basic fin dimensions are given in Figure 2 as follows.

Fin T11

s (semispan) = 2.5 in.

c_r (root chord) = 6.664 in.

c_t (tip chord) = 3.332 in.

x_H (hinge-line location) = 4 in.

λ (taper ratio) = 0.5.

$\mathcal{AR}$ (aspect ratio) = 1.0.

S_T (fin planform area) = 12.50 sq. in.

$\Lambda_{te} = 0°$

Other quantities

x_s (distance from center of moments to beginning of boattail) = 7.53 in.

x_B (distance along boattail from shoulder to hinge-line position) = 4.00 in.

γ (conical boattail half-angle) = $\tan^{-1}\left(\frac{1}{4}\right) = 14.04°$

D (body diameter) = 7 in.

We will calculate $(C_N)_{T(B)}$, $(C_H)_{T(B)}$, $(C_B)_{T(B)}$, $(C_N)_{B(T)}$, $(x_{cp}/c_r)_{B(T)}$, $(C_N)_{BT}$, and $(C_m)_{BT}$.

For coefficients $(C_N)_{T(B)}$, $(C_H)_{T(B)}$, and $(C_B)_{T(B)}$ the reference area is the planform area of one fin, while for $(C_N)_{BT}$ and $(C_m)_{BT}$ it is the body cross sectional area, S_R.

$$S_R = \frac{\pi(D^2)}{4} = 38.4 \text{ sq. in.}$$

For $(C_H)_{T(B)}$ the reference length is c_r, for $(C_B)_{T(B)}$ the reference length is s, and for $(C_m)_{BT}$ the reference length is D.

6.3 FIN NORMAL-FORCE COEFFICIENT, $(C_N)_{T(B)}$

Step 1. The first step is to determine the fin alone lift-curve slope from DATCOM. For this purpose we need aspect ratio $\mathcal{AR}$, and the sweep angle of the midchord line, $\Lambda_{c/2}$.

For no trailing -edge sweep

$$\tan\Lambda_{c/2} = \frac{c_r - c_t}{2s}$$

$$\tan\Lambda_{c/2} = \frac{6.664 - 3.332}{(2)(2.5)}$$

$$\tan\Lambda_{c/2} = 0.6664$$

$$AR = 1$$

From Equation (5)

$$\left(\frac{dC_L}{d\alpha}\right)_{DAT} = \frac{2(1)}{2 + \sqrt{1(1 + 0.6664^2) + 4}}$$

$$= \frac{6.28}{2 + 2.33} = 1.45 \text{ per radian}$$

$$\left(\frac{dC_L}{d\alpha}\right)_{DAT} = \frac{1.45}{57.3} = 0.0253 \text{ per degree} \quad .$$

Step 2. We now determine k_T from Equation (6). Since $s/R = 0.714$, the value of k_T^* from Figure 15 is

$$k_T^* = 0.915 \quad .$$

From Figure 16, F(s/R) is unity so that from Equation (6)

$$k_T = (0.915)(1) = 0.915 \quad .$$

Step 3. The fin-normal force coefficient with S_T as reference area is given without nonlinear correction from Equation (7) as

$$(C_N)_{T(B)} = (0.0253)(0.915)\delta; \qquad \delta \text{ in degrees}$$

$$= 0.0231\delta \quad .$$

Step 4. The nonlinear term in $(C_N)_{T(B)}$ is given by $b_2\delta|\delta|$ where b_2 is obtained from Figure 17. From this figure for $AR = 1$ and $s/R = 0.714$, we find $b_2 = 1\times10^{-4}$. The sum of the linear and nonlinear parts of the normal force coefficient are:

δ (deg.)	0.0231δ	$\delta\|\delta\|\times10^{-4}$	$(C_N)_{T(B)}$
0	0	0	0
4	0.0924	0.0016	0.0940
8	0.1848	0.0064	0.1912
12	0.2772	0.0144	0.2916
16	0.3696	0.0256	0.3952
20	0.4620	0.0400	0.5020
24	0.5544	0.0576	0.6120
28	0.6468	0.0784	0.7252

The nonlinear normal-force curve is plotted against δ in Figure 26(a) where it is compared with the measured data. The data represent the average of the two fins and has been shifted to go through the origin as a correction for the support tare. The figure exhibits good agreement between the prediction and the data. Actually, the predicted linear component is slightly high and the predicted nonlinear component is low, but the sum is close to the data.

6.4 FIN HINGE-MOMENT COEFFICIENT, $(C_H)_{T(B)}$

We follow Section 5.2.3.

Step 1. We first determine $(C_N)_{T(B)}$ using the method of Section 5.1.3. This has already been accomplished, and the values are listed in the preceding tabulation.

Step 2. The value of $(x_{cp}/c_r)_T$ for the fin alone is determined from the charts of Figure 20 to be $(x_{cp}/c_r)_T = 0.39$.

Step 3. From Figure 19 we obtain

$$(x_{cp}/c_r)_{T(B)} = 0.390$$

Step 4. From Equation (10)

$$(C_H)_{T(B)} = -(C_N)_{T(B)}\left[(x_{cp}/c_r)_{T(B)} - x_H/c_r\right]$$

$$= -(C_N)_{T(B)}\left(0.390 - \frac{4}{6.664}\right)$$

$$= -(C_N)_{T(B)}(-0.210)$$

δ (deg.)	$(C_N)_{T(B)}$	$(C_H)_{T(B)}$
4	0.0940	0.0200
8	0.1912	0.0400
12	0.2916	0.0610
16	0.3952	0.0830
20	0.5020	0.1050
24	0.6120	0.1290
28	0.7252	0.1520

The comparison between prediction and data is shown for $(C_H)_{T(B)}$ in Figure 26(b). The value of C_H is overpredicted for large control deflections.

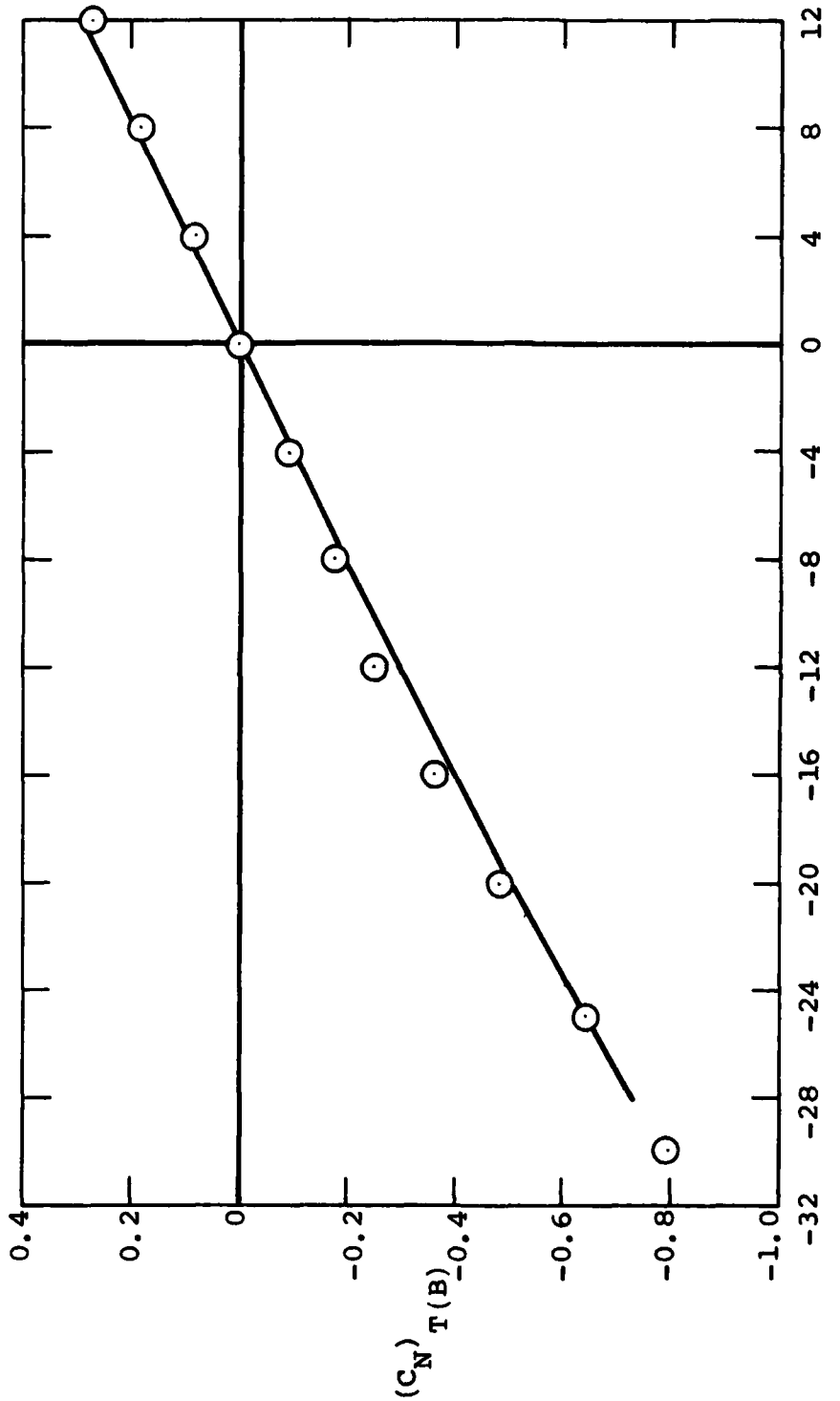

(a) Fin Normal Force

FIGURE 26. COMPARISON BETWEEN MEASURED AND PREDICTED QUANTITIES FOR TAIL FINS T11 ON BODY-TAIL COMBINATION

(Sheet 1 of 5)

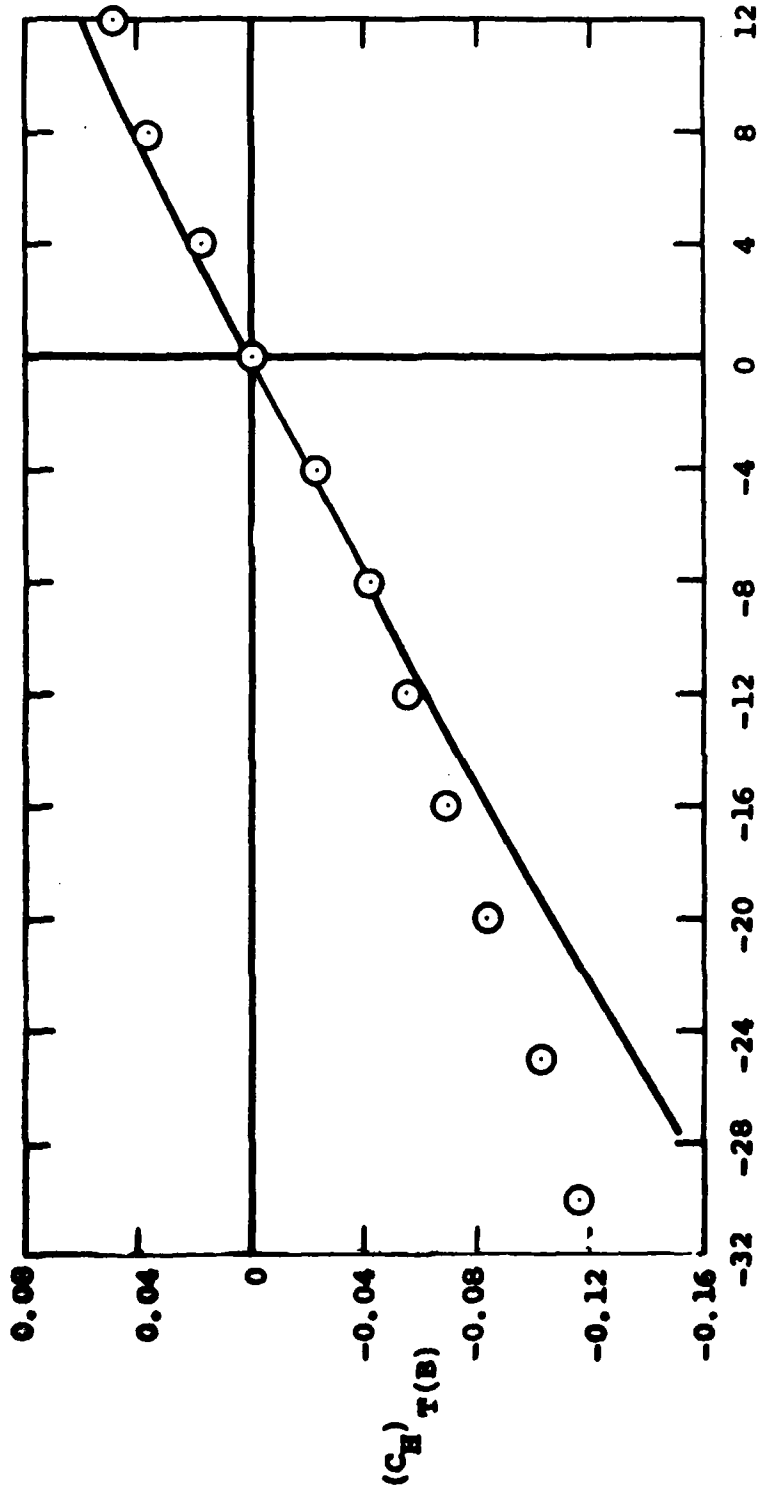

(b) Fin Hinge Moment

FIGURE 26. (Sheet 2 of 5)

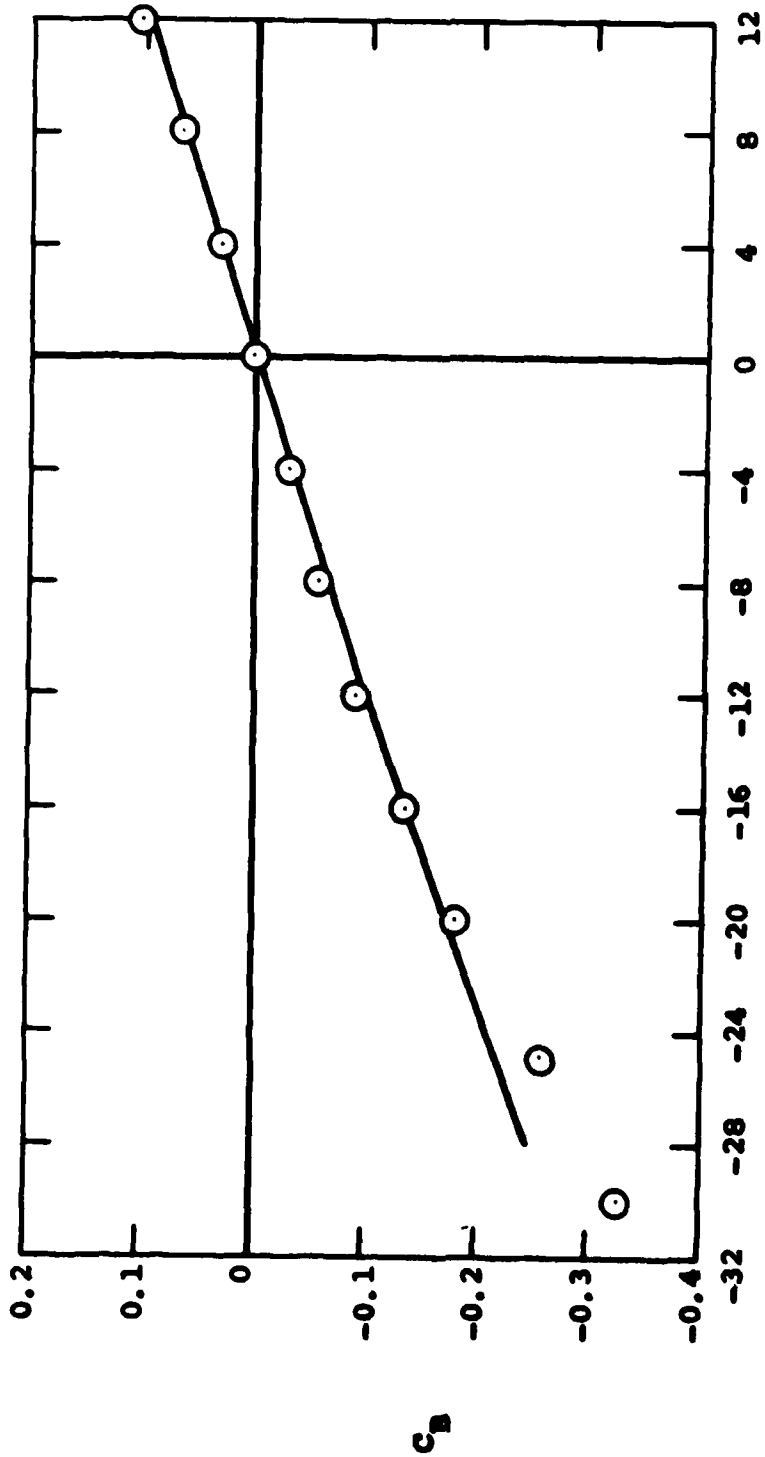

(c) Root-Bending Moment

FIGURE 26. (Sheet 3 of 5)

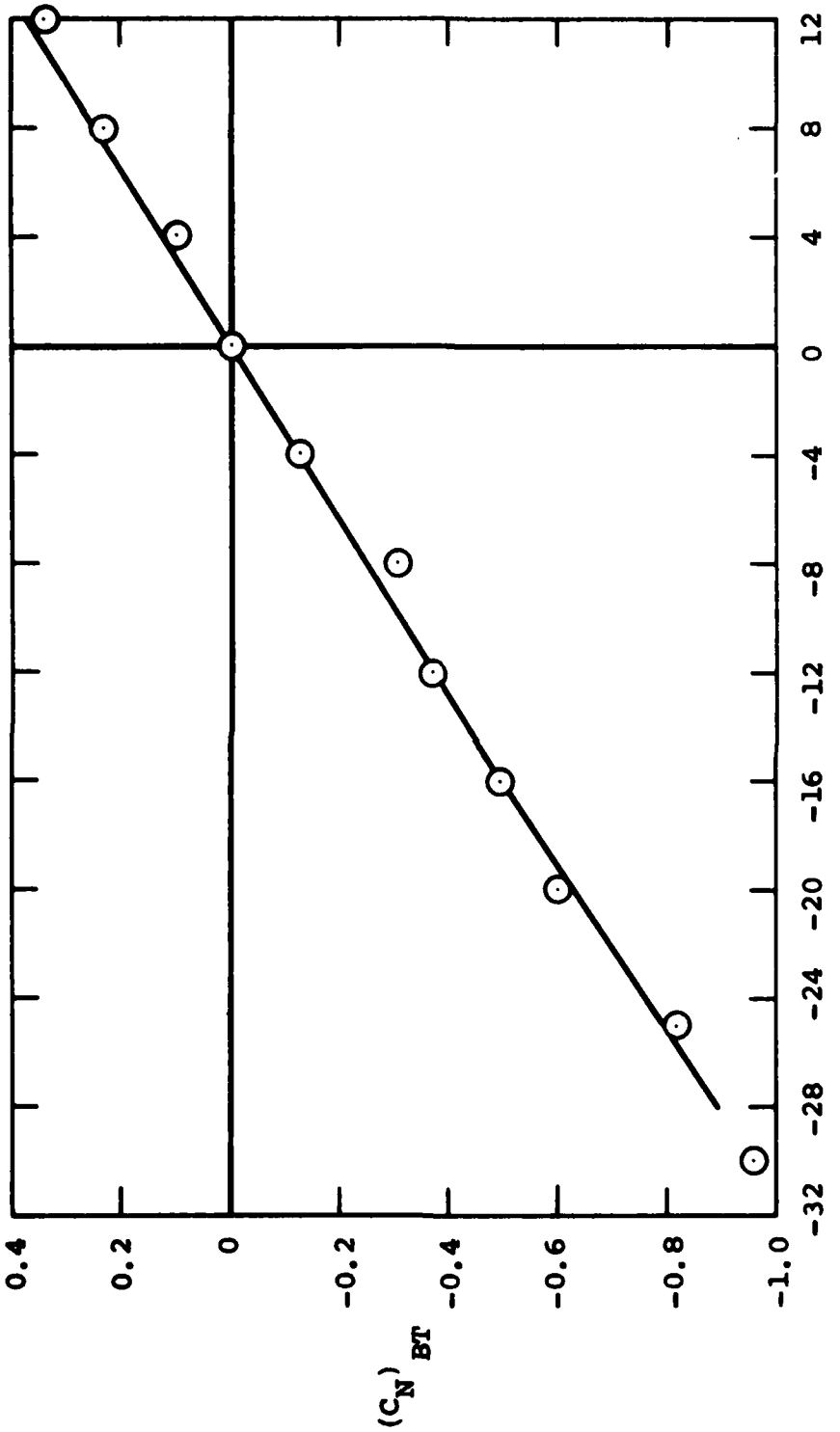

(d) Body-Tail Combination Normal Force

FIGURE 26. (Sheet 4 of 5)

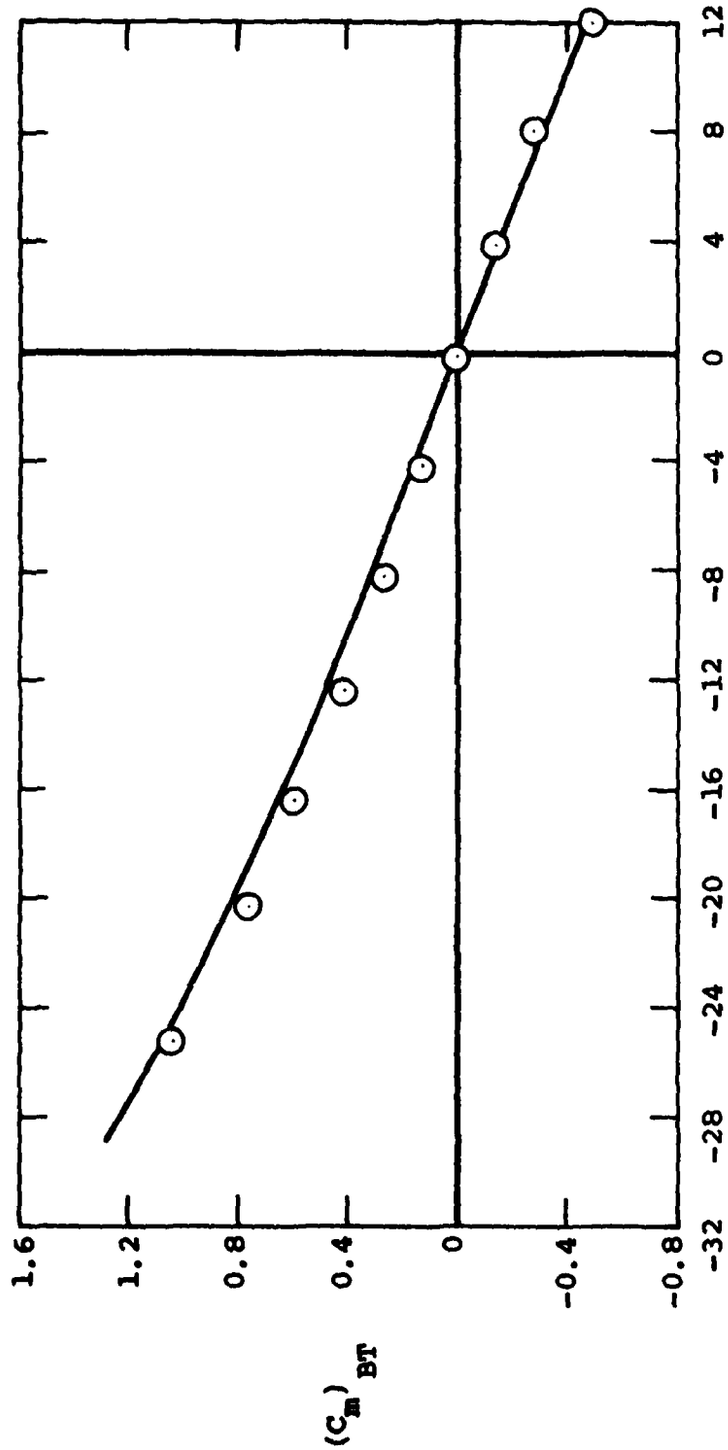

(e) Body-Tail Combination Pitching Moment

FIGURE 26. (Sheet 5 of 5)

6.5 FIN ROOT-BENDING-MOMENT COEFFICIENT, $(C_B)_{T(B)}$

We follow Section 5.3.3.

Step 1. Find $(C_N)_{T(B)}$ by method of Section 5.1.3. This has been accomplised.

Step 2. Find $(y_{cp}/s)_{T(B)}$ from Figure 21. We find that

$$(y_{cp}/s)_{T(B)} = 0.336$$

Step 3. From Equation (12)

$$(C_B)_{T(B)} = (C_N)_{T(B)} (y_{cp}/s)_{T(B)}$$

$$= (C_N)_{T(B)} (0.336)$$

δ (deg.)	$(C_N)_{T(B)}$	$(C_B)_{T(B)}$
4	0.0940	0.0316
8	0.1912	0.0642
12	0.2916	0.0980
16	0.3952	0.1330
20	0.5020	0.1690
24	0.6120	0.2060
28	0.7252	0.2440

Comparison between prediction and measurement for $(C_B)_{T(B)}$ is shown in Figure 26(c). The agreement is good up to δ = 20 degrees but deviates somewhat at higher δ.

6.6 NORMAL FORCE ON CONICAL BOATTAIL DUE TO FIN DEFLECTION, $(C_N)_{B(T)}$

We follow the steps of Section 5.4.3.

Step 1. Find k_B/k_T from Figure 23. From Figure 23 for $s/R = 0.714$, we find

$$k_B/k_T = 0.97$$

Step 2. The values of $(C_N)_{T(B)}$ are given in the preceding section.

Step 3. We evaluate Equation (17).

$$(C_N)_{B(T)} = (k_B/k_T)(C_N)_{T(B)}$$

The calculated results are:

δ (deg.)	$(C_N)_{T(B)}$	$(C_N)_{B(T)}$
4	0.0940	0.0911
8	0.1912	0.1855
12	0.2916	0.2830
16	0.3952	0.3830
20	0.5020	0.4870
24	0.6120	0.5940
28	0.7252	0.7030

6.7 CENTER-OF-PRESSURE OF LOADING ON CONICAL AFTERBODY, $(x_{cp}/c_r)_{B(T)}$

The only step in this calculation is to apply Equation (23) with $AR = 1$, $\lambda = 0.5$ and $s/R = 0.714$. The calculation proceeds as follows.

A_1:		$= 4.993$
$A_2(s/R)$:	$-10.818(0.714)$	$= -7.724$
$A_3(\lambda)$:	$-4.053(0.5)$	$= -2.027$
$A_4(AR)$:	$0.758(1)$	$= 0.758$
$A_5(s/R)^2$:	$(4.823)(0.714)^2$	$= 2.459$
$A_6(\lambda AR)$:	$-0.736(0.5)(1.0)$	$= -0.368$
$A_7(\lambda s/R)$:	$(6.450)(0.5)(0.714)$	$= 2.302$
$A_8(ARs/R)$:	$(-0.537)(1.0)(0.714)$	$= \underline{-0.383}$
		0.010

Thus

$$(x_{cp}/c_r)_{B(T)} = 0.010 \quad .$$

6.8 COMPLETE CONFIGURATION CHARACTERISTICS

6.8.1 Normal-Force Coefficient

The normal-force coefficient of the complete configuration based on S_R as reference area is given by Equation (24). Following this equation, with

$$\frac{2S_T}{S_R} = \frac{2(12.5)}{38.4} = 0.651$$

and the values of $(C_N)_{T(B)}$ and $(C_N)_{B(T)}$ from Section 6.6

δ (deg.)	$(C_N)_{T(B)}$	$(C_N)_{B(T)}$	$(C_N)_{BT}$
4	0.0940	0.0911	0.120
8	0.1912	0.1855	0.244
12	0.2916	0.2830	0.370
16	0.3952	0.3830	0.497
20	0.5020	0.4870	0.624
24	0.6120	0.5940	0.751
28	0.7252	0.7030	0.874

A comparison of $(C_N)_{BT}$ as predicted and measured is shown in Figure 26(d). The agreement between prediction and data is quite good. Since Figure 26(a) showed good agreement for $(C_N)_{T(B)}$, Figure 26(d) can be considered as verifying the $(C_N)_{B(T)}$ method since both components of configuration normal force are nearly equal.

6.8.2 Pitching-Moment Coefficient

Step 1. Determine the fin pitching moment about a lateral axis through the intersection of the hinge line and the conical boattail using Equation (25).

$$\frac{s}{c_r}\sin\gamma = \frac{(2.5)}{(6.664)}(0.2425) = 0.0910$$

δ (deg.)	C_H	C_B	$C_H\cos\gamma$	$\cos\delta$	$-0.0910\cos\delta C_B$	$C_{m_{Y'}}$
4	0.020	0.0316	0.0194	0.998	-0.00287	0.0165
8	0.040	0.0642	0.0388	0.990	-0.00579	0.0330
12	0.061	0.0980	0.0592	0.978	-0.00872	0.0505
16	0.083	0.1330	0.0805	0.961	-0.01160	0.0689
20	0.105	0.1690	0.1019	0.940	-0.01450	0.0874
24	0.129	0.2060	0.1251	0.914	-0.01710	0.1080
28	0.152	0.2440	0.1475	0.883	-0.01960	0.1279

Step 2. Determine the contribution of the fin to the pitching moment about the center-of-moments from Equation (26).

$$\frac{x_s + x_B\cos\gamma}{c_r} = \frac{7.53 + 4(0.970)}{6.664} = 1.713$$

δ (deg.)	$C_{m_{Y'}}$	$(C_N)_{T(B)}$	$1.713(C_N)_{T(B)}$	$C_{m_{Y''}}$
4	0.0165	0.0940	0.161	-0.144
8	0.0330	0.1912	0.327	-0.294
12	0.0505	0.2916	0.500	-0.450
16	0.0689	0.3952	0.677	-0.608
20	0.0874	0.5020	0.860	-0.773
24	0.1080	0.6120	1.048	-0.940
28	0.1279	0.7252	1.242	-1.114

Step 3. Find the axial position $(\bar{X}/c_r)_{B(T)}$ from Equation (27). From Section 6.7, $(x_{cp}/c_r)_{B(T)} = 0.010$.

$$\frac{x_s + x_B\cos\gamma}{c_r} = 1.713; \qquad \frac{x_H\cos\gamma}{c_r} = \frac{(4)(0.970)}{6.664} = 0.582$$

$$(\bar{X}/c_r)_{B(T)} = \cos\gamma\,\cos\delta\,(0.010) + 1.713 - 0.582\,\cos\delta$$

δ (deg.)	cosδ	0.582cosδ	0.010cosγcosδ	$(\bar{X}/c_r)_{B(T)}$
4	0.998	0.581	0.010	1.142
8	0.990	0.576	0.010	1.147
12	0.978	0.569	0.009	1.153
16	0.961	0.559	0.009	1.163
20	0.940	0.547	0.009	1.175
24	0.914	0.532	0.009	1.190
28	0.883	0.514	0.009	1.208

Step 4. Find $(C_m)_{BT}$ from Equation (29) using $(C_m)_{B(T)}$ from Equation (28). The values of $(C_N)_{B(T)}$ come from Subsection 6.8.1. The values of $(\bar{X}/c_r)_{B(T)}$ are from Step 3. The value of $(C_m)_{B(T)}$ is obtained from

$$(C_m)_{B(T)} = -(C_N)_{B(T)}\,(\bar{X}/c_r)_{B(T)} \quad .$$

The value of $C_{m_{Y''}}$ comes from Step 2. The value of $(C_m)_{BT}$ is given by

$$(C_m)_{BT} = 0.619\left[(C_m)_{B(T)} + C_{m_{Y''}}\right]$$

where

$$2\,\frac{c_r}{D}\,\frac{S_T}{S_R} = 2\left(\frac{6.664}{7}\right)\left(\frac{12.5}{38.4}\right) = 0.619$$

δ (deg.)	$(C_N)_{B(T)}$	$\left(\frac{\bar{X}}{c_r}\right)_{B(T)}$	$(C_m)_{B(T)}$	$C_{m_{Y''}}$	$C_{m_{Y''}}$ + $(C_m)_{B(T)}$	$(C_m)_{BT}$
4	0.0911	1.142	-0.104	-0.144	-0.248	-0.154
8	0.1855	1.147	-0.213	-0.294	-0.507	-0.314
12	0.2830	1.153	-0.326	-0.450	-0.776	-0.480
16	0.3830	1.163	-0.445	-0.608	-1.053	-0.652
20	0.4870	1.175	-0.572	-0.773	-1.345	-0.833
24	0.5940	1.190	-0.707	-0.940	-1.647	-1.019
28	0.7030	1.208	-0.849	-1.114	-1.963	-1.215

The predicted values of $(C_m)_{BT}$ were used to obtain the curve shown in Figure 26(e). The curve compares well with the measured data.

7. CONCLUSIONS AND RECOMMENDATIONS

7.1 CONCLUSIONS

A series of methods have been developed for estimating the normal force, hinge moment, and bending moment of all-movable fins at zero degrees angle-of-attack mounted on a conical boattail for a range of fin aspect ratios and taper ratios, and a range of fin spans. In addition methods have been developed for estimating the loading on the body due to fin deflection as well as its center-of-pressure location. The quantities are combined to predict the normal force and pitching moment of body-tail combinations. This methodology supplements similar methods developed earlier for similar configurations to estimate the angle-of-attack characteristics of the body-tail combinations with no fin deflection. These methods can be used together to estimate the combined effects of angle-of-attack and fin deflection within the range of validity of linear superposition.

Eleven fin configurations are used in the method development; testing additional configurations would enhance the accuracy of the method. The configuration space covers the following ranges of fin aspect ratio and taper ratio: $0.5 \leq AR \leq 3.7$; $0 \leq \lambda \leq 1.0$. The ratio of fin semispan (measured outward from the root chord) to body radius at the start of the boattail range from approximately 0.5 to 1.0.

The flat plate fins have rounded leading edges. When tested alone they gave lift-curve slopes and center-of-pressure positions in good agreement with low-speed wing theory.

The fin normal-force curves were fairly linear, but some fins showed 20 to 25 percent nonlinearity at deflection angles of 20 degrees. Generally the other quantities were fairly linear when plotted against fin normal-force coefficient, although some nonlinearities appeared in some quantities as the deflection angle approached 30 degrees. No effects of extensive flow separation on the boattail were evident in the measured results at zero angle of attack.

Since only one fin with an aspect ratio of less than 1 was tested in the present series, the method must be considered tentative for $AR < 1$.

7.2 RECOMMENDATIONS

Data were taken at combined angles-of-attack and horizontal control deflection for 11 independent tail configurations. These data should be sufficient to permit future development of methods for predicting the nonlinear effects of coupling between these two parameters, and it is recommended that this task be undertaken.

For the configurations with fins undeflected, tests were made through a roll angle range. It is possible that the data are adequate to enable methods to be developed for the effects of roll with $\delta = 0$ degree. This possibility needs investigation.

The configurations were also tested at an angle-of-attack with $\phi = 90$ degrees. In these tests the vertical fins were deflected. These data could be used to develop a yaw control prediction method.

Limited data are now available on the effects of sail position on the body-sail characteristics. These data should be analyzed with a view to the development of prediction methods for these effects. Further test data will probably be required.

The data base used in constructing the methods in the present document are sparse in certain ranges of the primary parameters. For instance, only one fin with an aspect ratio less than 1.0 was tested and only one greater than 2.5. Also one fin of zero taper ratio was tested. It would be desirable to fill out the data base in these regions.

APPENDIX A

CONTRIBUTION OF TAIL TO PITCHING MOMENT ABOUT CG

Consider the following planform sketch.

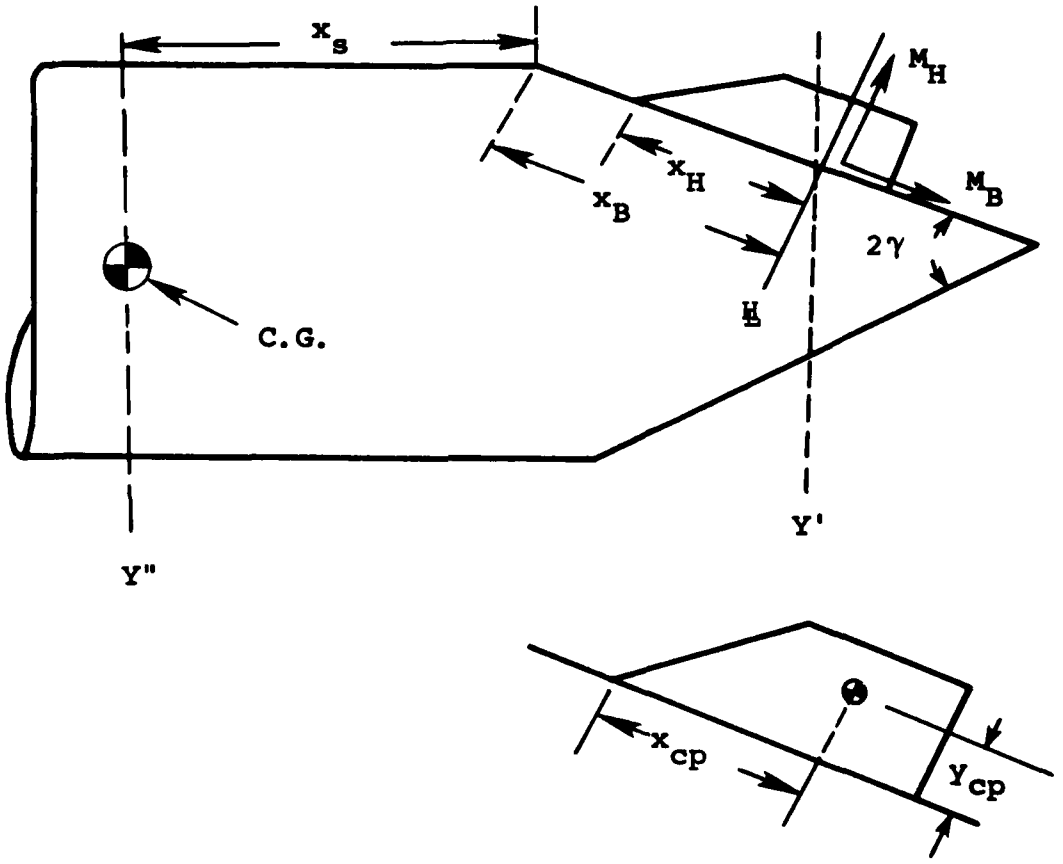

The moments measured on the fin are M_H, the hinge moment, and M_B, the bending moment. The normal force N is also measured. We desire to derive an expression for the moment $M_{T(B)}$ about the CG in terms of these quantities. It is assumed that the forces on the fin lying in the chord plane of the fin cause negligible moment.

Since the fin is at deflection δ, positive leading edge up, the moment M_Y, about axis Y' is

$$M_{Y'} = M_H \cos\gamma - M_B \cos\delta \sin\gamma \quad . \tag{A1}$$

For M_B, the reference length is s but for the other moments it is c_r. Thus, in coefficient form

$$C_{Y'} = C_H \cos\gamma - C_B \frac{s}{c_r} \cos\delta \sin\gamma \quad . \tag{A2}$$

By the parallel axis theorem

$$(C_m)_{T(B)} = C_{Y''} = C_{Y'} - C_Z \frac{(x_s + x_B \cos\gamma)}{c_r} \quad . \tag{A3}$$

Let x_{cp} and y_{cp} be the coordinates of the fin center-of-pressure as shown in the sketch, and let $(C_N)_{T(B)}$ be the fin normal force coefficient.

$$C_H = (C_N)_{T(B)} \frac{(x_H - x_{cp})}{c_r} \tag{A4}$$

$$C_B = (C_N)_{T(B)} \frac{y_{cp}}{s} \quad . \tag{A5}$$

Then

$$C_{Y'} = (C_N)_{T(B)} \left[\frac{(x_H - x_{cp})}{c_r} \cos\gamma - \frac{y_{cp}}{c_r} \cos\delta \sin\gamma \right] \quad . \tag{A6}$$

We assume that

$$C_Z = (C_N)_{T(B)} \cos\delta \quad . \tag{A7}$$

Then from Equation (A3)

$$(C_m)_{T(B)} = (C_N)_{T(B)} \left\{ \frac{(x_H - x_{cp})}{c_r} \cos\gamma - \frac{y_{cp}}{c_r} \cos\delta \sin\gamma - \cos\delta \frac{(x_s + x_B \cos\gamma)}{c_r} \right\}$$

or

$$(C_m)_{T(B)} = \frac{(C_N)_{T(B)}}{c_r}\Big[(x_H - x_{cp})\cos\gamma - y_{cp}\cos\delta\ \sin\gamma - (x_s + x_B\ \cos\gamma)\ \cos\delta\Big] \qquad \text{(A8)}$$

DISTRIBUTION LIST

		Copy No.
427	Commander, Naval Sea Systems Command	
	(SEA 035, Dr. T. Peirce)	1
	(SEA 032, Mr. Sejd)	2
	(SEA 034)	3
	(SEA 92)	4
	(PMS 393)	5
	(PMS 395)	6
	(Library)	7
001	Chief of Naval Material	
	(MAT 08T23, Mr. Vittucci, Mr. Remson, Mr. Romano)	8-10
003	Chief of Naval Operations	11
005	Commander, Naval Ship Engineering Center	
	(Library)	12
	(Code 6136, Mr. Keane, Mr. Louis, Mr. Golstein, Mr. Jones)	13-16
236	Commander, David Taylor Naval Ship R&D Center	
	(Library)	17
	(Code 1564, Dr. Feldman, Mr. Sheridan)	18-19
	(Code 1543, Mr. Folb)	20
266	Commanding Officer, Naval Underwater Systems Center	
	(Library)	21
	(Mr. Goodrich)	22
	(Mr. Nadolink)	23
265	Commander, Naval Oceans Systems Center, San Diego	
	(Library)	24
692	Director, Naval Oceans Systems Center, Hawaii Laboratory	
	(Library)	25
	(Code 5332)	26
	(Code 6302)	27
484	Director, Naval Research Laboratory	
	(Library)	28
210	Commander, Naval Surface Weapons Center, White Oak	
	(Library)	29
463	Commander, Naval Surface Weapons Center, Dahlgren	
	(Library)	30
154	Superintendent, Naval Academy, Annapolis	
	(Library)	31
222	Superintendent, Naval Postgraduate School, Monterey	
	(Library)	32
054	Chief of Naval Research	
	(ONR 211, Dr. Siegel, Dr. Whitehead)	33-34
	(ONR 438, Mr. Cooper)	35
268	Commander, Naval Weapons Center, China Lake	
	(Library)	36
162	Commander, Naval Air Systems Command	
	(Library)	37
---	Commanding Officer, Eglin Air Force Base	
	(Library)	38
---	Commanding Officer, Picatinny Arsenal, Dover, NJ 07801	
	(Library)	39

DISTRIBUTION LIST
(Continued)

		Copy No.
---	Commanding Officer, Redstone Arsenal, US Army Missile R&D Command	
	(Library)	40
---	Ames Research Center, National Aeronautics and Space Administration	
	(MS 202-3, Library)	41
---	Langley Research Center, National Aeronautics and Space Administration	
	(Library)	42
---	National Aeronautics and Space Administration, Washington	
	(Library)	43
621	Commanding Officer, Naval Oceans Research & Development Activity	44
693	Undersecretary of Defense for Research and Engineering	45
006	Director, Advanced Research Projects Agency	46
---	Library of Congress, Washington	
	(Science and Technology Library)	47
---	Nielsen Engineering & Research, Inc., Mountain View, CA 94040 (N61331-78-C-0032)	
	(Library)	48
	(Dr. J. Nielsen)	49
	(Mr. J. Fidler)	50
075	Director, Defense Technical Information Center	51-60